Analysis of Signal Propagation in Fiber Optic Links and Compensation Techniques for Propagation Impairments

ANALYSIS OF SIGNAL PROPAGATION IN FIBER OPTIC LINKS AND COMPENSATION TECHNIQUES FOR PROPAGATION IMPAIRMENTS

BY

JING SHAO, M.A.Sc.

A THESIS

SUBMITTED TO THE DEPARTMENT OF ELECTRICAL AND COMPUTER ENGINEERING

AND THE SCHOOL OF GRADUATE STUDIES

OF MCMASTER UNIVERSITY

IN PARTIAL FULFILMENT OF THE REQUIREMENTS

FOR THE DEGREE OF

DOCTOR OF PHILOSOPHY

Doctor of Philosophy (2015) McMaster University

(Electrical and Computer Engineering) Hamilton, Ontario, Canada

TITLE:	Analysis of Signal Propagation in Fiber Optic Links and Compensation Techniques for Propagation Impairments
AUTHOR:	Jing Shao M.A.Sc., (Optoelectronic Information Engineering) Huazhong University of Science and Technology,Wuhan, China
SUPERVISOR:	Prof. Shiva Kumar
NUMBER OF PAGES:	xix, 149

To my beloved parents

Abstract

This thesis deals with modeling of signal propagation in fiber links. The signal propagation in optical fiber is described by the nonlinear Schrödinger equation (NLSE) and this thesis discusses various schemes to solve NLSE. In addition, compensation of propagation impairments due to dispersion and nonlinearity in fiber optic systems are also dealt with. In order to reduce the bit error rate (BER) and enhance the reach, digital and optical equalization schemes are investigated.

Optical fiber is usually used as the transmission channel for optical signals. However, an optical fiber has loss, dispersive and nonlinear effects which bring distortions to the optical signal. Due to fiber loss, signal power decreases with propagation distance. Fiber dispersion results from the frequency dependence of transmission speed which leads to pulse broadening. Also, fiber nonlinearity, which is due to the dependence of refractive index on the signal intensity, brings nonlinear distortions to the optical signal. The total propagation effect is determined by the interplay among fiber loss, dispersion and nonlinearity, which is governed by the NLSE. Chapter 2 mainly focuses on efficient schemes for simulating propagation in optical fibers. Various schemes based on split-step Fourier techniques to solve the NLSE are compared. To solve the NLSE using split-step method, dispersive and nonlinear effects will be treated independently and interchangeably in small sections, and fiber loss can be

combined with dispersion or nonlinearity. In general, the schemes in which the loss operator is combined with nonlinearity operator are found to be more computationally efficient than the schemes in which the loss is combined with dispersion. When the global error is large, the schemes with variable step size outperform the ones with uniform stepsize. The scheme based on local error and/or minimum area mismatch(MAM) is investigated and futher improves the computational efficiency. In this scheme, by minimizing the area mismatch between the exponential profile and its stepwise approximation, an optimal step size distribution is found. The number of steps to get the desired accuracy is determined by the local error method. This scheme is found to have higher computational efficiency than the other schemes.

In Chapter 3, a digital back propagation (DBP) scheme with optimal step size for polarization division multiplexed transmission system is investigated. DBP is a digital compensation scheme to undo fiber dispersion and nonlinearity, which solves the NLSE using split-step method with parameters the opposite sign of the transmission fiber. For a fixed number of steps in DBP, the optimal step size is calculated by minimizing the mismatch between the area under the exponentially increasing nonlinearity profile and its stepwise approximation. In simulations, the vector NLSE or Manakov equations are used for forward propagation and Manakov equations are used for backward propagation. The simulation results show that at the same computational cost, the scheme using the optimum step size has higher tolerance to nonlinearity and a lower BER. In a single channel polarization multiplexing division system, the transmission reach can be increased from 4300 km to 5200 km while introducing the optimum step size, if two steps per span are used for DBP.

Although DBP is effective to compensate for fiber distortions, it has a relatively

high computational cost and is hard to implement in real time for WDM systems. Also it is not suitable for optical networks. In Chapter 4, a fiber-optic system design with optical backpropagation (OBP) that uses an optical phase conjugator, high-dispersion fibers (HDFs), and highly nonlinear fibers (HNLFs) is developed. The dispersion can be compensated by the HDFs, and the nonlinearity can be mitigated by HDFs and HNLFs. The analytical formulas of the lengths of HDFs and HNLFs are derived and match well with the numerical results. This technique outperforms the midpoint optical phase conjugation and DBP with the same step size. In a single channel system, when the step size equals the span length, BER of OBP is 8×10^{-4}, while BER of DBP is 2×10^{-3}. Also, another OBP scheme consisting of an optical phase conjugator, fiber Bragg gratings (FBGs), and HNLFs is investigated. Transmission fiber dispersion is compensated by the FBGs and the nonlinearity is compensated by HNLFs. Several sections of FBGs and HNLFs are concatenated in a way analogous to the split-step Fourier scheme used for solving the NLSE. The optimum accumulated dispersion of each section of the FBGs and the optimum nonlinear phase shift of each section of HNLF are calculated by minimizing the mismatch between the area under the exponentially increasing nonlinearity profile and its stepwise approximation. The mothod of Lagrange multipliers is used for optimization. The optimization technique leads to significant performance improvement and/or reach enhancement as compared to uniformly spaced sections, for the given number of sections. When 2 steps per span OBP are used in a single channel system , BER of uniform spacing step size is 2×10^{-3}, while BER of the optimum step size is reduced to 1×10^{-3}.

OBP is an effective scheme to compensate for fiber dispersion and nonlinearity. The more steps in a single span, the better the performance will be. However, fibers

and optical devices in OBP will introduce higher insertion loss if more steps are used. In Chapter 5, an ideal optical back propagation (OBP) scheme to compensate for dispersion and nonlinear effects of the transmission fibers is investigated. The scheme consists of an optical phase conjugator (OPC), N spans of dispersion-decreasing fibers (DDFs) and amplifiers, placed at the end of the fiber optic link. It is shown that a combination of DDFs and amplifiers can compensate for the nonlinear effects exactly. An analytical expression for the dispersion profile of the DDF is derived. Numerical simulations of wavelength division multiplexing (WDM) fiber-optic systems show that the proposed OBP scheme can enhance the system reach significantly as compared to DBP. The OBP scheme with DDF is also potential for applications in network communication systems, if a compensation unit with a DDF and amplifier is placed after the transmission fiber in each span.

In Chapter 6, an exact solution of NLSE is derived for impulse input in the presence of pre-dispersion. The phase factor of the exact solution is obtained in a closed form using the exponential integral. It is found that if the complex weights of a sequence of impulses at the input have a secant-hyperbolic envelope and a proper chirp factor, they will propagate over long distances without exchanging energy. To describe their interaction, a discrete version of NLSE is derived. The discrete NLSE is found to admit fundamental and higher order soliton solutions in the presence of high pre-dispersion. In the context of discrete NLSE, if the effective dispersion length is much longer than the effective nonlinear length, we have obtained the nonlinear eigenmodes of the highly pre-dispersed fiber-optic system which may be useful for the description of signal propagation, and signal and noise interaction.

Acknowledgements

I would like to express the deepest gratitude to my supervisor, Prof. Shiva Kumar. He taught me not only the knowledge about fiber optic communication systems, but also the method to think about and deal with problems. His patient guidance and constant encouragement on my research project make me conquer various obstacles and progress well. Also, I will give my sincere gratitude for his kindness and understanding, which is a great help in my Ph.D. years.

I would like to express my sincere thanks to the committee members, Prof. Xun Li and Prof. Jamal Deen, for their precious comments, suggestions and guidance during my research. Also, I would like to thank Dr. Jiankang Zhang, Dr. Max Wong, Dr. Steve Hranilovic, and Dr. Jun Chen, for their wonderful lectures. I would like to thank Dr. Sina N. Shaihi for his helpful discussion about the research. I would like to thank the ECE department staff, specially Cheryl, for helping me in various aspect. I would like to thank all the colleagues in Photonics CAD Lab, for their companionship and friendship.

Finally, I am deeply grateful to my parents for their love and supportive in my life, to my dear husband, Xiaojun, for his companionship, patience, understanding, and assistance throughout the memorable time.

Abbreviations

ADC	analog-to-digital converter
ASE	amplified spontaneous emission
BER	bit error rate
BPF	band pass filter
CW	continuous wave
DBP	digital back propagation
DCF	dispersion compensating fiber
DDF	dispersion-decreasing fiber
DFT	discrete Fourier transform
DM	dispersion-managed
DMUX	demultiplxer
DSP	digital signal processing
DST	discrete self-trapping
DU	dispersion-uncompensated
FBG	fiber Bragg grating
FEC	forward error correction
FFT	fast Fourier transforms
FIR	finite impulse response

FWM	four-wave mixing
GN	Gaussian noise
GVD	group-velocity dispersion
HDF	high-dispersion fiber
HNLF	highly nonlinear fiber
IDFT	inverse discrete Fourier transform
IFWM	intra-channel four wave mixing
ISI	inter-symbol interference
IST	inverse scattering transform
IXPM	intra-channel cross-phase modulation
LMS	least mean squares
LPF	low pass filter
LSM	least squares method
MAM	minimum area mismatch
MUX	multiplexer
NDF	negative dispersion fiber
NLIN	nonlinear interference noise
NLSE	nonlinear Schrödinger equation
OBP	optical back propagation
OBPF	optical back propagation fiber
OPC	optical phase conjugation
OSNR	optical signal-to-noise ratio
PDM	polarization division multiplexing
PMD	polarization mode dispersion

QAM	quadrature amplitude modulation
QPSK	quadrature phase shift keying
SPM	self-phase modulation
SSFS	split-step Fourier scheme
SSMF	standard single mode fiber
TF	transmission fiber
WDM	wavelength division multiplexing
XPM	cross-phase modulation

Contents

List of Figures

Chapter 1

Introduction

1.1 Introduction to fiber-optic communication systems

Fiber-optic communication systems are used to transmit datas from one point to another through lightwaves, whose frequency is very high ($\sim$ 200 THz). Compared to microwave communication systems, for which the typical frequency is about 1 GHz, the fiber optic communication systems have a much larger bandwidth because fibers can support the lightwave signals. Therefore, they have been widely used and advanced dramatically over the past 50 years, which has resulted in low cost and high bandwidth transmission. Fiber optics is now the back bone of internet and long distance telecommunication.

The evolution of fiber-optic communication systems traces back to 1960s, when a laser was invented that can be used as a coherent optical source of the transmission systems [1]. In 1966, optical fibers are considered to be the best candidate to guide

light and used as a transmission medium in the communication systems [2]. However, the high loss of fiber ($\sim$ 1000 dB/km) at that time was the main limitation of fiber to be utilized for transmission purposes. In 1970s, the fiber loss can be made less than 20 dB/km in the wavelength near 1 μm through a novel fabrication technique [3]. Also, GaAs semiconductor laser was investigated at the same time, which was a great enabler for the development of fiber-optic communications [4]. From 1975 to 2000, fiber-optic communication progressed four generations [5]. In the first generation, GaAs semiconductor laser was used as an optical source, whose wavelength was around 800 nm [4]. The transmission speed was 45 Mb/s and the repeater spacing could be increased to 10 km as compared to 1 km in coaxial systems [6]. The second generation began in 1980s, in which the fiber loss was 0.5 dB/km at the wavelength of 1.3 μm, and the bit rate was less than 100 Mb/s due to the dispersion of the multimode fibers [7]. The single mode fiber was introduced to solve this problem [8]. In the third generation, fibers operated at 1.5 μm was developed as the transmission fiber, which had a low loss ($\sim$ 0.2 dB/km) [9], but it had a large dispersion. By introducing the dispersion-shifted fiber (DSF), the zero chromatic dispersion (CD) was able to shift to 1.55 μm from 1.3 μm, which made it feasible to achieve both low loss and small dispersion of the transmission fiber [10]. To further increase the system capacity and transmission reach, the fourth generation of fiber-optic communication systems utilized the optical amplifier as well as wavelength-division multiplexing (WDM) [5]. The optical amplifier was used to compensate for fiber loss in the transmission link, and it could be used to enlarge the repeater spacing. In a WDM system, signals in different channels will be modulated on separate frequencies (or wavelengths) and launched to the fiber by a multiplexer at the transmitter, and then the signals propagated in

fibers simultaneously. The signals in different channels would be demultiplexed at the receiver side. As a result, the WDM scheme considerably increased the transmission capacity without using extra fibers, and it brought a new era to fiber-optic communication system . The bit rate could increase up to 10 Tb/s by 2001 [11].

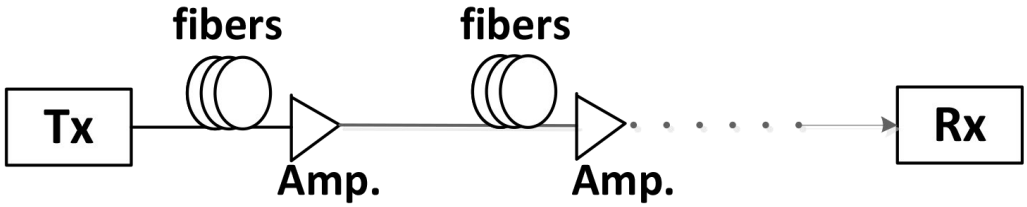

Figure 1.1: A typical fiber-optic communication system. TX: transmitter, RX: receiver.

A typical fiber-optic communication system includes a transmitter, a transmission link and a receiver, as shown in Fig. 1.1. The transmitter consisting of an optical source, electronic circuits, and a modulater, is used to modulate the electric signals into optical signals and launch the signals into the fiber links. The transmission link consists of transmission fibers and amplifiers; the transmission fibers are the medium to guide light. As the optical signal propagates down the fiber, it suffers losses due to Rayleigh scattering and absorption. To compensate for loss, optical amplifiers are introduced along the transmission line. The advantage of introducing lightwave as the carrier is its high frequency so that the transmission capacity can be significantly improved. The role of the receiver is to convert the optical signal back into electrical domain. The generic receiver includes a photodetector, electric circuits, and a demodulator. In the past decade, coherent receiver, converting the optical signals into electrical domain using homodyne or heterodyne technique, has drawn significant attention. The coherent detection technique makes it possible to

compensate for fiber distortions using high-speed digital signal processing (DSP), and it will be discussed further in subsection 1.3.

1.2 Impairments in fiber-optic links

1.2.1 Linear distortions

Chromatic dispersion (CD) is one of the major limitation factors in long-haul fiber-optic communication systems, which results in pulse broadening and inter-symbol interference (ISI) [12]. Therefore, it degrades the performance of the transmission system severely. When optical signals are launched into a single mode fiber, there is no intermodal dispersion. However, the optical pulses still broaden due to intra-modal dispersion. That is, different frequency components have different speeds in fibers, hence they arrive at different times leading to pulse broadening, as shown in Fig. 1.2.

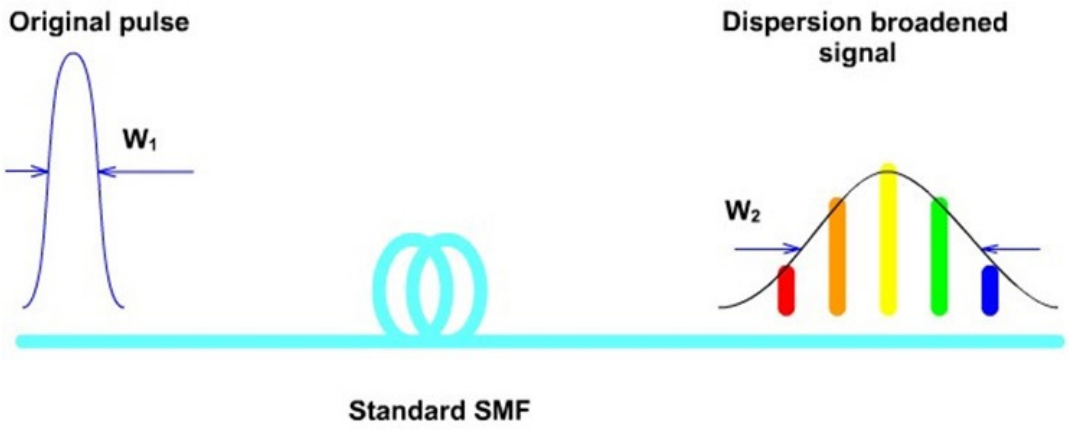

Figure 1.2: Pulse broadening due to dispersion.

To explain CD in more detail, let us consider a single-mode fiber of length L. The propagation delay T for a spectral component at frequency ω can be written as

$$T = \frac{L}{v_g}, \tag{1.1}$$

where v_g is the group velocity [13],

$$v_g = (d\beta/d\omega)^{-1}. \tag{1.2}$$

If the optical pulse has a spectral width of $\Delta\omega$, different spectral component will not arrive at the end of the fiber at the same time. The time difference is [14]

$$\Delta T = \frac{dT}{d\omega}\Delta\omega. \tag{1.3}$$

Plug Eqs. (1.1) and (1.2) into Eq. (1.3),

$$\Delta T = L\frac{d^2\beta}{d\omega^2}\Delta\omega = L\beta_2\Delta\omega, \tag{1.4}$$

where β_2 is defined as group velocity dispersion (GVD) parameter and equals to $d^2\beta/d\omega^2$. From Eq. (1.4), the extent of broadening is proportional to the spectral width $\Delta\omega$, fiber length L, and β_2.

In a polarization division multiplexing (PDM) transmission systems, another source of pulse broadening called polarization-mode dispersion (PMD) will exist [15–21]. In a PDM transmission system, the two polarization components have different group velocities, as a result the input pulse will be broadened, which could severely limits the performance of fiber-optic communication systems. In a fiber with constant

birefringence, the time delay between two polarization components can be written as

$$\Delta T = \left| \frac{L}{v_{gx}} - \frac{L}{v_{gy}} \right| = L|\beta_{1x} - \beta_{1y}|, \tag{1.5}$$

where β_1 is the inverse of group velocity,

$$\beta_{1r} = \frac{d\beta_r}{d\omega}, \quad r = x \text{ or } y. \tag{1.6}$$

In a real fiber, refractive index changes randomly due to stress, temperature and other environmental fluctuations. As a result, the propagation constants β_{1x} and β_{1y} change randomly as a function of propagation distance and time, which makes the delay ΔT to change randomly. However, β_{1x} and β_{1y} change over a time scale that is lower than the symbol period and therefore, it is possible to compensate for PMD using DSP in coherent communication systems.

1.2.2 Nonlinear impairments

When the launch power of the fiber-optic communication system is low, the fiber link can be roughly regarded as a linear medium, and the system performance can be improved by increasing the launch power due to the increase of signal-noise ratio (SNR). However, when the launch power is relatively high, the transmission quality of the fiber-optic communication systems will degrade by further increasing the launch power, due to the fiber nonlinearity. A typical relationship between launch power and bit error rate (BER) is shown in Fig. 1.3. When the launch power is less than P_1, the amplified spontaneous emission (ASE) is the main limitation in the transmission system, and the BER can be reduced by increasing the launch power. When the

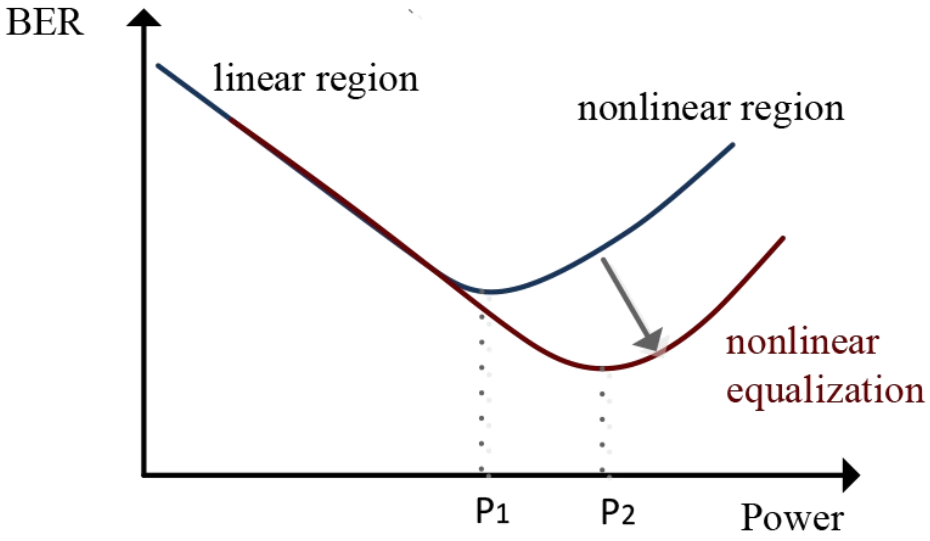

Figure 1.3: Typical relationship between launch power and BER in fiber-optic communication systems.

launch power is larger than P_1, the nonlinearity is dominant and it is the main factor to limit the system performance. By introducing a nonlinear equalizer, the nonlinear tolerance can be improved, a lower BER can be achieved, and the optimum power can be increased from P_1 to P_2 (see Fig. 1.3). The compensation techniques for fiber impairments will be discussed in Section 1.3.

Fiber nonlinearity originates from the Kerr effects, that is the refractive index increases with optical intensity [22, 23]. The refractive index is a function of launch power and can be written as [22]

$$n(\omega, P) = n_0(\omega) + n_2 \frac{P}{A_{eff}}, \tag{1.7}$$

where n_0 is the refractive index when the launch power is very low, n_2 is the nonlinear-index coefficient with typical value in the order of 2×10^{-20} m^2/W, P is the launch

power, and A_{eff} is the effective core area. As a result, the propagation constant β is also related to the light intensity and can be written as [22]

$$\beta(\omega, P) = \frac{2\pi}{\lambda} n(\omega, P) = \beta_0(\omega) + \gamma P, \tag{1.8}$$

where $\beta_0(\omega)$ is chromatic dispersion coefficient, and γ is the fiber nonlinear coefficient, which is

$$\gamma = \frac{2\pi n_2}{\lambda A_{eff}}. \tag{1.9}$$

The nonlinear effects will induce phase shift to the optical signal, which can be written as

$$\phi^{NL} = \int_0^L (\beta - \beta_0) dz = \int_0^L \gamma P(z) dz. \tag{1.10}$$

If fiber loss is considered,

$$P(z) = P_{in} \exp(-\alpha z), \tag{1.11}$$

where P_{in} is the input signal intensity, α is the fiber loss coefficient. Plug Eq. (1.11) into Eq. (1.10), the nonlinear phase shift can be obtained as

$$\phi_{NL} = \gamma P_{in} L_{eff}, \tag{1.12}$$

where L_{eff} is defined as the effective length

$$L_{eff} = \frac{1 - \exp(-\alpha L)}{\alpha}. \tag{1.13}$$

As an optical pulse propagates down an optical fiber, it interacts not only with the pulses of the same channel, but also with the pulses of the neighboring channels.

The nonlinear interaction among pulses of the same channel is known as intra-channel nonlinear effects [12, 22, 24]. The nonlinear interaction between pulses of different channels in WDM system is called inter-channel nonlinear effects [12, 22].

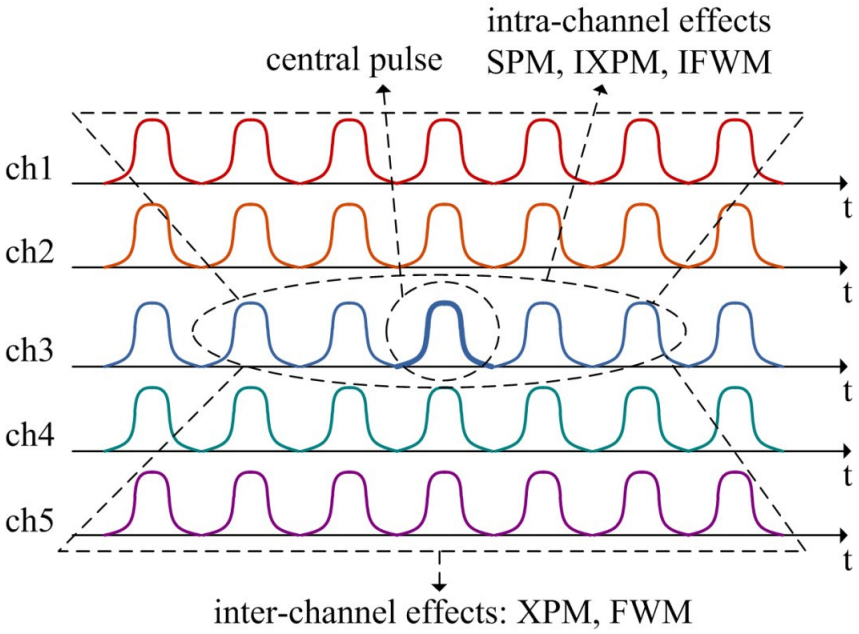

Figure 1.4: Illustration of the difference between intra-channel and inter-channel nonlinear effects.

Intra-channel nonlinear effects include self-phase modulation (SPM), intra-channel cross-phase modulation (IXPM) and intra-channel four wave mixing (IFWM). For the central pulse of channel 3 in Fig. 1.4, the change in refractive index due to the Kerr effect translates into a phase shift, so the signal phase is modulated by its own power distribution. This is known as SPM. If the central pulse interacts with the other pulses in channel 3, it will result in IXPM, which also brings in a phase shift of the central pulse. When two or more pulses of channel 3 interact nonlinearly, echo or ghost pulses are generated, which is called IFWM. In the case of IFWM, the nonlinear interaction between pulses centered at t_1, t_2, and t_3 leads to echo pulses at $t_1 + t_2 - t_3$

and $t_2 + t_3 - t_1$.

In WDM systems, the nonlinear interaction between pulses of different channels is called inter-channel nonlinear effects [12, 22]. The inter-channel nonlinear effects can be divided into two types: cross-phase modulation (XPM) and four-wave mixing (FWM). The phase of a signal in a channel is modulated not only by its channel power, but also by other channels, which is called XPM, and the phase shift of the jth channel can be written as

$$\phi_{NL}^{j} = \underbrace{\gamma P_{in,j} L_{eff}}_{\text{SPM}} + \underbrace{2\gamma L_{eff} \sum_{m \neq j} P_{in,m}}_{\text{XPM}}, \tag{1.14}$$

The second term of Eq. (1.14) refers to the phase shift brought out by XPM, and it is twice that from SPM. Nonlinear interactions between channels of center frequencies f_1, f_2, and f_3 results in a new frequency components at $f_1 + f_2 - f_3$ and $f_2 + f_3 - f_1$ which is known as FWM [25, 26]. The new frequency components generated through FWM act as noise on channels centered at $f_1 + f_2 - f_3$ and $f_2 + f_3 - f_1$.

Nonlinear interaction between signal and noise leads to nonlinear phase noise [27–31]. The signal instantaneous power fluctuates due to ASE noise and it is translated into phase shift due to Kerr nonlinear effect. Hence, the phase changes randomly which is known as nonlinear phase noise. In the absence of fiber dispersion, nonlinear phase noise could lead to significant performance degradation to the coherent fiber optic systems [27, 29]. However, in the presence of moderate to large dispersion, nonlinear phase noise is significantly reduced [28, 30].

Fiber optic system can be categorized into two types: (i) dispersion managed (DM) systems in which dispersion of transmission fiber is partially compensated by inline

dispersion compensating fibers (DCFs) and (ii) dispersion uncompensated (DU) systems in which the transmission fiber dispersion is compensated only at the transmitter or at the receiver in digital domain. Intra- and inter-channel nonlinear effective have attracted enormous research attention for decades. The intra-channel nonlinearity in DM fiber optic systems has been investigated by analytical techniques and numerical simulations [32–34]. For dispersion unmanaged systems, a perturbation theory has been used to study intra-channel nonlinear effects [35, 36]. The inter-channel nonlinear effects have been studied under different system configurations, such as in intensity modulation-direct detection (IM-DD) systems [37, 38], or in WDM systems [25, 39, 40]. The distortion caused by XPM leads to major impairments in WDM systems. Impact of XPM effects on the system performance have been studied taking into account its dependence on the number of WDM channels [41], its frequency response [42], and the intensity interference caused by XPM [43]. Also, theoretical models based on perturbation theory have been developed to study inter-channel nonlinear effects [44–46]. The properties of nonlinear noise have been studied by simulations [47, 48]. The capacity bound of fiber optic communication systems in presence of nonlinear effect has also been studied and the results show that the capacity increases with signal power in the linear regime, but when the signal power is very large, capacity decreases due to nonlinear noise caused by XPM. [49, 50]. Recently, a Gaussian-noise (GN) based model has been reported [51–53] for DU fiber optic systems. The accuracy of the GN model has been validated by experiments [54]. Also, in fiber-optic systems with large pre-dispersion, the nonlinear distortion behaves as decoupled modes in frequency domain [55].

1.3 Compensation techniques for fiber dispersive and nonlinear effects

Unlike direction detection in the receiver side of fiber-optic communication systems, coherent detection technique makes it possible to obtain both the amplitude and phase information of the complex signals. In a coherent receiver, the output signal from the fiber optic link and the continuous wave (CW) signal from a local oscillator are mixed together in a way such that the in-phase and quadrature components of information signal can be detected using photo diodes. As a result, compensation for distorted signals at the receiver side using DSP have advanced significantly in the past decades.

Various schemes based on DSP were proposed to compensate for the distortion due to the interplay of dispersion and nonlinearities in fibers. The commonly used technique to compensate for fiber impairment is digital back propagation (DBP) [56, 57]. The basic idea of DBP is as follows: Let the output of optical signal go into the DSP unit. Virtual fibers with the loss, dispersive and nonlinear coefficient the opposite sign of the transmission fiber are realized on the DSP unit, so as to undo the distortion due to the transmission links. In DBP, nonlinear Schrödinger equation (NLSE), which is used to describe optical pulse propagating in fibers, are solved numerically using split-step Fourier scheme (SSFS). In the absence of noise, DBP can fully compensate for both the dispersion and nonlinearity if the step size is small enough. In practice, the noise exists and the noise-nonlinearity interaction cannot be compensated by DBP. Also, the small step size will increase the computational burden, although it can increase the DBP performance. Li *et al.* applied DBP in WDM systems by

introducing finite impulse response (FIR) filters for the dispersion step and a parallel architecture for real-time implementation [56]. Nonlinearity compensation can be achieved by using two samples per symbol hardware sampling with up-sampling in DSP. A system performance of 10×10 Gbit/s binary-phase-shift-keying (BPSK) signals with 20 GHz channel spacing over 800 km has been demonstrated. Ip and Kahn [57] proposed a noniterative asymmetric SSFS to solve the inverse NLSE, which reduced the computational complexity. Their simulation results showed that it is a reasonable compromise to set the step size equaling to span length when the symbol rate is 10 Gsymbol/s. Mateo *et al.* analyzed the impact of XPM and FWM via DBP [58]. In their work, XPM is compensated using coupled NLSE, and XPM+FWM are compensated using total field NLSE. The results showed that the FWM is weak relative to XPM, and DBP with coupled NLSE is sufficient to compensate for most nonlinearities in long-haul systems with large accumulated dispersion. Mateo and Li investigated an enhanced coupled NLSE to implement DBP for fully compensating XPM and partially compensating FWM. In their work, the increased computational cost is negligible as compared to that compensates for XPM only, and the scheme is 20 times more efficient in terms of computational cost as compared to full FWM compensation scheme [59]. Mateo *et al.* proposed an advanced split-step method for DBP including the effect of the inter-channel walk off in the nonlinear step to compensate for XPM. This scheme reduced the computational cost by a factor of 4 [60]. In Ref. [61], Du and Lowery presented an improved SSFS in DBP to compensate for fiber impairment in a PDM-WDM systems. Manakov equations are used for DBP. In the improved SSFS, new terms are added in the nonlinear step to deal with inter-polarization mixing effects, and the effect of inter-channel walk off is included. Zhu

and Li proposed an efficient DBP algorithm for DM transmission systems, in which the nonlinearity of many spans can be folded into one span. As a result, computational cost can be reduced significantly with negligible penalty [62]. In Ref. [63], Zhu and Li proposed a dispersion-folded DBP in DM fiber-optic links. Their experimental results show that the computational cost in a single channel system can be reduced by 43, and the simulation results show that the computational cost in WDM can be reduced by 39. In Ref. [64], Mateo *et al.* reported an improved SSFS for DBP in PDM-WDM transmission systems. The governing equation used for DBP are derived from Manakov equation. In this scheme, DBP can be implemented in a channel by channel basis by including inter-channel nonlinear terms and new terms to calculate the inter-polarization mixing effects.

DBP is a universal technique to compensate for deterministic fiber distortions, which is based on solving NLSE numerically. In optical links, dispersion is considered to be the dominant distortions, and nonlinearity can be treated as a small perturbation. Therefore, analytical or semi-analytical models to solve NLSE can be used in digital domain to undo the fiber impairments based on perturbation theory, and it can substantially reduce the computational complexity. Mecozzi *et al.* analyzed intrachannel nonlinearities of short optical pulses transmitting in dispersion compensated transmission systems and they obtained closed-form expressions for the echo pulses and the timing jitter based on a perturbative method [35]. In Ref. [44], Kumar and Yang investigated a second-order perturbation technique for nonlinear effects in a fiber-optic transmission system. They found that if the dispersion distance is much smaller than the nonlinear distance, the first order perturbation technique works. However, if the dispersion length equals or is larger than the nonlinear distance, the

second-order perturbation technique can obtain a good result as compared to the numerical results. Poggiolini *et al.* [51] and Carena *et al.* [52] have modeled the nonlinear interference noise (NLIN) in dispersion-uncompensated transmission systems as excess additive Gaussian noise and its variance is calculated using a perturbation technique. A semi-analytical expression is obtained and shown to provide good performance. Dar *et al.* have studied the properties of NLIN in a DU transmission system with large accumulated dispersion and found that the NLIN is not additive Gaussian, but it depends on the transmitted data [47]. Mecozzi and Essiambre proposed a general first-order perturbation theory of pulse propagation in fibers taking into account the amplification and nonlinear effects. In their work, both intra- and inter- channel nonlinear effects are considered. This scheme is in a good agreement as compared to the numerical simulation results [49]. In Ref. [65], Tao *et al.* have developed a multiplier-free predistortion algorithm operating at the symbol rate to compensate for the intrachannel nonlinearity. They validated the algorithm by experiment and found that it is comparable with the back propagation method, which has a higher computational cost. Gao *et al.* demonstrated that the complexity can be reduced by a factor up to 6.8 by combining symmetric electronic dispersion compensation and root-raised-cosine pulse shaping [66]. In Ref. [67], Gao *et al.* reduced the number of multiplications by jointly using perturbation-based nonlinear pre compensation at the transmitter side and selective perturbation-based nonlinear post compensation at the receiver side.

Also, signal distortions due to fibers can be compensated using optical techniques. DCF and fiber Bragg grating (FBG) can be used to undo the dispersion in the transmission fiber [68, 69]. In order to compensate for both the linear and the nonlinear

effects, mid-point optical phase conjugation (OPC) are utilized to obtain the conjugate of the transmission signals in the middle point. Then, the fiber dispersion and nonlinearity can be compensated at the second half of the transmission link, if the power profile is symmetric [70, 71]. However, it is hard to realize the symmetric power profile, which severely limits the performance of mid-OPC scheme. We note that a scheme in which the OPC in the receiver is followed by the DBP has been investigated before [72]. Recently, optical back propagation (OBP) techniques have been developed to compensate for fiber dispersion and nonlinearities [73, 74]. The basic idea of OBP is to solve the NLSE in a similar way of SSFS using optical devices with the opposite signs of the loss, dispersive and nonlinear coefficients at the receiver side. The main difficulty for OBP is the absence of the negative nonlinear coefficient fibers. In Ref. [74], Kumar and Yang proposed a technique to realize an effective negative nonlinear coefficient using two highly nonlinear fibers, which can be used to implement OBP.

1.4 Main contributions of the thesis

This thesis mainly focuses on the modeling of signal propagation in fiber-optic links and compensation of fiber dispersive and nonlinear effects using digital and optical techniques.

To study signal propagation in fiber-optic communication systems, the NLSE needs to be solved numerically. We investigated and compared various methods for solving the NLSE. We developed a novel scheme by combining a local error method with a minimum area mismatch method, which reduces the computational cost by a factor up to 5.8 as compared with existing NLSE solvers.

With the development of DSP techniques, DBP has been widely applied to compensate for fiber dispersion and nonlinearity. Currently, the performance and applications of DBP are limited due to its high computational cost. We proposed a simplified DBP algorithm by optimizing the DBP step sizes. The proposed scheme increases the system reach from 4300 km to 5200 km when the number of DBP steps is two.

We also studied OBP schemes to compensate for fiber dispersion and nonlinearities. One OBP module consists of high-dispersion fibers (HDFs) and highly nonlinear fibers (HNLFs). The fiber dispersion is compensated using the HDFs, and the nonlinearity is compensated using the HNLFs and HDFs. The simulation results show that this OBP scheme outperforms the schemes using midpoint OPC and DBP with the same step size. We further improved the OBP performance by designing the OBP module based on the minimum area mismatch method. Another OBP scheme is developed using dispersion-decreasing fibers (DDFs) and optical amplifiers, which fully compensates for the nonlinear effects. Numerical simulations show that the proposed OBP scheme can enhance the system reach by 54% as compared to DBP.

Also, we derived an exact solution of NLSE for impulse input in the presence of high pre-dispersion. We have obtained the nonlinear eigenmodes of the highly pre-dispersed fiber-optic system which may be useful for the description of signal propagation, and signal and noise interaction.

The research work has resulted in the following publications:

Journal papers:

1. J. Shao and S. Kumar,"Optical back propagation for fiber-optic communications

using optical phase conjugation at the receive," Optics Letters, vol. 37, issue 15, pp. 3012-3014, (2012).

2. S. Kumar and J. Shao, "Optical back propagation with optimal step size for fiber optic transmission systems," Photonics Technology Letters, vol. 25, no. 5, 523-526, (2013).
3. X. Liang, S. Kumar, and J. Shao, "Ideal optical backpropagation of scalar NLSE using dispersion-decreasing fibers for WDM transmission," Optics Express, vol. 21, no. 23, pp. 28668-28675, (2013).
4. J. Shao, S. Kumar, and X. Liang, "Digital back propagation with optimal step size for polarization multiplexed transmission," *IEEE* Photonics Technology Letters, vol. 25, no. 23, pp. 2327-2330, (2013).
5. J. Shao, X. Liang, and S. Kumar, "Comparison of split-step Fourier schemes for simulating fiber optic communication systems," *IEEE* Photonics Journal, vol. 6, no. 4, pp. 7200515, (2014).
6. X. Liang, S. Kumar, J. Shao, M. Malekiha, and D. V. Plant, "Digital compensation of cross-phase modulation distortions using perturbation technique for dispersion-managed fiber-optic systems," Optics Express, vol. 22, no. 17, pp. 20634-20645, (2014).
7. S. Kumar, J. Shao, and X. Liang, "Impulse response of nonlinear Schrödinger equation and its implications for pre-dispersed fiber-optic communication systems," Optics Express, vol. 22, no. 26, pp. 32282-32292, (2014).

Conference papers:

1. S. Kumar, S.N. Shahi and J. Shao, "Analysis and compensation of nonlinear impairments in fiber optic systems," invited talk, international conference on optical engineering (ICOE-12), Belgaum, India, 2012.
2. J. Shao, X. Liang, and S. Kumar, "An efficient scheme of split-step Fourier method for fiber optic communication systems," in Proc. of SPIE, Photonics North (Montreal Canada, 2014), paper 928806.
3. S. Kumar, X. Liang and J. Shao, "Digital and optical compensation of fiber nonlinear impairments in coherent fiber optic systems", *invited paper*, Energy materials and nanotechnology meeting on Optoelectronics (Beijing China, 2015).

Book chapter:

X. Liang, J. Shao, and S. Kumar, "Optical back propagation for compensation of dispersion and nonlinearity in fiber-optic transmission systems", in the book *Odyssey of Light in Nonlinear Optical Fibers: Theory and Applications*, K. Porsezian and R. Ganapathy, ed., CRC Press, 2015. (in press)

Chapter 2

Comparison of split-Step Fourier schemes for simulating fiber optic communication systems

2.1 Introduction

The SSFS is widely used to solve the NLSE, which describes the evolution of optical field envelope in optical fibers[22, 75–77]. In SSFS, dispersion and nonlinearity operators are assumed to act independently over a small step size. A pair of FFTs is used to solve the NLSE when there is only dispersion and/or loss and then, a phase shift is introduced to account for the nonlinear effects when the dispersion is absent. Recently DBP has drawn significant attention to mitigate the linear and nonlinear impairments [56, 57, 60, 61, 78–80]. In DBP, the NLSE is solved in digital domain with the reversed signs of dispersion, loss and nonlinear coefficients. Therefore, efficient algorithms to solve the NLSE have become even more important.

In solving the NLSE, smaller step size leads to results closer to the exact solution, but it takes more computational time. Thus, there is a trade-off between the accuracy and computational cost. The objective of this chapter is to compare the accuracy of various SSFSs for the given computational cost. In the conventional approach [22], the linear operator, $\hat{D}$ takes into the account of dispersive and loss effects while the nonlinear operator, $\hat{N}$ takes into account only the Kerr effect. Instead, it is possible to include the loss effect along with the Kerr effect in $\hat{N}$ and we find that this scheme has higher computational efficiency than the conventional approach. It is because the path-averaged nonlinear phase shift is introduced which takes into account the power attenuation due to fiber loss within the step while in the conventional scheme, nonlinear phase shift is determined by the power at the beginning or the middle of the step. If the losses were to vary with frequency, introducing losses into the nonlinear operator would not be a simple task. For optical waveguides, the losses change across the relevant spectrum of the optical signal and hence, this scheme is not suitable. However, for optical fibers, over the simulation bandwidth, the loss is nearly constant.

In the presence of fiber loss, the uniform step size is not optimum since the nonlinear phase shift accumulated in each step decreases exponentially with distance due to loss. The step size distribution can be optimized using the local error method [77] or minimum aera mismatch (MAM) [81–83] or the combination of both. Local error method is a powerful technique to solve the NLSE, in which the step size is adaptively chosen so as to bound the relative local error. In MAM, the step size distribution is optimized by minimizing the area mismatch between the exponential curve and its stepwise approximation. In this chapter, a scheme that combines the merits of local

error method and MAM is introduced [84]. Using this approach, the computational efficiency can be improved by a factor 2.5 to 5, and a factor 1.6 to 3.1 as compared to the conventional and local error methods, respectively, when the global error is in the range of practical interest.

2.2 Theory

2.2.1 Principle of the Split-Step Fourier scheme (SSFS)

The NLSE is used to describe the optical pulse propagation in fibers. When the pulse width is large ($>$ 5 ps) and the higher order dispersion and the delayed nonlinear response are neglected, the NLSE can be written as

$$\frac{\partial A}{\partial z} = -\frac{\alpha}{2}A - \frac{i}{2}\beta_2\frac{\partial^2 A}{\partial T^2} + i\gamma|A|^2 A, \tag{2.1}$$

where A is the complex field envelope, α, β_2, and γ are loss coefficient, second order dispersion parameter, and nonlinear coefficient. Eq. (2.1) has an analytical soliton solution for a specific case when $\beta_2 < 0$. However, for most cases, it has to be solved numerically. SSFS is extensively used to solve the NLSE numerically. To explain the SSFS clearly, it's convenient to write Eq. (2.1) in the following form:

$$\frac{\partial A}{\partial z} = \left[\hat{D} + \hat{N}(A)\right] A. \tag{2.2}$$

Here, $\hat{D}$ and $\hat{N}$ are the operators that account for dispersion and nonlinearity, respectively. If we neglect the fiber loss,

$$\hat{D} = -\frac{i}{2}\beta_2\frac{\partial^2}{\partial T^2}, \quad \hat{N}(A) = i\gamma|A|^2. \tag{2.3}$$

The cases when the fiber loss is taken into account will be discussed later. In fibers, dispersion and nonlinearity act simultaneously, but they can be roughly treated as being independent in a very small distance. If the unsymmetric split-step scheme is employed, Eq. (2.2) has an approximate solution as [22]

$$A(z+h,T) \approx \exp(h\hat{D}) \exp\left(\int_z^{z+h} \hat{N}(z')dz'\right) A(z,T). \tag{2.4}$$

Fig. 2.1 illustrates the unsymmetric SSFS if the length of fiber is L. This technique can be summarized as follows:

(i) Initial field $A(0,t)$ is known. First, fiber dispersion ($\hat{D}$) is ignored. The NLSE is analytically solved with the initial signal $A(0,t)$ and the output of a lossless, nonlinear fiber $A^{nl}(h,t)$ can be calculated analytically.

(ii) Next, the nonlinear effects ($\hat{N}$) is ignored, and the output of a lossless, linear fiber is calculated using the Fourier transformation technique, and $A(h,t)$ can be obtained.

(iii) $A(2h,t)$ is calculated by repeating steps (i) and (ii) with $A(h,t)$ as the initial condition.

This process is repeated until $z = L$. The step size h should be chosen sufficiently small so that the absolute value of the nonlinear phase shift accumulated over a distance h should be much smaller than π.

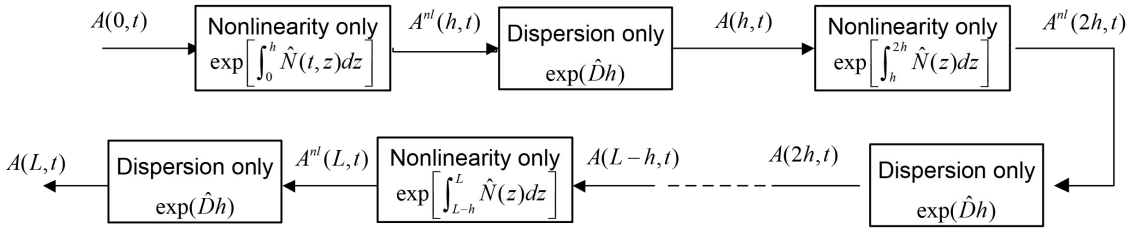

Figure 2.1: Unsymmetric split-step Fourier scheme for forward propagation.

In the symmetric scheme for a single step, Eq. (2.2) can be approximated as

$$A(z+h,T) \approx \exp\left(\frac{h}{2}\hat{D}\right) \exp\left(\int_{z}^{z+h} \hat{N}(z')dz'\right) \exp\left(\frac{h}{2}\hat{D}\right) A(z,T). \tag{2.5}$$

Eq. (2.4) and Eq. (2.5) are not the exact solutions of Eq. (2.2) since $\hat{D}$ and $\hat{N}$ don't commute. Using Baker-Hausdorff formular [85], the dominant error term of Eq. (2.4) is of the order h^2, and the leading error of Eq. (2.5) is of the order h^3. Since the symmetric scheme is more accurate than the unsymmetric one, it has been utilized in the numerical calculation throughout this chapter. The operation $\exp\left(h\hat{D}/2\right) A(z,T)$ can be realized using a pair of FFTs and hence, the computational cost of a single-step symmetric scheme is approximately twice that of the unsymmetric scheme. However, after multiple steps, the computational cost is approximately the same. This can be seen by dividing the fiber length into m steps and the optical field envelope after m steps is obtained by concatenation of operators in Eq. (2.5), [22]

$$\begin{aligned} A(z+mh,T) \cong \exp\left(\frac{h}{2}\hat{D}\right) \exp\left(ih\gamma\left|A(z+(m-1)h,T)\right|^2\right) \exp\left(h\hat{D}\right) \\ \times \exp\left(ih\gamma\left|A(z+(m-2)h,T)\right|^2\right) ... \times \exp\left(h\hat{D}\right) \\ \times \exp\left(ih\gamma\left|A(z,T)\right|^2\right) \exp\left(\frac{h}{2}\hat{D}\right) A(z,T). \end{aligned} \tag{2.6}$$

To evaluate Eq. (2.6), it requires only $(m+1)$ FFT pairs since the dispersion operators of the neighboring steps are combined while the unsymmetric scheme requires m FFT pairs. Throughout this chapter, the dispersion operators of the neighboring steps are combined whenever it is feasible, which reduces the computational cost by a factor of 2.

When the fiber loss is included, there are two options. It could be included with dispersion or with nonlinearity. For the first case (Sections 2.2.2 and 2.2.4), Eq. (2.3) is modified as

$$\hat{D}_1 = -\frac{i}{2}\beta_2\frac{\partial^2}{\partial T^2} - \frac{\alpha}{2}, \quad \hat{N}_1(A) = i\gamma|A|^2. \tag{2.7}$$

For the latter case, we have (Sections 2.2.3 and 2.2.5),

$$\hat{D}_2 = -\frac{i}{2}\beta_2\frac{\partial^2}{\partial T^2}, \tag{2.8}$$

$$\hat{N}_2(A) = i\gamma|A|^2 - \frac{\alpha}{2}. \tag{2.9}$$

The efficiency of the scheme depends on whether the loss is included with dispersion or nonlinearity. Also, the step size distribution can affect the scheme performance. In the following subsections, several schemes of SSFS to solve the NLSE will be reviewed and a scheme based on MAM and local error method will be introduced.

2.2.2 Uniform step size, loss with dispersion (Scheme Ia)

The simplest way to realize the SSFS is to introduce uniform step size, in which the accuracy can be improved by selecting a smaller step size. In scheme Ia, the loss is combined with dispersion (see Eq. (2.7)). Using the rectangular rule for the integrals

in Eqs. (2.4) and (2.5), they become

$$A(z+h,T) \approx \exp\left(h\hat{D}_1\right) \exp\left(ih\gamma \left|A(z,T)\right|^2\right) A(z,T), \tag{2.10}$$

$$A(z+h,T) \approx \exp\left(\frac{h\hat{D}_1}{2}\right) \exp\left(ih\gamma \left|A_{l1}\left(z+\frac{h}{2},T\right)\right|^2\right) \exp\left(\frac{h\hat{D}_1}{2}\right) A(z,T), \tag{2.11}$$

where $A_{l1}(z+h/2,T) = \exp\left(h\hat{D}_1/2\right) A(z,T)$.

For a certain nonlinear phase rotation ϕ^{NL}, the step size is determined by

$$h = \frac{\phi^{NL}}{\gamma P_{peak}}, \tag{2.12}$$

where P_{peak} is the peak power of the optical signal launched to a fiber span. The same step size is used in the following steps within the span.

Using the Baker-Hausdorff formular, the leading error term is found to be (see Appendix A)

$$\begin{aligned} E_I = \Bigg(&\frac{i}{24}\beta_2\gamma^2|A_{l1}|^4\frac{\partial^2}{\partial T^2} - \frac{i}{12}\beta_2\gamma^2|A_{l1}|^2\frac{\partial^2}{\partial T^2}|A_{l1}|^2 - \frac{i}{48}\beta_2^2\gamma\frac{\partial^2}{\partial T^2}|A_{l1}|^2\frac{\partial^2}{\partial T^2} \\ &+ \frac{i}{96}\beta_2^2\gamma\frac{\partial^4}{\partial T^4}|A_{l1}|^2 + \frac{i}{96}\beta_2^2\gamma|A_{l1}|^2\frac{\partial^4}{\partial T^4} + \frac{i}{24}\beta_2\gamma^2\frac{\partial^2}{\partial T^2}|A_{l1}|^4\Bigg) h^3 A(0,T). \end{aligned} \tag{2.13}$$

2.2.3 Uniform step size, loss with nonlinearity (Scheme IIa)

This scheme is almost the same as scheme Ia except that the fiber loss is included in $\hat{N}$ (see Eqs. (2.8) and (2.9)). Let us first ignore the operator $\hat{D}$ in Eq. (2.2). Using Eq. (2.9) for $\hat{N}$, we find

$$\frac{dA}{dz} = \left(i\gamma|A|^2 - \frac{\alpha}{2}\right) A. \tag{2.14}$$

Let

$$A = |A|e^{i\theta}. \tag{2.15}$$

Substituting Eq. (2.15) in Eq. (2.14) and separating the real and imaginary parts, we find

$$\frac{d|A|}{dz} = -\frac{\alpha}{2}|A|, \tag{2.16}$$

$$\frac{d\theta}{dz} = \gamma|A|^2. \tag{2.17}$$

Solving Eqs. (2.16) and (2.17), we obtain

$$A(z+h,T) = \exp\left(-\frac{\alpha}{2}h + i\gamma h_{eff}|A(z,T)|^2\right)A(z,T), \tag{2.18}$$

where

$$h_{eff} = \frac{1-\exp(-\alpha h)}{\alpha}. \tag{2.19}$$

Therefore, Eqs. (2.4) and (2.5) are modified as

$$A(z+h,T) \approx \exp\left(h\hat{D}_2\right)\exp\left(-\frac{\alpha}{2}h + i\gamma h_{eff}|A(z,T)|^2\right)A(z,T), \tag{2.20}$$

$$A(z+h,T) \approx \exp\left(\frac{h}{2}\hat{D}_2\right)\exp\left(-\frac{\alpha}{2}h + i\gamma h_{eff}\left|A_{l2}\left(z+\frac{h}{2},T\right)\right|^2\right)\exp\left(\frac{h}{2}\hat{D}_2\right)A(z,T), \tag{2.21}$$

where $A_{l2}\left(z+h/2,T\right) = \exp\left(h\hat{D}_2/2\right)A(z,T)$.

For this scheme, the leading error is found to be (Appendix A),

$$E_{II} = \left(\frac{i}{24} h_{eff} \beta_2 \gamma^2 |A_{l2}|^4 \frac{\partial^2}{\partial T^2} - \frac{i}{12} h_{eff} \beta_2 \gamma^2 |A_{l2}|^2 \frac{\partial^2}{\partial T^2} |A_{l2}|^2 - \frac{i}{48} h \beta_2^2 \gamma \frac{\partial^2}{\partial T^2} |A_{l2}|^2 \frac{\partial^2}{\partial T^2} + \frac{i}{96} h \beta_2^2 \gamma \frac{\partial^4}{\partial T^4} |A_{l2}|^2 + \frac{i}{96} h \beta_2^2 \gamma |A_{l2}|^2 \frac{\partial^4}{\partial T^4} + \frac{i}{24} h_{eff} \beta_2 \gamma^2 \frac{\partial^2}{\partial T^2} |A_{l2}|^4 \right) h h_{eff} A(0, T). \tag{2.22}$$

As it will be shown later, given the same step size, the performance of the scheme when loss is clubbed with nonlinearity is better than that when loss is with dispersion, especially when the field change due to loss within the interval $[z, z + h]$ is larger than that due to dispersion. This is because the operator $\hat{N}_2$ in Eq. (2.21) represents the mean nonlinear phase shift in the interval $[z, z + h]$ taking into account the power loss in that interval. In contrast, the operator $\hat{N}_1$ in Eqs. (2.10) or (2.11) includes only the power $|A(z, T)|^2$ at the beginning or the middle of the step and it ignores the nonlinear phase variations within the step due to fiber loss. Although it is possible to set up an iterative procedure to approximate the integrals in Eqs. (2.4) and (2.5) instead of the rectangular rule [22], we found that the computational efficiency (computational cost for the given accuracy) is lower for the schemes based on the iterative procedure.

2.2.4 Variable step size, loss with dispersion (Scheme Ib)

The disadvantage of scheme Ia is that the nonlinear phase accumulated over a step decreases with distance due to fiber loss and the step size determined by the fiber launch power (see Eq. (2.12)) is too small for steps closer to the end of the span. If we ignore the pulse broadening due to dispersion, the peak power decreases exponentially

with distance. So, Eq. (2.12) is modified as

$$h_{m+1} = \frac{\phi^{NL}}{\gamma P_{peak} e^{-\alpha z_m}}, \quad m = 0, 1, 2, ... \tag{2.23}$$

where h_m is the step size at z_m, $z_0 = 0$ and $z_m = \sum_{k=1}^{m} h_k$. In this scheme, loss is combined with dispersion and, $\hat{D}$ and $\hat{N}$ are given by Eqs. (2.7).

2.2.5 Variable step size, loss with nonlinearity (Scheme IIb)

In this scheme, the selection of step size is the same as that of scheme Ib. In each step, loss is combined with nonlinearity, and $\hat{D}$ and $\hat{N}$ operators are given by Eqs. (2.8) and (2.9), respectively. This scheme brings both the advantages of loss with nonlinearity and an efficient step size distribution.

2.2.6 Local-Error method (scheme III))

The method developed in Ref. [77] is summarized as follows. Suppose the field A at z is known. The field at $z + 2h$ can be obtained using Eq. (2.5) as

$$A_c(z+2h) = \exp\left(h\hat{D}_1\right) \exp\left(\int_z^{z+2h} \hat{N}_1(z')dz'\right) \exp\left(h\hat{D}_1\right) A(z) = A_{exact}(z+2h) + e_1. \tag{2.24}$$

For the symmetric SSFS, the error e_1 is of the order $(2h)^3$ and hence, Eq. (2.24) may be written as

$$A_c(z+2h) = A_{exact}(z+2h) + C\,(2h)^3 + O\left(h^4\right), \tag{2.25}$$

where $A_c(z+2h)$ and $A_{exact}(z+2h)$ represent the coarse and exact solutions at $z+2h$, respectively, and C is a constant. The solution at $z + 2h$ can also be obtained by

using Eq. (2.5) twice with a step size of h, which we call the fine solution A_f,

$$\begin{aligned} A_f(z+2h) =& \exp\left(\frac{h}{2}\hat{D}_1\right)\exp\left(\int_{z+h}^{z+2h}\hat{N}_1(z')dz'\right)\exp\left(h\hat{D}_1\right)\exp\left(\int_{z}^{z+h}\hat{N}_1(z')dz'\right)\exp\left(\frac{h}{2}\hat{D}_1\right)A(z) \\ =& A_{exact}(z+2h)+e_2, \end{aligned} \tag{2.26}$$

where the error e_2 is of the order $2h^3$. Eq. (2.26) may be rewritten as

$$A_f(z+2h) = A_{exact}(z+2h) + 2Ch^3 + O\left(h^4\right). \tag{2.27}$$

By taking appropriate linear combination of A_c and A_f, the term proportional to h^3 can be eliminated so that the leading order error is $O\left(h^4\right)$, i.e.,

$$A_4(z+2h) = \frac{4}{3}A_f(z+2h) - \frac{1}{3}A_c(z+2h) = A_{exact}(z+2h) + O\left(h^4\right). \tag{2.28}$$

$A_4(z+2h)$ is the solution at $z+2h$ with a higher accuracy and used as the input of the next step. The local error in the coarse solution relative to the fine solution is a measure of the relative local error, defined as

$$e = \frac{\|A_f(z+2h) - A_c(z+2h)\|^2}{\|A_f(z+2h)\|^2}, \tag{2.29}$$

and $\|\cdot\|$ is the norm that equals to $\left(\int|\cdot|^2dt\right)^{1/2}$. The main principle of this method is that, given a target local error e_{target}, if the current relative local error is larger than the target error, the next step size should be reduced accordingly and vice versa. Although the local-error method introduces additional computational cost

while calculating the local error, it's still a very efficient method to control the local error in a certain range, especially when the target global error is very small.

2.2.7 MAM combined with local-error method (scheme IV)

In order to further increase the efficiency, we develop a scheme by roughly bounding the local error of the first step, fixing the total number of steps M per span, and then using an optimal distribution of the dispersion operator and nonlinear operator in SSFS [84]. The optimal step size distribution has an elegant feature that the local error within a fiber span has a relatively less variance, so that the local error of the first step is a rough estimate of those of the following steps.

Before describing this scheme in detail, the principle and technique to optimize the $\hat{D}$ and $\hat{N}$ operator will be presented. To explain the method more clearly, it is better to transform the NLSE into a lossless form by the transformation

$$A(z,T) = e^{-\alpha z/2}U(z,T) \tag{2.30}$$

to obtain

$$\frac{\partial U}{\partial z} = -\frac{i}{2}\beta_2\frac{\partial^2 U}{\partial T^2} + i\gamma'|U|^2U, \tag{2.31}$$

where

$$\gamma' = \gamma\exp(-\alpha z). \tag{2.32}$$

γ' is the effective nonlinear coefficient that exponentially decreases with the distance. In the numerical methods like SSFS, the efficient way is to divide the fiber into several segments with fixed dispersion and effective nonlinear coefficients. As a result, the effective nonlinear coefficient is an approximated stepwise nonlinearity-decreasing

curve instead of an ideal exponential one. It is easy to see from Fig. 2.2(a) that because of the limited number of steps, there is a mismatch between the area under the exponential curve (solid line) and its stepwise approximation (dashed line) and the total absolute area mismatch is $\chi = \sum_{j=1}^{3}(A_j + A_j')$. If the area mismatch is minimized, the stepwise curve is expected to provide the closest approximation to the ideal exponential curve. A similar idea was investigated in the context of soliton communications to approximate the exponentially decreasing dispersion profile by stepwise decreasing profile with an additional constraint of soliton average condition [82]. If the total number of steps M is sufficiently large, these two curves will almost coincide. Define the nonlinear multiplication factor K_j, $j = 1, 2, .., M$, for each step, and the stepwise effective nonlinear coefficient is

$$\gamma_j' = K_j \gamma. \tag{2.33}$$

Fig. 2.2(a) shows the ideal exponential curve and its stepwise approximation (K_j) as a function of distance for $M = 3$, and Fig. 2.2(b) shows a more general case for the kth step. The split-step algorithm may be written as

$$U(z + l_j) = \exp\left(\frac{l_j}{2}\hat{D}_2\right) \exp\left(iK_j\gamma \left|U_l\left(z + \frac{l_j}{2}\right)\right|^2 l_j\right) \exp\left(\frac{l_j}{2}\hat{D}_2\right) U(z), \tag{2.34}$$

where $U_l\left(z + l_j/2\right) = \exp\left(l_j\hat{D}_2/2\right) \cdot U(z)$. We have $2M - 1$ adjustable parameters, namely, K_1, K_2, ... ,K_M and l_1, l_2, ... , l_{M-1}. The parameters could be so chosen that the global error is minimum. Alternatively, these parameters can be determined using the MAM technique [81–83]. In Section 2.3, it will be shown that the optimum step size determined using the minimum area mismatch technique minimizes the global

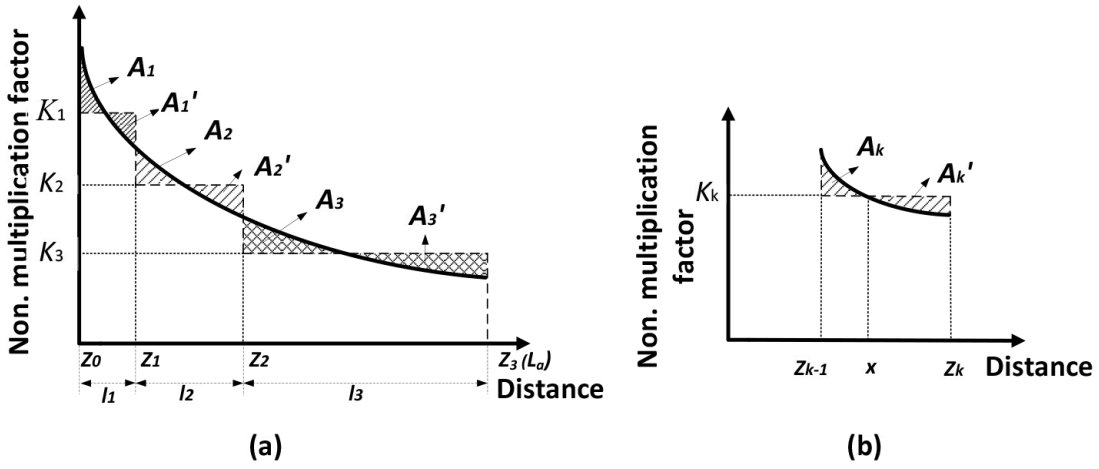

Figure 2.2: Stepwise approximation of the effective nonlinear coefficient. (a) The case when the number of steps per span $M = 3$. (b) The general case. A_j and A'_j denote area mismatch of the jth section.

error, for the case of $M = 2$. In Fig. 2.2(a), the absolute area mismatch between the area under the ideal exponential curve (solid line) and its stepwise approximation (dashed line) is $\chi = \sum_{j=1}^{3} \left(A_j + A'_j\right)$ with $A_j > 0$ and $A'_j > 0$. l_j and K_j are so chosen that the total area under the exponential curve should be the same as that under its stepwise approximation curve and the area mismatch χ should be minimum. So, we have

$$\int_0^{L_a} \exp(-\alpha z) dz = \sum_{j=1}^{M} K_j l_j. \tag{2.35}$$

Eq. (2.35) states that the total nonlinear phase shift accumulated over a span of length L_a should be equal to the sum of the nonlinear phase shifts in each step l_j. This is an optimization problem with $2M-2$ parameters. The number of parameters can be reduced by a factor of 2 if we impose a constraint that K_j is the mean of

exponential function in the segment l_j, i.e.,

$$K_j = \frac{1}{l_j} \int_{z_{j-1}}^{z_j} \exp(-\alpha z)\, dz = \frac{\exp(-\alpha z_{j-1}) - \exp(-\alpha z_j)}{\alpha l_j}, \tag{2.36}$$

where

$$z_j = \sum_{k=1}^{j} l_k, \tag{2.37}$$

$z_0 = 0$, $z_M = L_a$, and L_a is the fiber span length. Now, we consider the optimization problem with $M-1$ unknown parameters (z_j, $j = 1, 2, \ldots, M-1$) with the condition that χ should be minimum. We solve this problem using the steepest descent algorithm [86]. In Fig. 2.2(b), let x be the distance at which the exponential curve and its stepwise approximation line intersect. So, we have

$$K_k = \exp(-\alpha x). \tag{2.38}$$

The area mismatch A_k and A'_k are given by

$$A_k = \frac{e^{-\alpha z_{k-1}} - K_k}{\alpha} - K_k(x - z_{k-1}), \tag{2.39}$$

$$A'_k = K_k(z_k - x) - \frac{K_k - e^{-\alpha z_k}}{\alpha}. \tag{2.40}$$

Using Eq. (2.36), we have $A_k = A'_k$.

We randomly choose an initial set of z_k, $k = 1, 2, \ldots, M-1$, and iteratively update the value of every z_k towards the inverse gradient direction until the optimum points are reached. So, taking the derivative of the total mismatch area χ with respect to

z_k, we find

$$\frac{\partial \chi}{\partial z_k} = 2\left(\frac{\mathrm{In}K_k}{\alpha} + z_{k-1}\right)\left[\frac{e^{-\alpha z_k}}{z_k - z_{k-1}} - \frac{e^{-\alpha z_{k-1}} - e^{-\alpha z_k}}{\alpha(z_k - z_{k-1})^2}\right] + 2\left(\frac{\mathrm{In}K_{k+1}}{\alpha} + z_k\right)\left[-\frac{e^{-\alpha z_k}}{z_{k+1} - z_k} + \frac{e^{-\alpha z_k} - e^{-\alpha z_{k+1}}}{\alpha(z_{k+1} - z_k)^2}\right] - 2e^{-\alpha z_k} + 2K_{k+1}. \tag{2.41}$$

Then use the following iterative procedure to update z_k,

$$z_k^{(n+1)} = z_k^{(n)} - \frac{\partial \chi}{\partial z_k}\Delta_k, \quad k = 1, 2, \ldots, M-1 \tag{2.42}$$

where $z_k^{(n)}$ is the value of z_k in the nth iterative step and Δ_k is the step size of the steepest descent algorithm. Once the optimum values of z_k are found, Eqs. (2.36) and (2.37) can be used to obtain the best distribution of the nonlinear multiplication factor K_j and the segment length l_j.

The constraint of Eq. (2.36) is not really essential. If we do not impose this constraint, computational complexity of the steepest descent algorithm increases roughly by a factor of 2. However, the improvement in accuracy (in terms of global error) is only marginal and hence, the simulation results of Section 2.3 are obtained by imposing the constraint of Eq. (2.36).

The steepest descent algorithm converges quickly and Table 2.1 shows the look-up table for the optimum segment lengths when $\alpha = 0.2$ dB/km and $L_a = 80$ km. One of the advantages of this method is that the optimum segment lengths neither depend on the launch power nor on the nonlinear coefficient. Once the look-up table such as that shown in Table 2.1 is made for a particular fiber type, it can be used for a range of launch powers and other system parameters. Using Eq. (2.34), the optical field at

Table 2.1: Look-up table for the optimal step size distribution

Length (km)	$M = 2$	$M = 3$	$M = 4$	$M = 5$	$M = 6$	$M = 7$	$M = 8$
l_1	24.4	14.5	10.4	8.06	6.59	5.58	4.84
l_2	55.6	21.8	13.6	9.88	7.77	6.40	5.45
l_3	—	43.7	19.8	12.8	9.46	7.51	6.23
l_4	—	—	36.3	18.1	12.1	9.08	7.27
l_5	—	—	—	31.1	16.8	11.5	8.73
l_6	—	—	—	—	27.3	15.6	10.9
l_7	—	—	—	—	—	24.3	14.6
l_8	—	—	—	—	—	—	22.0

Parameters: $\alpha = 0.2$ dB/km, $L_a = 80$ km.

the end of the link can be calculated for the given M. However, M is undetermined. To relate M with the desired accuracy, we introduce a technique that combines the local error method with the MAM.

Given an initial M and a target local error e_{target}, calculate the relative local error for the first step e_1 by Eq. (2.29). If e_1 is larger than $10e_{target}$, M will be updated by $2M$. Else if e_1 is larger than e_{target} and less than or equaling to $10e_{target}$, then M will be replaced by $\lceil 2^{1/3}M \rceil$. Here, $\lceil x \rceil$ rounds the element of x to the nearest integer towards infinity. If e_1 is less than or equal to $e_{target}/10$, M will be decreased to $\lfloor M/2^{1/3} \rfloor$, where $\lfloor x \rfloor$ rounds the element of x to the nearest integer towards minus infinity. Finally, if e_1 is in the target range which is $(e_{target}/10, e_{target}]$, that M will be used to find the optimal parameters in the look-up table, which will be used to model the pulse propagation.

In this scheme, the local error for each step will not have a large fluctuation since the step size distribution is optimized for every M. As a result, we can roughly bound the local error by controlling that of the first step. The implementation for this scheme is different from the local-error method in that we find the total number

of steps as well as the step size distribution at the very beginning, instead of adjusting the step size along the fiber length, which saves the computational cost. Since we can combine the dispersion operator (the same way as in Eq. (2.6)) of the neighboring steps, the computational cost can further be reduced by a factor of 2. We will discuss the simulation results in the later subsection. Since we do not make any assumptions about the system configuration, or the modulation format of the signal, this scheme is system independent and can be widely used for various cases with high efficiency.

2.3 Comparison of schemes

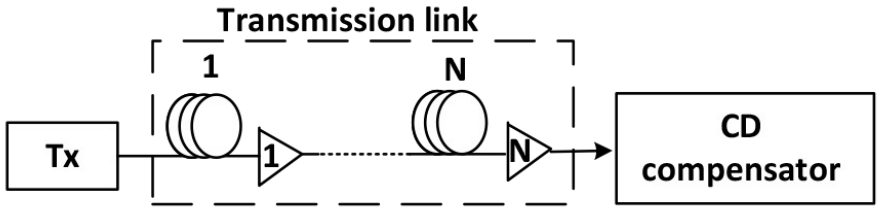

Figure 2.3: Schematic of a fiber-optic transmission system.

In this subsection, we compare the performance of the different schemes described in Section 2.2 of the SSFS. The system schematic is shown in Fig. 2.3, which includes a transmitter, a fiber-optic link consisting of N spans of fibers and amplifiers, and a chromatic dispersion (CD) compensator. The amplifier compensates for the fiber loss exactly, without adding noise. Before implementing the schemes, we simulate a signal propagation in the fiber by the split-step method using a very small step size with the nonlinear phase accumulated per step of 0.00001 radians, such that the fiber output is very close to the exact solution of NLSE. This output is the reference signal with which we compare the outputs of various schemes. Then, using the same fiber

input signal as that used to obtain the reference signal, NLSE is solved by different schemes, and the accuracy and the computational cost are compared. To measure the accuracy, we define the global error by

$$e_{global} = \frac{\|A_n - A_{ref}\|^2}{\|A_{ref}\|^2}, \tag{2.43}$$

where A_n is the numerical result for scheme n, and A_{ref} is the reference signal. Note that we use the square of the norm instead of the norm itself in Eq. (2.43). We use the number of FFTs as a measure of computational cost since the computational time is roughly proportional to the number of FFTs.

At first, a fiber-optic system shown in Fig. 2.3 is simulated for 32 quadrature amplitude modulation (QAM) at a symbol rate 25 Gbaud. The following parameters are used throughout this chapter unless otherwise specified. A random symbol sequence consisting of 8192 raised-cosine pulses with a roll-off factor of 0.8 is launched to the fiber. The fiber-optic link consists of 10 fiber spans, each 80 km long, and 10 amplifiers. The parameters of the fibers are as follows, the loss coefficient $\alpha = 0.046$ km^{-1}, the dispersion parameter $\beta_2 = 5$ ps^2/km, and the nonlinear coefficient $\gamma = 2.2$ $\text{W}^{-1}\text{km}^{-1}$. Different schemes in Section 2.2 were employed to carry out the SSFS. After that, a CD compensator is introduced right after the fiber link. Finally, the global error of each scheme is calculated using Eq. (2.43).

Table 2.2 shows the error in a single step for 10 Gbaud and 25 Gbaud systems, respectively. When the loss is combined with nonlinearity (scheme IIa or b), the single-step error is significantly lower for 10 Gbaud as compared to the case when the loss is combined with dispersion (scheme Ia or b). However, for 25 Gbaud, scheme II has a lower error only when $h < 40$ km. When h is larger, scheme II does not

perform better because of larger variation of the optical field within the step size due to dispersion.

Table 2.2: Single-step error versus step size.

h (km)	10 Gbaud		25 Gbaud	
	Single-step error (scheme I)	Single-step error (scheme II)	Single-step error (scheme I)	Single-step error (scheme II)
0.5	1.29e-15	3.43e-17	5.38e-15	4.69e-15
1	8.05e-14	2.15e-15	3.39e-13	2.96e-13
2	5.01e-12	1.33e-13	2.17e-11	1.89e-11
5	1.05e-9	2.85e-11	5.07e-9	4.48e-9
10	5.45e-8	1.45e-9	2.86e-7	2.50e-7
20	2.22e-6	6.10e-8	9.41e-6	7.76e-6
25	6.87e-6	1.88e-7	2.16e-5	1.77e-5
30	1.68e-5	4.59e-7	3.94e-5	3.57e-5
40	6.12e-5	1.73e-6	1.02e-4	1.19e-4
50	1.53e-4	4.46e-6	2.26e-4	2.74e-4
60	3.07e-4	9.79e-6	4.14e-4	4.34e-4

Fig. 2.4(a) and 2.4(b) show the computational cost (in units of number of FFTs) as a function of the global error for schemes Ia, IIa, Ib and IIb when the fiber launch power is 0 dBm and 3 dBm, respectively. As can be seen, when the global error is greater than 10^{-7}, scheme IIb (loss combined with nonlinearity and variable step size) is the most efficient scheme of the four schemes. When the global error is large, it corresponds to small number of steps. In this case, uniform step size is not a good choice because the nonlinear phase shift accumulated in a low power region is small and the step size is unnecessarily large wasting the computational resources. When the global error is 10^{-5}, the number of FFTs required for scheme IIb is reduced by a factor of 2 as compared to scheme Ia when the launch power equals to 0 dBm. However, when the global error is less than 10^{-7}, scheme IIa (loss combined with nonlinearity and uniform step size) is the most efficient scheme of the four schemes

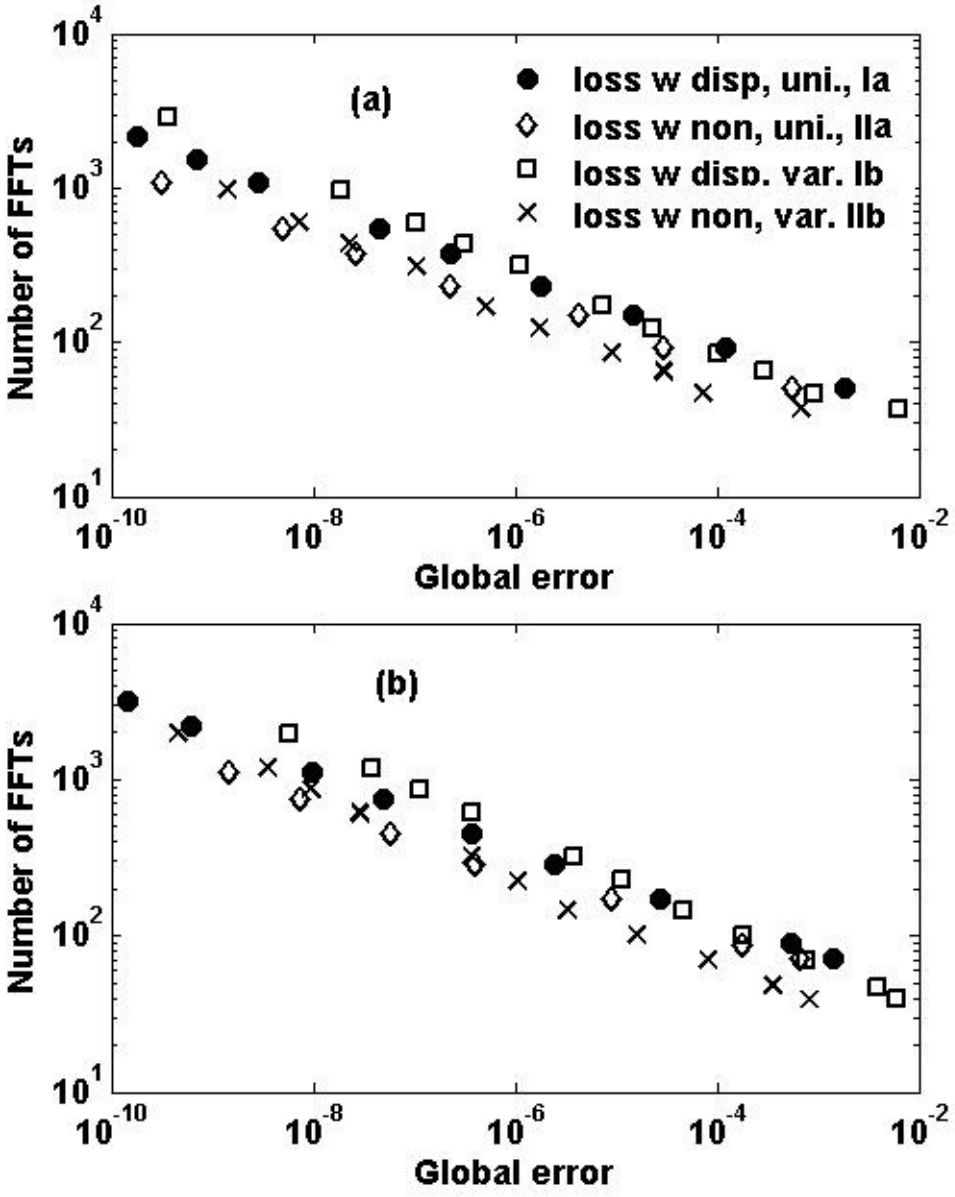

Figure 2.4: Plot of the number of FFTs vs global error of the 32QAM system at 25 GBaud for the schemes Ia, IIa, Ib and IIb. (a) 0 dBm and (b) 3 dBm.

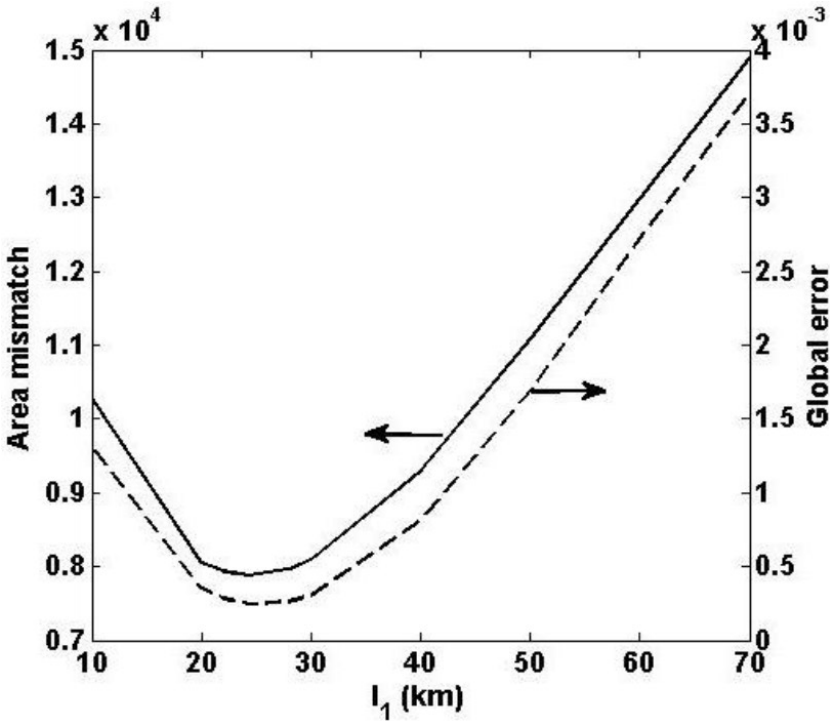

Figure 2.5: Area mismatch vs l_1 and global error vs l_1 for the case when $M = 2$, launch power = 0 dBm.

and it is marginally better than scheme IIb. In either case, schemes in which loss is combined with nonlinearity (schemes IIa and b) outperform the schemes in which the loss is combined with dispersion (schemes Ia and b). For the simulation of fiber-optic transmission system, the region of most practical interest corresponds to a global error in the range of 10^{-8} - 10^{-2}. Typically, practical power of telecom systems range from -6 dBm to 3 dBm depending on the reach and modulation format. The purpose of simulations with higher power (3 dBm) is to evaluate the effect of stronger nonlinear effect in various schemes. Comparing Figs. 2.4(a) and 2.4(b), we find that the scaling of error is quite similar.

Fig. 2.5 shows the area mismatch and global error (calculated using Eq. (2.43)) as a function of l_1, for $M = 2$. As can be seen, the value of l_1 that minimizes the area mismatch (χ) also corresponds to minimum global error.

Next the performance of the local error method (scheme III) and MAM combined with local error method (scheme IV) are considered. The results are shown in Figs. 2.6(a) and 2.6(b). Scheme III gives a better performance than the schemes Ia, IIa, Ib and IIb when the global error is less than 10^{-8}, and it has a flatter slope, which means the required additional computational cost to achieve a smaller error is the minimum. However, when the global error is large ($> 10^{-8}$), the local error method is not efficient. Similar results are found in Ref. [77] in which the efficiency of the local error method is comparable to the other schemes when the global error is large. Figs. 2.6(a) and 2.6(b) show that the MAM combined with local error method is the most efficient one in that, for obtaining the same error, it needs the least number of FFTs. In Fig. 2.6(a), when the global error is 10^{-8}, the number of FFTs needed for scheme Ia is 4.4 times that of scheme IV, and the number of FFTs required for scheme III is

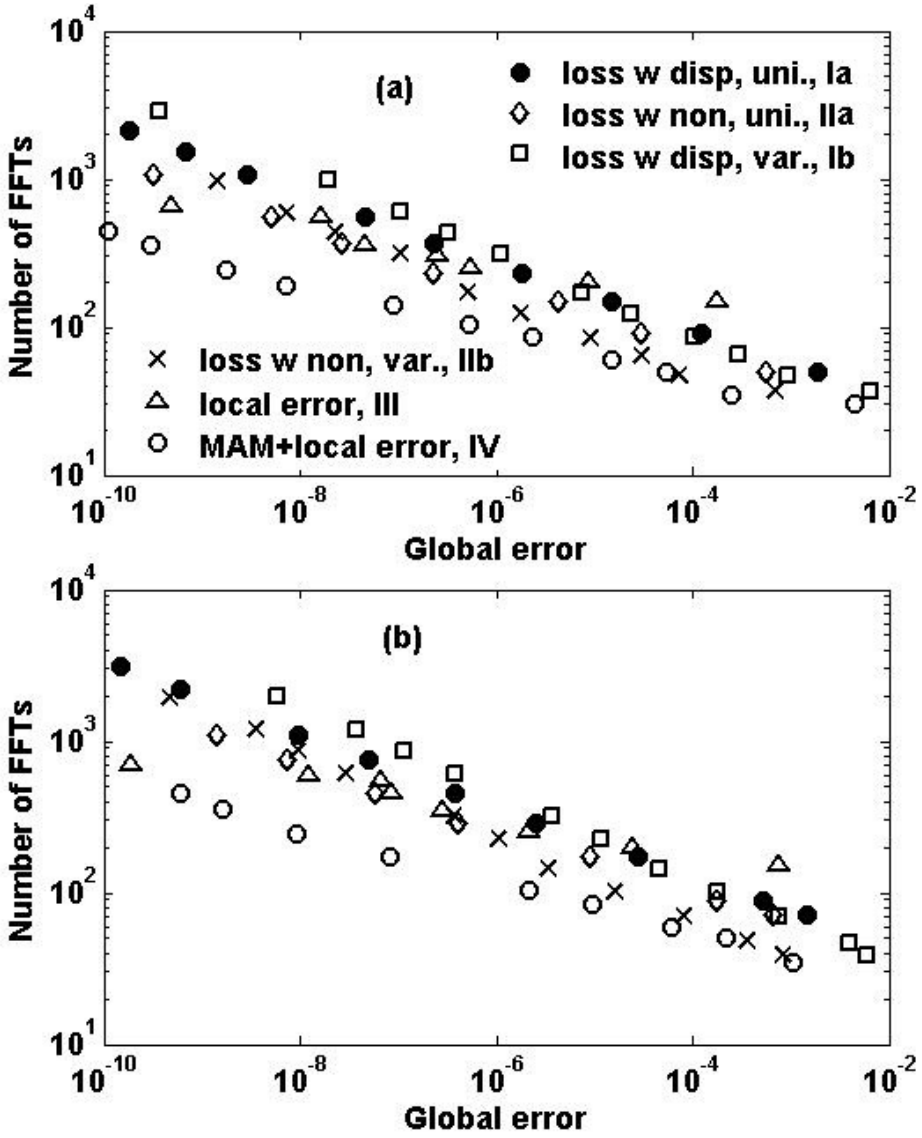

Figure 2.6: Plot of the number of FFTs vs global error of the 32QAM system for the schemes I-IV. (a) 0 dBm and (b) 3 dBm.

3.1 that of scheme IV. When the global error is 10^{-6}, the number of FFTs needed for scheme Ia is 2.7 times that of scheme IV and the number of FFTs required for scheme III is 2.5 times that of scheme IV. Comparing Fig. 2.6(a) and 2.6(b), we find that the scheme that combines MAM with the local error method is the most efficient scheme even at higher launch power. Fig. 2.7 shows the computational time as a function of the global error. Comparing Fig. 2.6 and Fig. 2.7, we find that the number of FFTs is a good measure of the computational cost.

Fig. 2.8 shows the relative local error as a function of distance when the launch power is 0 dBm and the number of steps per span is 5. Dashed and solid lines in Fig. 2.8 show the results for the case of uniformly distributed step size (scheme Ia) and an optimally distributed step size using MAM (scheme IV), respectively. Both curves show a periodic characteristic due to the system configuration. When the uniformly distributed step size is utilized, the local error is the maximum at the beginning and decreases with distance in each span. This is because the accumulated nonlinear phase per step decreases exponentially with distance in each span due to fiber loss and, smaller accumulated nonlinear phase leads to a more accurate result. In the case when the step size is distributed through the MAM technique, the nonlinear phase accumulated is optimized such that the local error will be smaller and has less variation. From Fig. 2.8, we see that the local error fluctuation for scheme IV is about one or two orders of magnitude smaller than that for scheme Ia.

As a next example, we have simulated a fiber-optic system based on quadrature phase shift keying (QPSK). The system configuration and all the parameters of the system are the same as the previous ones. Fig. 2.9 shows the number of FFTs as a function of global error for all the schemes. Fig. 2.9(a) and Fig. 2.9(b) are obtained

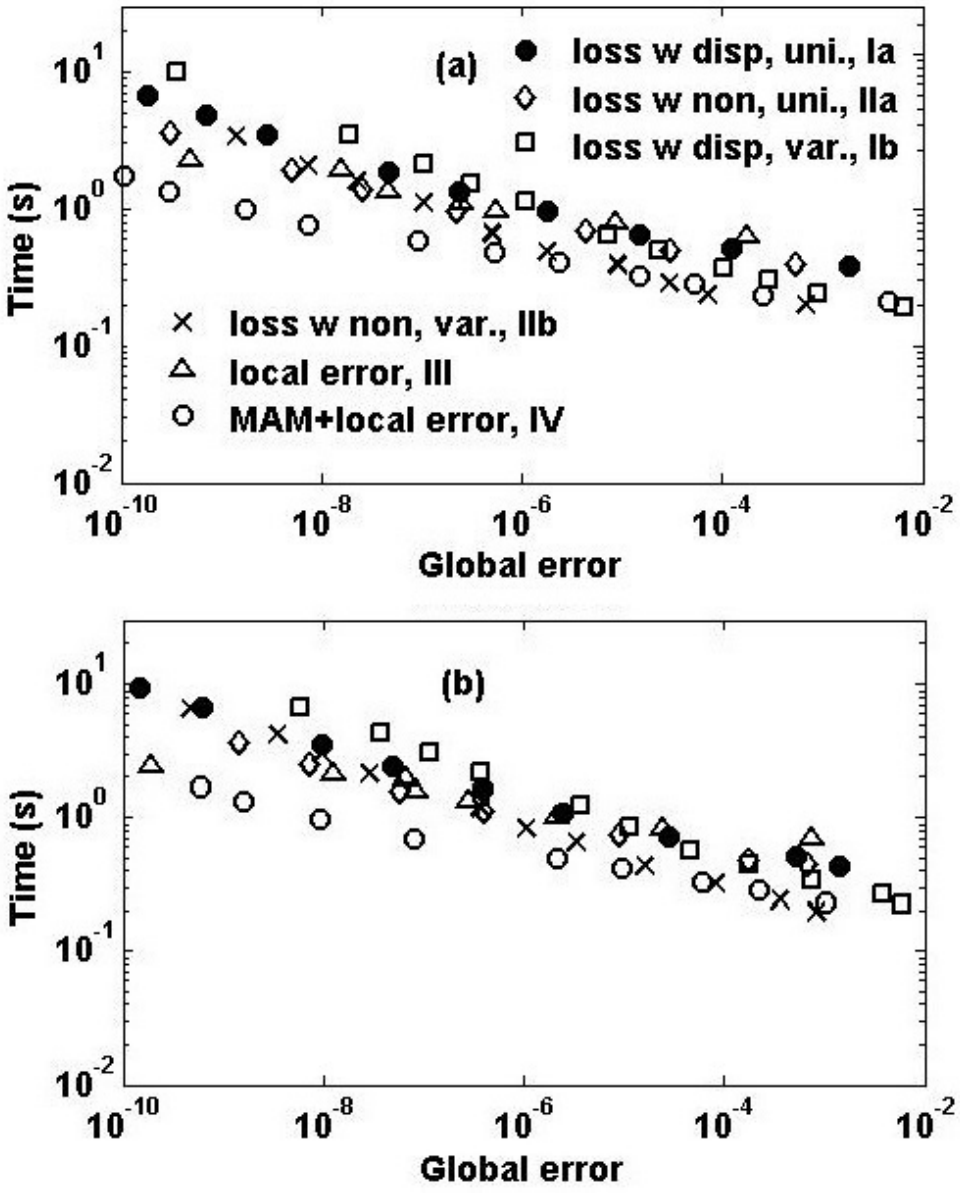

Figure 2.7: Plot of the time vs global error of the 32QAM system for the schemes I-IV. (a) 0 dBm and (b) 3 dBm.

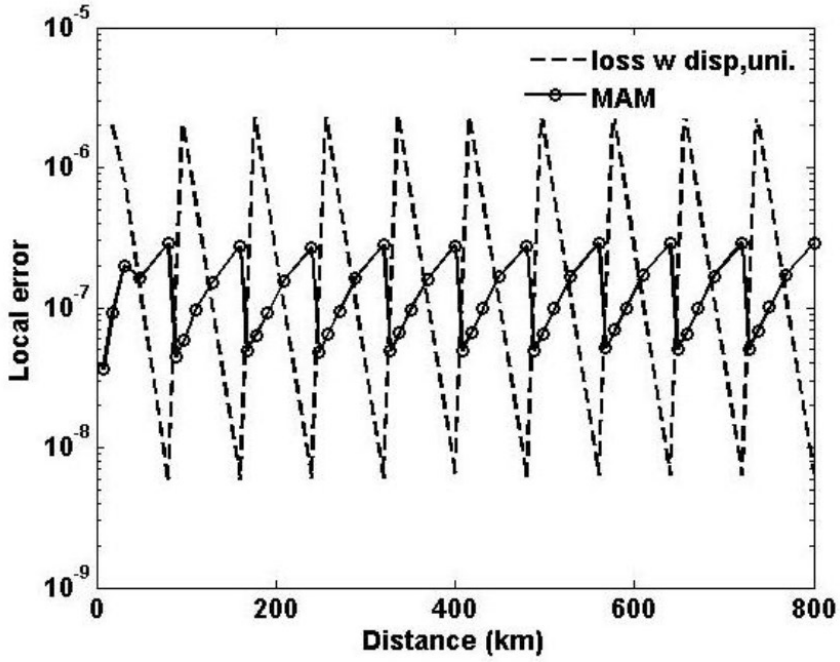

Figure 2.8: Local error as a function of distance for schemes Ia and IV for 32 QAM system, when the launch power is 0dBm and the number of steps per span $M = 5$.

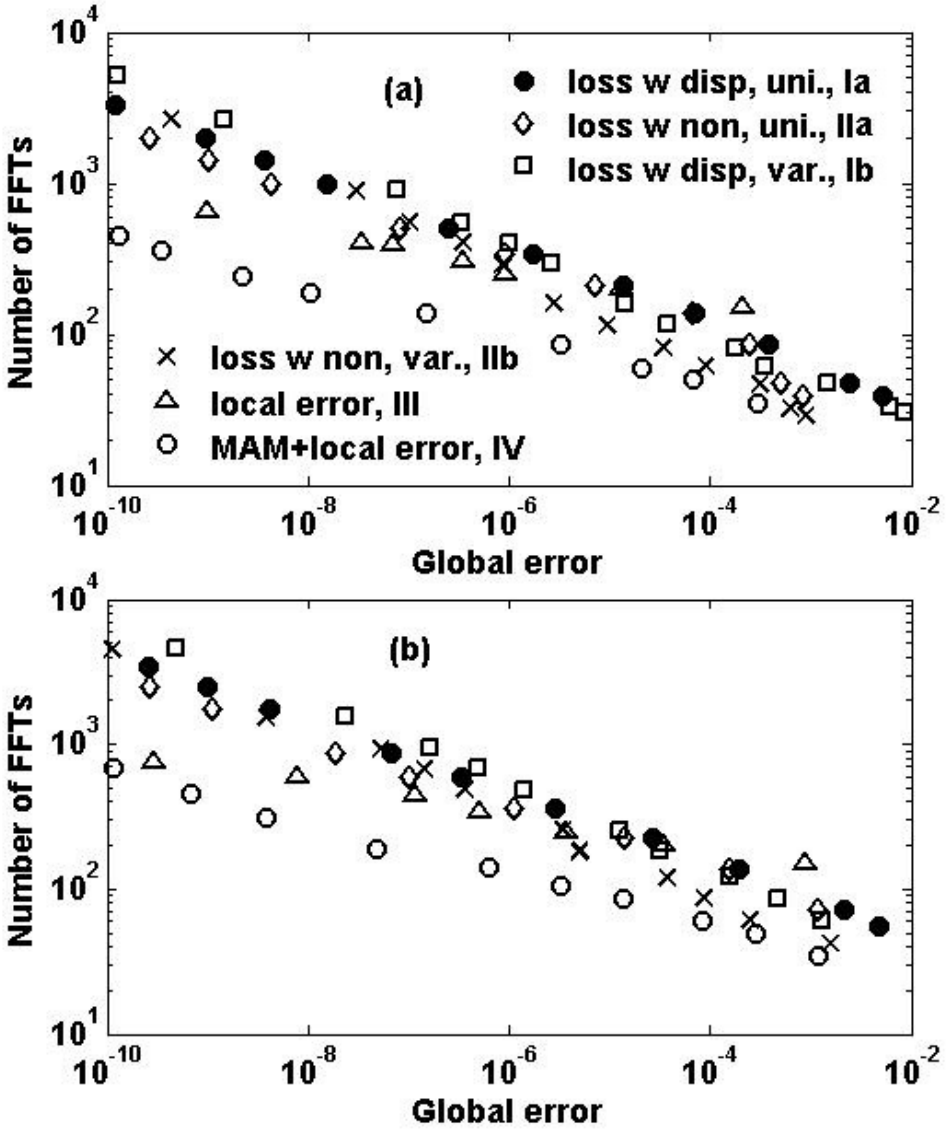

Figure 2.9: Plot of the number of FFTs vs global error of the QPSK system for the schemes I-IV. (a) 0dBm and (b) 3dBm.

when the launch power is 0 dBm and 3 dBm, respectively. In Fig. 2.9(a), when the global error is 10^{-8}, numbers of FFTs needed for scheme Ia and scheme III are 5.8 and 2.5 times that of scheme IV, respectively. When the global error is 10^{-6}, the numbers of FFTs required for scheme Ia and scheme III are 3.7 and 2.4 times that of scheme IV, respectively. Similar results are obtained when the launch power is 3 dBm (Fig. 2.9(b)).

2.4 Conclusion

In this chapter, we have studied various schemes using SSFS to solve the NLSE for a fiber-optic system based on two different modulation formats and compared their performances. A scheme combining the local error method with the method based on MAM is introduced. The optimum step size for the given number of steps (M) is found by minimizing the area mismatch between the exponential curve and its stepwise approximation. The steepest descent algorithm is used for this optimization. The number of steps to have the desired accuracy is determined using the local error method. The advantage of this scheme is that the local error is not calculated at each step which saves the computational cost. The step size distribution is pre-determined by the steepest descent algorithm so that the dispersion operators of the neighboring steps can be combined. The simulation results show that this scheme outperforms the other schemes.

In general, the schemes in which the fiber loss is combined with nonlinearity have higher computational efficiency than the schemes in which the fiber loss is combined with dispersion. When the global error is large ($> 10^{-7}$), the schemes with variable step size outperform the schemes with uniform step size. As for the local error method,

it has a flatter slope and outperforms the schemes with uniform or variable step size distribution, especially when the global error is very small.

Chapter 3

Digital back propagation with optimal step size for polarization multiplexed transmission systems

3.1 Introduction

DBP is now widely used to compensate for fiber distortions due to linear and nonlinear effects, in which the signs of loss, dispersion and nonlinear coefficients in DBP are opposite of those of the transmission fiber [58, 61, 78, 79, 87–89]. In DBP, SSFS is used to solve the NLSE in digital domain and it provides significant performance improvement if the step size is sufficiently small. In practice, the choice of step size is usually determined by the trade-off between performance and implementation complexity. In [79], the step size used to solve the NLSE is chosen equal to the amplifier spacing and in [58, 78], sub-amplifier spacing step size is chosen, but the step size is uniform. In this chapter, a DBP scheme with non-uniform step size

based on MAM is investigated [83]. For the ideal compensation of dispersion and nonlinearity, the power in the virtual fiber should increase exponentially with distance if the nonlinear coefficient is constant or equivalently the nonlinear coefficient should increase exponentially with distance if the power is fixed. This ideal exponential profile can be approximated by a stepwise increasing profile. The nonlinear coefficients of these virtual fiber sections (or steps) are obtained by minimizing the area mismatch between the ideal exponential profile and its stepwise approximation. The dispersion and nonlinear coefficients of each of the virtual fiber section are optimized using the Lagrange function. For the given number of virtual fiber sections, the MAM scheme outperforms the uniform spacing scheme without additional computational cost. In [61], the step size is chosen larger than the amplifier spacing so as to lower the computational complexity and power consumption. However, the method proposed in this chapter is not valid for such cases.

3.2 Digital back propagation theory

Let us first consider a single-span system with constant fiber dispersion, nonlinear and loss coefficients. The evolution of the field envelope in a fiber is described by the NLSE (see details in Chapter 2),

$$\frac{\partial q}{\partial z} = (D + N)q, \tag{3.1}$$

where D denotes the fiber dispersion effect given by Eq. (2.8), and N denotes the nonlinear and loss effects given by Eq. (2.9). The solution, $q(t, L)$ of Eq. (3.1) can

be written as:

$$q(t, L) = Mq(t, 0), \tag{3.2}$$

where

$$M = \exp\left\{\int_0^L [N(t, z) + D(t)]dz\right\}, \tag{3.3}$$

is the tranfer function of the transmission fiber, and L is the total transmission length. To compensate for the fiber distortions due to fiber dispersion and nonlinearity, DBP is introduced after the transmission link. If the transfer function of DBP is inverse of that of the fiber optic link, the initial field envelope can be recovered. Multiplying Eq. (3.2) by M^{-1} (transfer function of DBP) on both sides, we find

$$q_{DBP,out}(t) = M^{-1}q(t, L) = q(t, 0), \tag{3.4}$$

where

$$M^{-1} = \exp\left\{-\int_0^L [N(t, z) + D(t)]dz\right\} \tag{3.5}$$

In Eq. (3.4), $q_{DBP,out}(t)$ represents the signal after DBP, and $q(t, L)$ represents the received field envelope which is distorted due to fiber dispersion and nonlinear effects. Eq. (3.4) with M^{-1} given by Eq. (3.5) is equivalent to solving the following partial differential equation,

$$\frac{\partial q_b}{\partial z} = -[N + D]q_b, \tag{3.6}$$

with the initial condition $q_b(t, 0) = q(t, L)$. Solving Eq. (3.6) is similar to let the pulse propagate reversely, so this is referred to as back propagation. Eq. (3.6) may be rewritten as

$$\frac{\partial q_b}{\partial z} = [N_b + D_b]q_b, \tag{3.7}$$

with $q_b(t,0) \equiv q(t,L)$ and

$$D_b = -D = i\frac{\beta_2}{2}\frac{\partial^2}{\partial t^2}, \tag{3.8}$$

$$N_b = -N = -i\gamma|q_b|^2 + \frac{\alpha}{2}. \tag{3.9}$$

Eq. (3.7) is NLSE with reversed signs of dispersion, loss and nonlinear coefficients, which can be solved in digital domain to compensate for fiber distortions. Fig. 3.1 illustrates the forward propagation of signals in fibers and backward propagation using virtual fibers in digital domain.

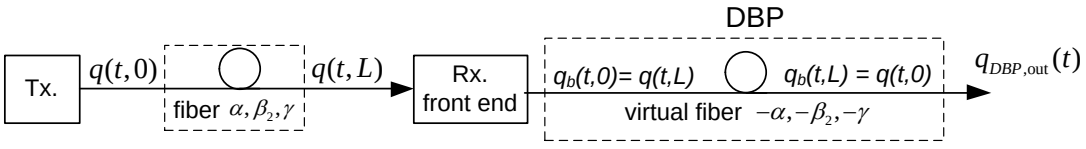

Figure 3.1: Propagation in a single-span fiber (Forward propagation) and digital back propagation. Tx: transmitter, Rx: receiver.

Eq. (3.7) can be solved numerically using the SSFS described in Chapter 2 [22]. Let us take the symmetric split-step scheme as an example. The received field $q(t,L) = q_b(t,0)$. We need to find $q_b(t,\Delta z)$ which corresponds to $q(t,L-\Delta z)$. The operator M^{-1} in this propagation step can be approximated as

$$\begin{aligned} M^{-1} &= \exp\left\{\int_0^{\Delta z}[N_b(t,z) + D_b(t)]dz\right\} \\ &\cong \exp\left[D_b(t)\frac{\Delta z}{2}\right]\exp\left\{\int_0^{\Delta z}[N_b(t,z)]dz\right\}\exp\left[D_b(t)\frac{\Delta z}{2}\right]. \end{aligned} \tag{3.10}$$

And

$$q_b(t,\Delta z) = M^{-1}q_b(t,0) \cong \exp\left[D_b(t)\frac{\Delta z}{2}\right]\exp\left[\int_0^{\Delta z} N_b(t,z)dz\right]q_b^l\left(t,\frac{\Delta z}{2}\right), \tag{3.11}$$

where

$$q_b^l\left(t, \frac{\Delta z}{2}\right) = \exp\left[D_b(t)\frac{\Delta z}{2}\right] q_b(t,0). \tag{3.12}$$

The linear solution $q_b^l\left(t, \frac{\Delta z}{2}\right)$ is obtained using fiber linear transfer function [22]

$$q_b^l\left(t, \frac{\Delta z}{2}\right) = F^{-1}\left[\tilde{q}_b^l\left(\omega, \frac{\Delta z}{2}\right)\right], \tag{3.13}$$

where

$$\tilde{q}_b^l\left(\omega, \frac{\Delta z}{2}\right) = \tilde{q}_b^l(\omega,0)\exp\left[-i\beta_2\frac{\Delta z}{2}\omega^2/2\right], \tag{3.14}$$

$$\tilde{q}_b^l(\omega,0) = F\left[q_b^l(t,0)\right], \tag{3.15}$$

F and F^{-1} are the Fourier transformation and inverse Fourier transformation, respectively. When only taking into account of the nonlinear operator in Eq. (3.11), we have

$$\frac{\partial q_b}{\partial z} = N_b q_b = \left(-i\gamma|q_b|^2 + \frac{\alpha}{2}\right) q_b, \tag{3.16}$$

with initial field of Eq. (3.16) being $q_b^l\left(t, \frac{\Delta z}{2}\right)$. Following the procedure in Section 2.2.3, the solution of Eq. (3.16) is

$$q_b^{nl}(t, \Delta z) = q_b^l\left(t, \frac{\Delta z}{2}\right)\exp\left(-i\gamma\Delta z_{eff}\left|q_b^l\left(t, \frac{\Delta z}{2}\right)\right|^2 + \alpha\Delta z\right), \tag{3.17}$$

where

$$\Delta z_{eff} = \frac{\exp(\alpha\Delta z) - 1}{\alpha}. \tag{3.18}$$

The leftmost term corresponding to dispersion in Eq. (3.11) can be calculated in the same way as in Eq. (3.13).

Fig. 3.2 shows the propagation in a N-span fiber-optic system, which consists of

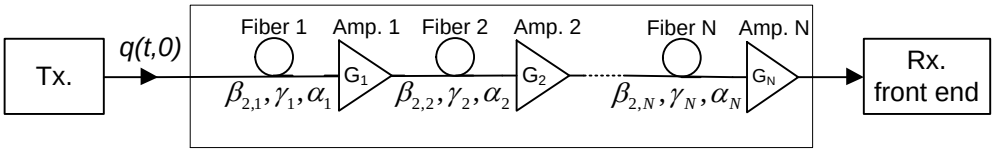

Figure 3.2: Propagation in a N-span fiber optic system. Tx: transmitter, Rx: receiver.

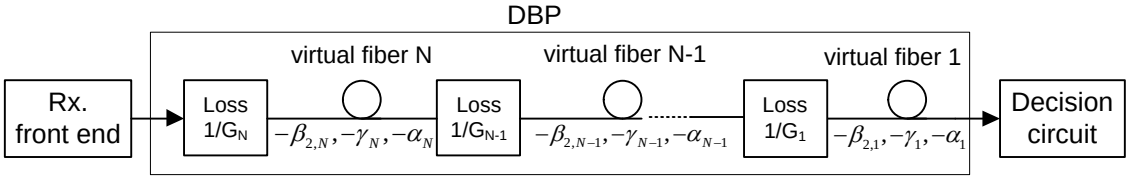

Figure 3.3: Digital back propagation for a N-span fiber-optic system. Rx: receiver.

an amplifier in each span. In DBP, shown in Fig. 3.3, amplifiers with Gain G_n are replaced by attenuation with loss $1/G_n$. Also, the parameters of the virtual fiber in DBP are set to have the opposite signs of those of the TF. Note that the distortions results from the first fiber span will be compensated for in the last span of DBP, and the impairments of the second span of TF will be compensated in the last but two span in DBP. Although the digital back propagation can compensate for deterministic (and bit-patter dependent) nonlinear effects, it can not undo the impact of ASE and nonlinearity-ASE coupling[27].

3.3 DBP with optimal step sizes

In polarization division multiplexing (PDM) systems, the evolution of the electric field in the fiber can be described by the vector NLSE

$$\frac{\partial A_x}{\partial z} = -\beta_{1x}\frac{\partial A_x}{\partial t} - \frac{i\beta_2}{2}\frac{\partial^2 A_x}{\partial t^2} - \frac{\alpha}{2}A_x + i\gamma\left(|A_x|^2 + \frac{2}{3}|A_y|^2\right)A_x, \tag{3.19a}$$

$$\frac{\partial A_y}{\partial z} = -\beta_{1y}\frac{\partial A_y}{\partial t} - \frac{i\beta_2}{2}\frac{\partial^2 A_x}{\partial t^2} - \frac{\alpha}{2}A_y + i\gamma\left(|A_y|^2 + \frac{2}{3}|A_x|^2\right)A_y, \tag{3.19b}$$

where A_x and A_y are the electric field in x- and y- polarization, respectively; β_{1x}, β_{1y}, β_2, γ and α are inverse group velocities for x- and y- polarization components, dispersion, nonlinear and loss coefficients, respectively. To model PMD in the fiber, we employed the method of [90, 91] in which fibers with randomly varying birefringence are approximated by multiple short fiber sections with constant birefringence in each fiber section. The power transfer between the polarization components and the random phase changes due to refractive index fluctuations are accounted for by introducing a matrix

$$F = \begin{bmatrix} \cos\theta & \sin\theta e^{i\phi} \\ -\sin\theta e^{i\phi} & \cos\theta \end{bmatrix} \tag{3.20}$$

between the fiber sections. Here, θ and ϕ are the random variables with uniform distribution in the interval $-\pi < \theta < \pi$, $-\pi/2 < \phi < \pi/2$.

Since the residual birefringence in the transmission fiber changes randomly much faster than the nonlinear interaction, by averaging the vector NLSE over the Poincare sphere, Manakov equations are obtained as

$$\frac{\partial A_r}{\partial z} = -\frac{i\beta_2}{2}\frac{\partial^2 A_r}{\partial t^2} - \frac{\alpha}{2}A_r + \frac{i8\gamma}{9}\left(|A_x|^2 + |A_y|^2\right)A_r, \quad r = x, y. \tag{3.21}$$

Consider a single span of a transmission fiber of length L_a. The output field of the fiber in two orthogonal polarizations may be written as [22]

$$A_r(t, L_a) = \exp\left\{\int_0^{L_a}\left[D(t) + N(t, z)\right]dz\right\}A_r(t, 0), \quad r = x, y. \tag{3.22}$$

where

$$D(t) = -\frac{i}{2}\beta_2\frac{\partial^2}{\partial t^2}, \tag{3.23}$$

$$N(t,z) = \frac{8}{9}i\gamma\left(|A_x(t,z)|^2 + |A_y(t,z)|^2\right) - \frac{\alpha}{2}. \tag{3.24}$$

After coherent detection and analog to digital conversion, the distorted field passes through the virtual fiber in digital domain. The virtual fiber in DBP has loss, dispersion and nonlinear coefficients with the opposite sign of the transmission fiber, i.e.,

$$D_{DBP}(t) = \frac{i}{2}\beta_2\frac{\partial^2}{\partial t^2} = -D(t), \tag{3.25}$$

$$N_{DBP}(t,z) = -\frac{8}{9}i\gamma\left(|A_x(t,z)|^2 + |A_y(t,z)|^2\right) + \frac{\alpha}{2} = -N(t,z). \tag{3.26}$$

Then, the digital signal after the DBP may be written as

$$\begin{aligned} A_{r,out}(t) &= e^{\int_0^{L_a}[D_{DBP}(t)+N_{DBP}(t,z)]dz}\cdot e^{\int_0^{L_a}[D(t)+N(t,z)]dz}A_r(t,0) \\ &= e^{-\int_0^{L_a}[D(t)+N(t,z)]dz}\cdot e^{\int_0^{L_a}[D(t)+N(t,z)]dz}A_r(t,0) \\ &= A_r(t,0). \qquad (r=x,y) \end{aligned} \tag{3.27}$$

Thus, the transmitted electric field can be fully recovered after the DBP if there is no noise. Eq. (3.27) can also be expressed in the following form

$$\frac{\partial A_{r,b}}{\partial z} = \left[D_{DBP} + N_{DBP}\right]A_{r,b} = -\left[D+N\right]A_{r,b}, \tag{3.28}$$

with $A_{r,b}(t,0) = A_r(t,L_a)$. Using $A_{r,b} = e^{\alpha z/2}u_{r,b}$, Eq. (3.28) can be written as

$$i\frac{\partial u_{r,b}}{\partial z} - \frac{\beta_2}{2}\frac{\partial^2 u_{r,b}}{\partial t^2} + \frac{8\gamma'(z)}{9}\left(|u_{x,b}|^2 + |u_{y,b}|^2\right)u_{r,b} = 0, \quad r = x,y, \tag{3.29}$$

where $\gamma'(z) = \gamma e^{\alpha z}$ is the effective nonlinear coefficient. In DBP, if the step size is small enough such that the effective nonlinear coefficient has an exponential profile, it provides the ideal compensation of dispersion and nonlinearity. However, this ideal case is unfeasible due to the enormous computational cost. One realistic method to implement DBP is to divide the virtual fiber into M cascaded sections, which can compensate for the signal distortion from the transmission fiber by solving Manakov equations using SSFS [22]

$$\begin{aligned} u_{r,b}(t, z_{j-1} + l_j) \approx & e^{-iD(t)l_j/2} \cdot e^{-i\frac{8}{9}\left(|u_{x,b}(t,z_{j-1})|^2 + |u_{y,b}(t,z_{j-1})|^2\right) \int_{z_{j-1}}^{z_{j-1}+l_j} \gamma'(z)dz} \\ & \times e^{-iD(t)l_j/2} u_{r,b}(t, z_{j-1}), \end{aligned} \tag{3.30}$$

where $r = x, y$, l_j is the length of the section of the virtual fiber, and $z_j = \sum_{k=1}^{j} l_k$, $z_0 = 0$ and $z_M = L_a$. In this chapter, we investigate the DBP scheme by optimizing the accumulated dispersion and nonlinear phase shift of each section, and compare its performance with that of the uniform spacing scheme.

For the uniform spacing case, the virtual fiber is divided into M sections with equal length $l_j = L_a/M$, $j = 1, 2, , M$ (see Fig. 3.4a). The accumulated dispersion of each section is $\xi_j = \beta_2 l_j$, and the nonlinear phase shift imparted by the jth section is

$$\varphi_j = \frac{8}{9\alpha}\gamma \left(|u_{x,b}|^2 + |u_{y,b}|^2\right) e^{\alpha z_{j-1}} \left(e^{\alpha L_a/M} - 1\right). \tag{3.31}$$

Let $M = 3$, see Fig. 3.4. In this case, we have 5 unknowns, $l_1, l_2, \gamma_1, \gamma_2,$ and γ_3. The DBP can compensate for the linear and nonlinear distortions if it satisfies the

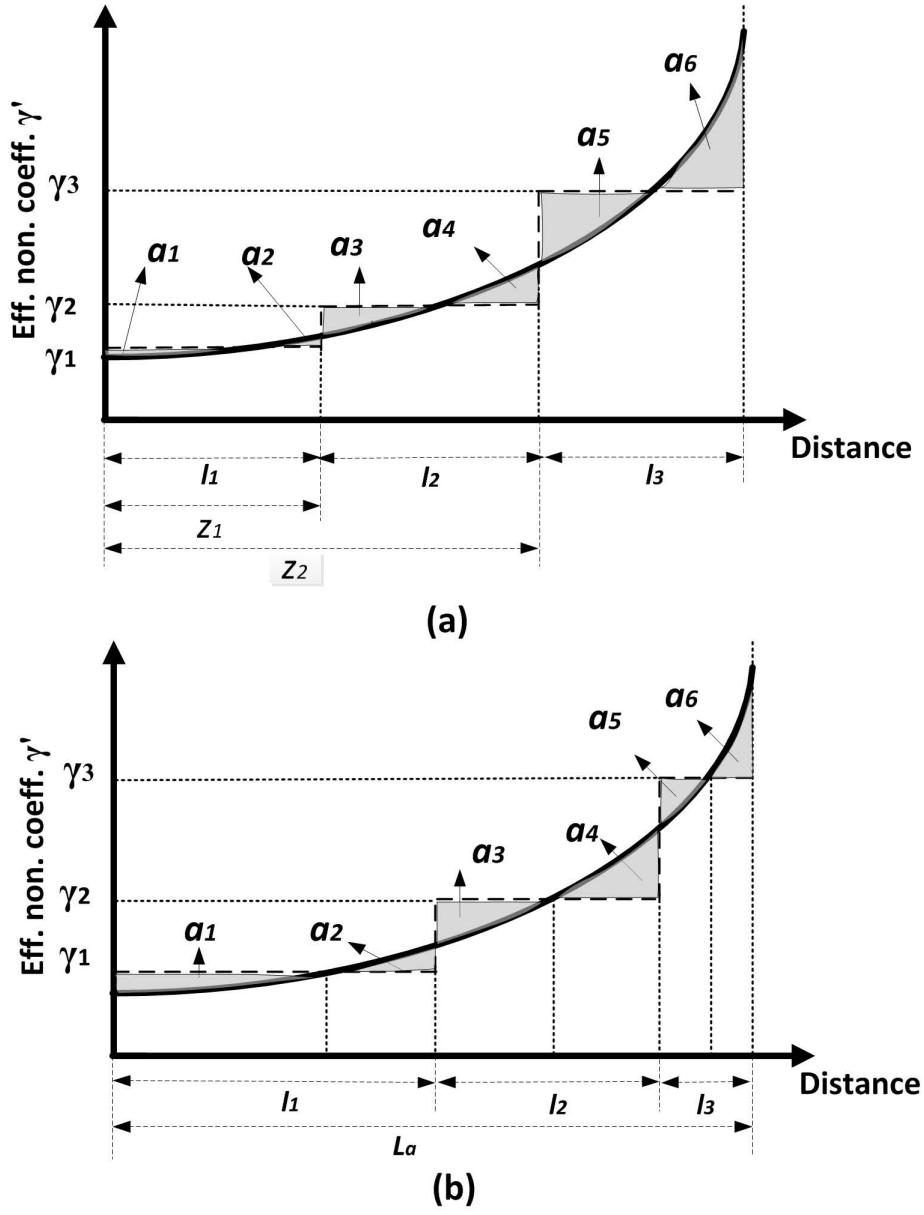

Figure 3.4: Effective nonlinear coefficient and its stepwise approximation for the number of sections $M = 3$. (a) Uniform spacing, (b) MAM.

following conditions,

$$l_1 + l_2 + l_3 = L_a, \qquad \sum_{j=1}^{3} \gamma_j l_j = \gamma \int_0^{L_a} e^{\alpha z} dz = \gamma \left(\frac{e^{\alpha L_a - 1}}{\alpha} \right). \tag{3.32}$$

We construct a Lagrange function

$$L(l_1, l_2, \gamma_1, \gamma_2, \gamma_3, \lambda) = \sum_{j=1}^{6} a_j + \lambda \left[\sum_{j=1}^{3} \gamma_j l_j - \gamma \left(\frac{e^{\alpha L_a - 1}}{\alpha} \right) \right], \tag{3.33}$$

where λ is the Lagrange multiplier. Setting the derivative of L with respect to each of its arguments, we obtain a set of nonlinear equations and their solutions yield the optimum values of $l_1, l_2, \gamma_1, \gamma_2,$ and γ_3. Then the dispersion in the jth section is

$$\xi_j = \beta_2 l_j, \tag{3.34}$$

and the nonlinear phase shift in the jth section is

$$\varphi_j = \frac{8}{9} \gamma_j l_j \left(|u_{x,b}(t, z_{j-1})|^2 + |u_{y,b}(t, z_{j-1})|^2 \right). \tag{3.35}$$

The Lagarange multiplier method is effective when the number of unknown parameters is not too many. For the case of a large number of steps, the number of unknown parameters become large and the least squares method (LSM) together with the steepest descent method is used to optimized the lengths and nonlinear coefficients [84]. The detailed derivation of LSM has been given in Chapter 2. Table 3.1 shows the optimum section lengths and their nonlinear coefficients for various M.

So far we considered a single span system. Fig. 3.5 shows a fiber optic transmission system consisting of K spans with an amplifier in each span. At the receiver, the

Table 3.1: Optimum values of the parameters in DBP

M	l_1	l_2	l_3	l_4	γ_1	γ_2	γ_3	γ_4
2	55.8	24.2	—	—	5.13	26.3	—	—
3	43.7	21.8	14.5	—	3.54	14.17	31.94	—
4	36.3	19.8	13.6	10.4	2.84	9.53	20.2	34.8

Parameters: α=0.2 dB/km, γ=1.1 $\mathrm{W^{-1}km^{-1}}$, and L_a=80 km. l_j has the unit of km and γ_j has the unit of $\mathrm{W^{-1}km^{-1}}$. $(j = 1, 2, 3, 4)$

DBP consists of K spans of virtual fibers. It is followed by a least mean square (LMS) equalizer to compensate for PMD.

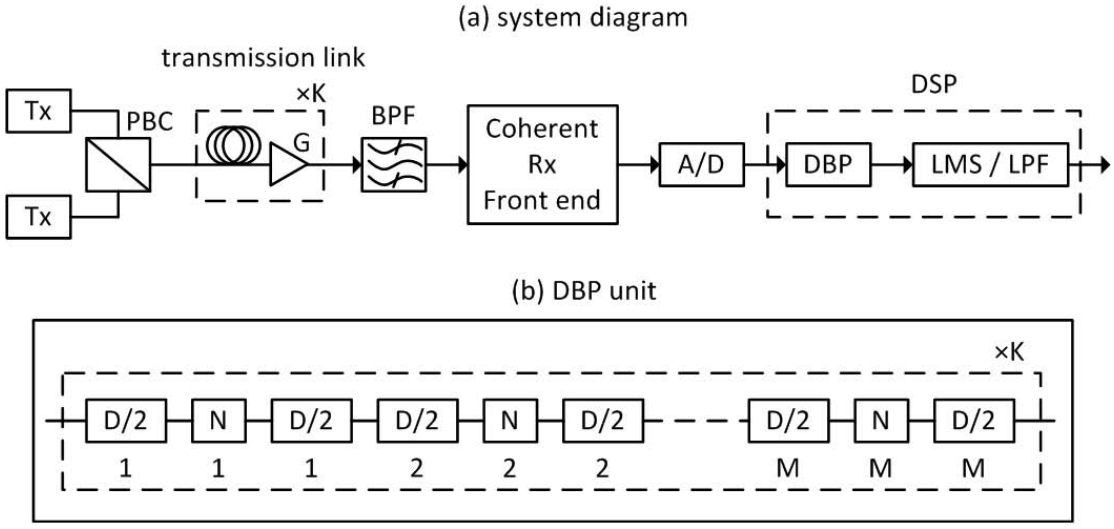

Figure 3.5: (a) Block diagram of a fiber-optic link with DBP; (b) The dispersion and nonlinear operator in DBP. PBC: polarization beam combiner, BPF: band pass filter, LMS: least mean square equalizer, LPF: low pass filter.

3.4 Simulation results and discussions

Monte-Carlo simulations of a single-channel dual-polarization fiber optic system with DBP at the receiver are carried out. 25 Gbaud per polarization and 16-QAM signal

is used in the simulation. Total number of symbols is 32768 symbols per polarization. Standard single mode fiber (SSMF) is used as the transmission fiber with following parameters, $\alpha = 0.046$ km^{-1}, $\beta_2 = -21$ ps^2/km, $\gamma = 1.1$ W^{-1}km^{-1}, and the PMD parameter $D_p = 0.04$ ps/$\sqrt{\text{km}}$. The amplifier spacing L_a is 80 km, the gain of the amplifier is 16 dB and the spontaneous emission noise factor n_{sp} is 1.5. Eight and two samples per symbol are used for optical forward propagation and digital processing, respectively, unless otherwise specified. A second order Gaussian filter with 50 GHz bandwidth (band pass filter (BPF) in Fig. 3.5a) is used before the coherent receiver. The polarization diversity coherent receiver provides four outputs: I and Q components of each polarization. These outputs after DBP pass through an adaptive equalizer based on decision-directed LMS algorithm. The adaptive equalizer calculates the inverse Jones matrix adaptively and compensates for the polarization rotation, phase shift and delay between polarization components [92]. Number of taps of the LMS equalizer is 12 and the number of training symbols per polarization is 15360. The symbol sequence after the equalizer is compared with the symbol sequence at the transmitter and those symbols which have crossed the boundaries are counted as error symbols.

The forward propagation is simulated in two different ways-with vector NLSE and random rotational matrix between fiber sections (case 1), and with Manakov equations (case 2). For both cases, standard SSFS is used for simulation with a nonlinear phase per step of 0.0005 rad. For case 2, LMS equalizer is not required since there is no PMD in the system. Instead a second order Gaussian low pass filter (LPF) with 20 GHz bandwidth is used to limit the noise.

Let us first consider case 1. Fig. 3.6 shows the BER as a function of the launch

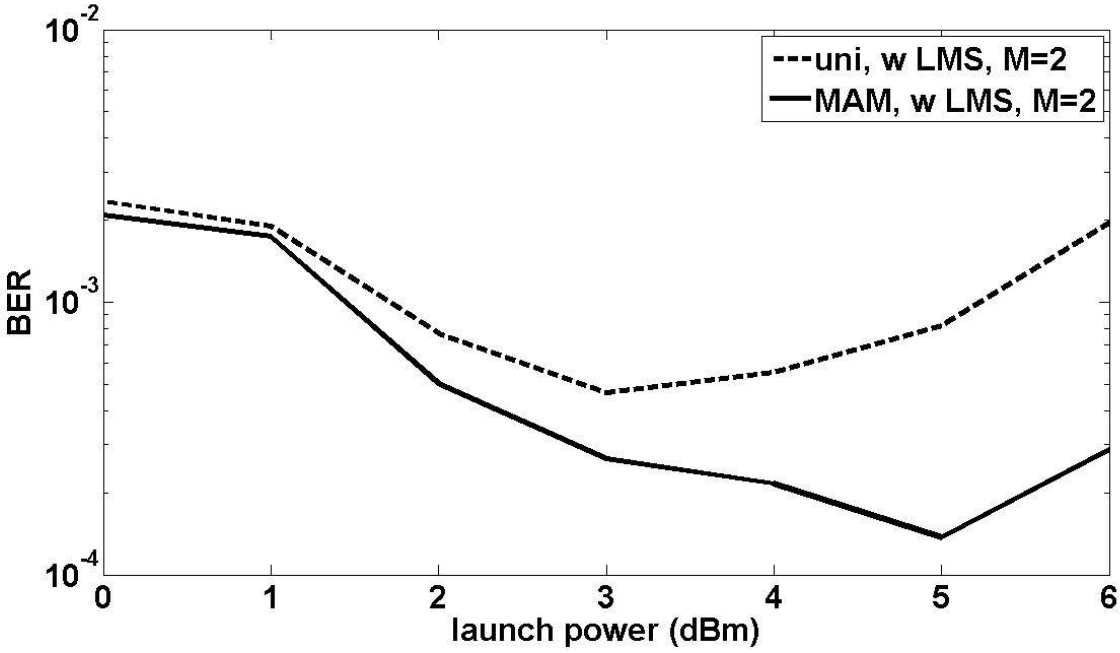

Figure 3.6: BER versus launch power when vector NLSE is used for forward propagation and LMS adaptive equalizer is introduced to remove PMD after DBP. Transmission distance = 2800 km. 2 samples/symbol is used. M: number of steps per span.

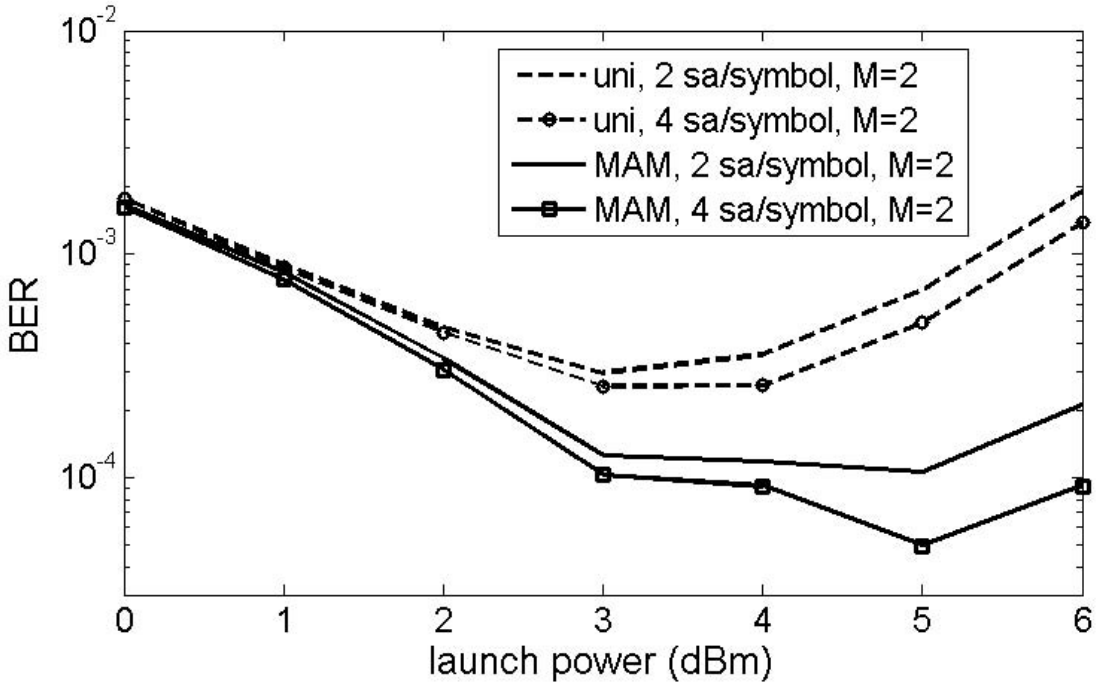

Figure 3.7: BER versus launch power when Manakov equation is used for forward propagation. Transmission distance = 2800 km. Optical signal-to-noise ratio (OSNR) is 24.2 dB when launch power is 3 dBm.

power to the SSMF at 2800 km transmission distance. The number of steps per span M is 2 in DBP. The solid line and dashed line show BER versus launch power when the MAM and uniform spacing methods are used in DBP, respectively. As can be seen, the DBP with MAM method outperforms that using uniform spacing method at the same computational cost. When the launch power is less than 1 dBm, the performance of the two techniques are almost the same, but DBP with MAM is better when launch power is large and nonlinearity becomes dominant. Fig. 3.7 shows BER as a function of launch power at the same transmission distance except that the Manakov equations are solved in the forward propagation (case 2). Although the LMS equalizer can effectively mitigate linear PMD impairments, neither LMS nor DBP compensates for the PMD-nonlinearity interactions. Hence, comparing Fig. 3.6 and Fig. 3.7, with 2 samples per symbol, we see that the performance is slightly worse at larger launch power for case 1, for both uniform spacing and MAM techniques. When 4 samples per symbol are used, the Q-factor is improved by 0.1 dB and 0.4 dB for uniform and MAM schemes, respectively (as compared with 2 samples per symbol).

The minimum BER (such as the minimum point in Fig. 3.7) is plotted as a function of the transmission reach in Fig. 3.8 with different M. As M increases, the maximum reach increases. The MAM technique has a longer reach than that of the uniform spacing case. When $M = 2$, the maximum transmission distance at the forward error correction (FEC) limit of BER $= 2.1 \times 10^{-3}$ is limited to 4300 km for the uniform spacing, which can be extended to 5200 km with the MAM technique. Also, the transmission reach of the uniform spacing case is 5600 km and 6480 km when $M = 3$ and $M = 4$, respectively, which can be increased to 6640 km and 6880

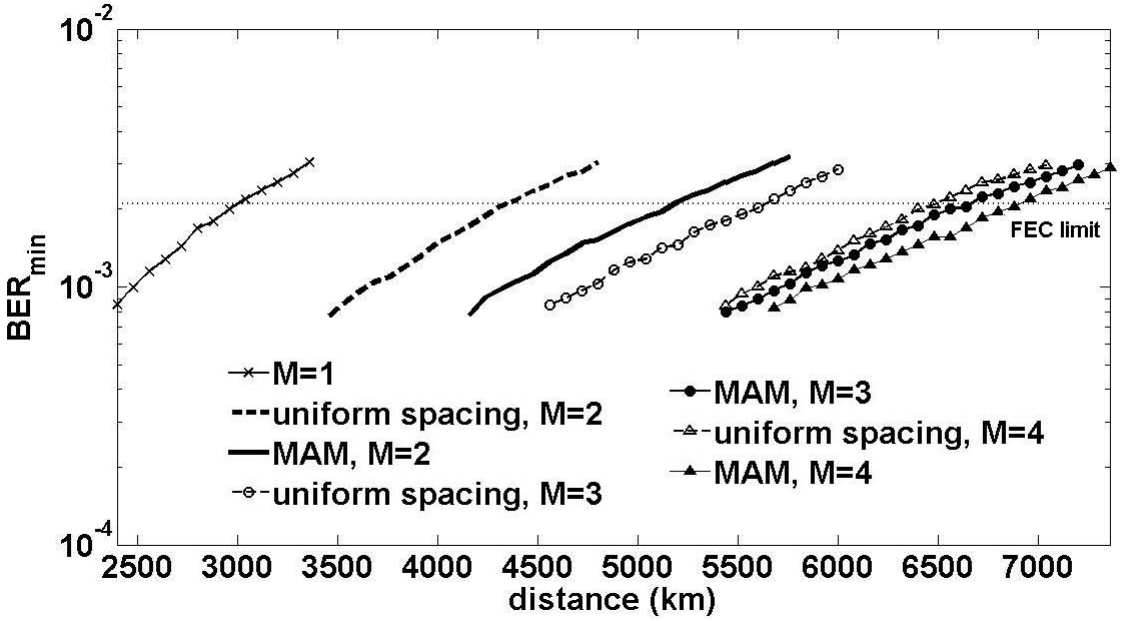

Figure 3.8: BER versus transmission distance. Manakov equation is used for forward propagation. 2 samples/symbol is used.

km, respectively, by using the MAM method. So, only optimizing the parameters of DBP without additional computational cost and system complexity, MAM technique can make a better compensation of the fiber dispersion and nonlinearity compared with the uniform spacing method.

Next, we consider a wavelength division multiplexing (WDM) system with the following additional parameters: number of channels = 5, channel spacing = 100 GHz, a second order Gaussian filter with a bandwidth of 50 GHz is used to demultiplex channels. Coupled vector NLSEs [78] without FWM are solved in digital domain with 2 samples per symbol. As pointed out in [58], the step size of a WDM system has to be really small (of the order of 3 km for uniform spacing). Therefore, we considered a relatively larger M in our WDM simulation. Fig. 3.9 shows the BER versus launch power per channel. As can be seen, the performance improvement is larger with

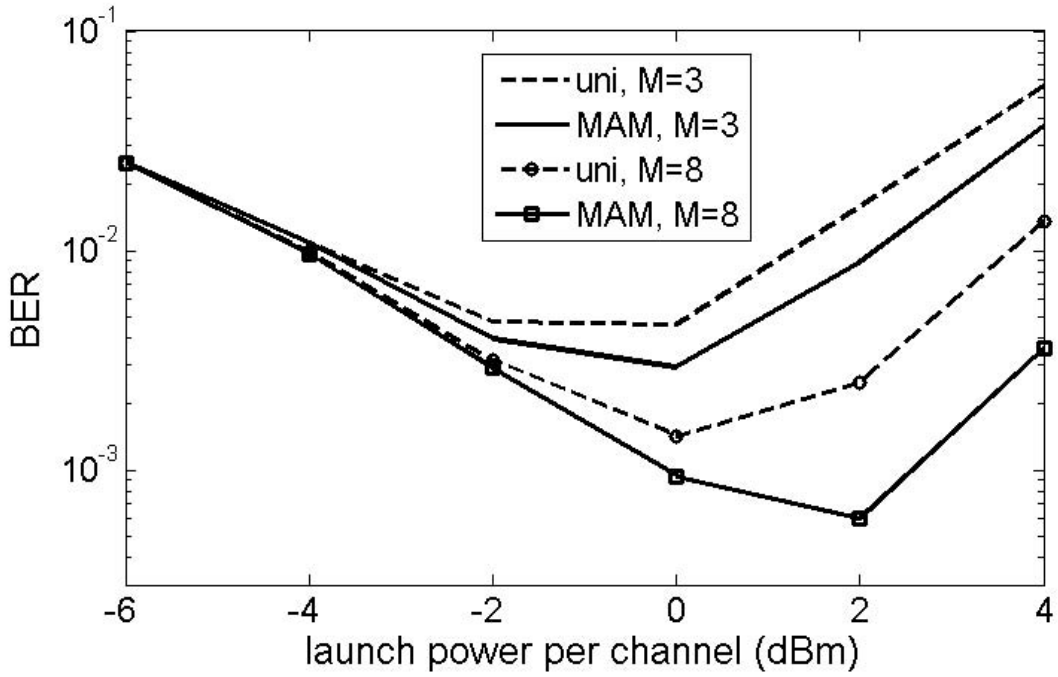

Figure 3.9: BER versus launch power per channel for a WDM system. Transmission distance = 2000 km. 2 samples/symbol is used. OSNR is 22.5 dB when launch power is 0 dBm.

MAM, $M = 8$ as compared to the case of $M = 3$. Relatively smaller improvement for $M = 3$ with MAM is due to the fact that WDM nonlinear impairments are much stronger when the step sizes are larger and both uniform and MAM schemes do not provide substantial improvements.

3.5 Conclusions

We have investigated a DBP scheme to compensate for the dispersion and nonlinearity of the transmission fibers. By optimizing the step size of each section through minimizing the area mismatch between the exponential profile of the effective nonlinear coefficient and its stepwise approximation, a better system performance can be obtained without additional computational cost and system complexity. The optical forward propagation is simulated in two different ways: (i) vector NLSE with random polarization rotation. (ii) Manakov equations. An adaptive LMS equalizer is employed after the DBP to compensate for the randomly changing birefringence when the vector NLSE is used for forward propagation. The simulation results show that the two approaches have almost the same performance, except that PMD-nonlinearity interaction results in a slight degradation for case (i). In both the approaches, DBP with uniform spacing and MAM are simulated and results show that the MAM technique can increase the system reach significantly as compared to the uniform spacing.

Chapter 4

Optical back propagation for fiber-optic communications using optical phase conjugation at the receiver

4.1 Introduction

The compensation of fiber dispersion and nonlinear effects in either the optical or electrical domain has drawn considerable attention [56, 57, 70, 72, 74]. Midpoint OPC can undo the distortion due to dispersion and nonlinearity, if the nonlinearity, dispersion, and power profiles are symmetric with respect to the location of the OPC [70]. Although the midpoint OPC could provide substantial benefits to the point-to-point links, they are not suitable for optical networks since the midpoint cannot be

defined. With the advent of coherent detection, the receiver has access to the complex optical field envelope and hence, DBP can be used to compensate fiber distortions [56, 57]. DBP is found to be effective in mitigating intra-channel impairments. However, to compensate the nonlinear impairments of a WDM system in real time, DBP would require enormous amounts of computational resources. An OBP scheme employing DCFs and HNLFs has been investigated [74]. Although the OBP provides very good transmission performance, it requires pumps and polarization alignment of the pumps with signal, which increases the complexity of the receiver. In this chapter, we consider an improved form of the OBP that does not require pumps. The OBP module consists of an OPC followed by short lengths of HDFs and HNLFs. The HDF provides the accumulated dispersion that is the same as the corresponding transmission fiber section and the set of HDF and HNLF provides a nonlinear phase shift that is the same as the corresponding transmission fiber section. Also, another OBP scheme consisting of OPC, fiber Bragg grating (FBG) and highly nonlinear fiber (HNLF) is investigated in this chapter. In this scheme, we extend the approach of [93] for arbitrary step sizes and find an optimal step size for OBP using the MAM constraint and the method of Lagrange multipliers. We find that the transmission performance can be significantly improved when the OBP section lengths are chosen using MAM as compared to uniform section lengths, for the given number of sections. In the case of DBP, step size can also be changed to improve the performance. The step size could be adaptively chosen to keep the error within a certain tolerance level [77] or an iteration technique [94] could be used to improve the performance. The MAM technique can be used to minimize the computational efforts of DBP as well (see Chapter 3). However, for OBP, the techniques presented in Ref. [77] and [94]

cannot be implemented easily as they require feedback loops. Using the MAM technique, the optical component count in the OBP system can be reduced as compared to the uniform step size, to achieve the same performance. The OBP has the following advantages.(1) It provides compensation in real time whereas the DBP is currently limited to off-line signal processing because of extensive computational requirements. (2) A very large bandwidth (∼4 THz) is available for OBP while the bandwidth of the DBP is limited by the bandwidth of the coherent receiver.

4.2 OBP for fiber optic communications using OPC, HDFs and HNLFs

4.2.1 System setup

The evolution of the optical field envelope in a fiber-optic system is described by the NLSE

$$\frac{\partial q}{\partial z} = i\left[D(t) + N(q)\right] q(t,z), \tag{4.1}$$

$$D(t) = -\frac{\beta_2}{2}\frac{\partial^2}{\partial t^2}, \tag{4.2}$$

$$N(q) = \gamma|q(t,z)|^2 + i\frac{\alpha}{2}, \tag{4.3}$$

Consider a single span of a transmission fiber of length L_a.The output field of the fiber may be written as

$$q(t, L_a) = \exp\left\{ i \int_0^{L_a} [D(t) + N(q)]\, dz \right\} q(t, 0) \tag{4.4}$$

$$= Mq(t, z). \tag{4.5}$$

Here, M is the transfer function of the fiber-optic link. To compensate for the distortion due to fiber dispersion and nonlinear effects, an OBP module is placed at the end of the fiber-optic link, as shown in Fig. 4.1(a). If the transfer function of the OBP is inverse of that of the fiber-optic link, we recover the initial field envelope at the output of the OBP. However, OBP module with transfer function

$$M^{-1} = \exp\left\{ -i \int_0^{L_a} [D(t) + N(q)]\, dz \right\} \tag{4.6}$$

is not available, because the fiber nonlinear coefficient is positive. Then, let the output of the transmission fiber be phase-conjugated using an OPC, so that

$$q^*(t, L_a) = \exp\left\{ -i \int_0^{L_a} [D(t) + N^*(q)]\, dz \right\} q^*(t, 0). \tag{4.7}$$

The conjugated signal $q^*(t, L_a)$ will pass through an OBP fiber that is identical to the transmission fiber except that its loss profile (or equivalently, the power profile) is inverted. In other words, the nonlinear operator corresponding to the OBP fiber is

$N^*(q)$. The output of the OBP fiber is

$$\begin{aligned} q_{OBP,out} &= e^{i\int_0^{L_a}[D(t)+N^*(q)]dz} q^*(t, L_a), && (4.8) \\ &= e^{i\int_0^{L_a}[D(t)+N^*(q)]dz} e^{-i\int_0^{L_a}[D(t)+N^*(q)]dz} q^*(t, 0), && (4.9) \\ &= q^*(t, 0). && (4.10) \end{aligned}$$

Thus, the input field envelope can be recovered at the receiver after performing a phase conjugation in electrical domain. Eq. (4.8) is equivalent to

$$\frac{\partial q_b}{\partial z} = i[D(t) + N^*(q_b)]q_b, \tag{4.11}$$

with $q_b(t, 0) = q^*(t, L_a)$. Using a transformation $q_b = e^{\alpha z/2}u_b$, Eq. (4.11) can be written as

$$i\frac{\partial u_b}{\partial z} - \frac{\beta_2}{2}\frac{\partial^2 u_b}{\partial t^2} + \gamma'(z)|u_b|^2 u_b = 0, \tag{4.12}$$

where

$$\gamma'(z) = \gamma \exp(\alpha z) \tag{4.13}$$

is the effective nonlinear coefficient. Eq. (4.12) is equivalent to

$$\frac{\partial u_b}{\partial z} = i[D(t) + N'(u_b)]u_b(t, z), \tag{4.14}$$

where $u_b(t, 0) = u^*(t, L_a)$, $u(t, z) = \exp(\alpha z/2)q(t, z)$, and

$$N'(u_b) = \gamma'(z)|u_b|^2 = \gamma \exp(\alpha z)|u_b|^2. \tag{4.15}$$

By solving Eq. (4.14),

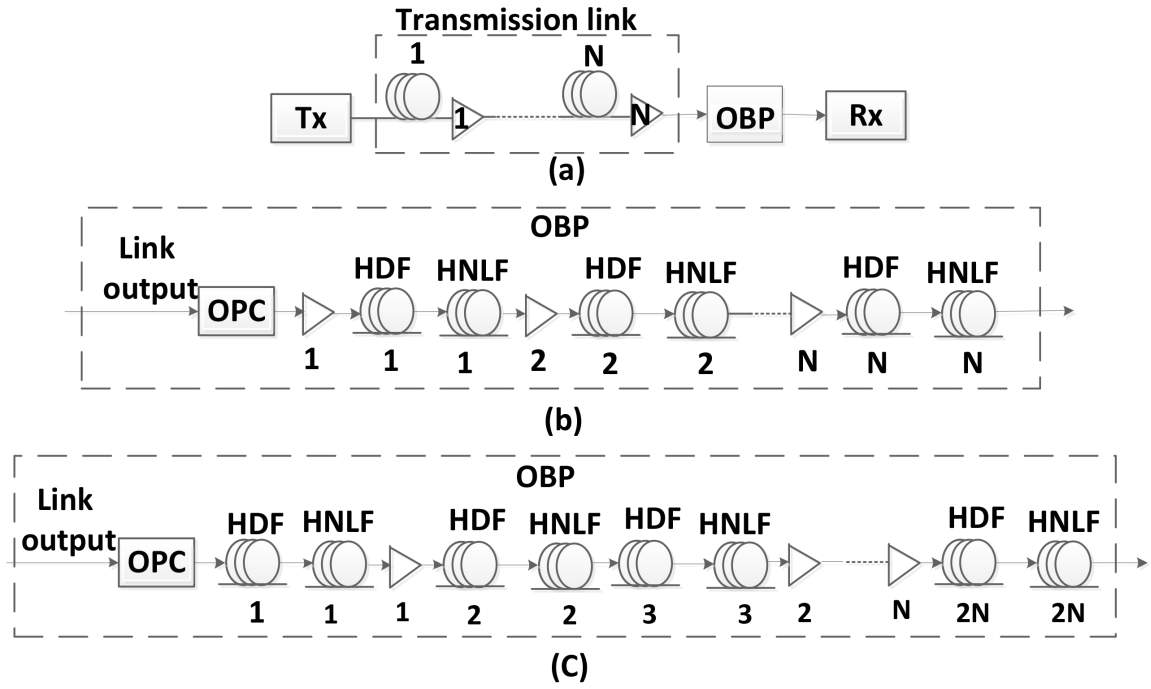

Figure 4.1: (a) Schematic of a fiber-optic link with OBP; (b) block diagram of the OBP with stepsize= L_a; (c) block diagram of the OBP with stepsize= $L_a/2$. TX, transmitter; RX, receiver.

$$\begin{aligned} u^*_{OBP,out}(t) &= e^{i\int_0^{L_a}[D(t)+N'(u_b)]ds}u^*(t,L_a), \\ &= M'u^*(t,L_a), \\ &= u^*(t,0), \end{aligned} \tag{4.16}$$

where M' is the channel matrix of the optical equalizer. We utilize a split-step Fourier technique with a step size of Δz [22], and

$$M' \approx A(t)\cdot B(t,\Delta z)\cdot A(t)\cdot B(t,2\Delta z)\cdot \ldots \cdot A(t)\cdot B(t,L_a), \tag{4.17}$$

where

$$A(t) = \exp\left[iD(t)\cdot\Delta z\right], \tag{4.18}$$

$$B(t,x) = \exp\left[i\int_{x-\Delta z}^{x}\gamma\exp(\alpha z)|u_b(t,z)|^2dz\right]. \tag{4.19}$$

The solution of Eq. (4.14) is $u_b(t,L_a) = u^*(t,0)$. Hence the complex field envelope at the transmitter can be recovered by taking the complex conjugate of the output of the OBP in electrical domain.

Here, $A(t)$ and $B(t,x)$ are the operators corresponding to the fiber dispersive effect over a length Δz and the nonlinear effect over the interval $[x-\Delta z \;\; x]$. Typically, $\exp(\alpha z)$ varies more rapidly than $|u_b(t,z)|^2$, and therefore, $|u_b(t,z)|^2$ can be approximated to be independent of z and now the integral in Eq. (4.19) can be evaluated analytically as [74],

$$B(t,x) = \exp\left[i\gamma\Delta z_{eff}(\Delta z)\exp(\alpha x)|u_b(t,x)|^2\right], \tag{4.20}$$

where

$$\Delta z_{eff} = \frac{1 - e^{-\alpha \Delta z}}{\alpha}, \tag{4.21}$$

If there are multiple spans in fiber optic link. The first OBP module will compensate for the distortion brought by the last fiber span, and the second OBP module will compensate for the impairment due to the second last span of the transmission fiber. We try to realize the functions of operator A and B in optical domain. The operator A can be realized using a HDF as shown in Fig. 4.1(b), if its nonlinearity is ignored. Later we will discuss the impact of the HDF nonlinearity. Since the dispersion of the transmission fibers are only compensated by HDF, the length of HDF in each step can be easily calculated as

$$L_{HDF} = \frac{|\beta_{2,TR}| \Delta z}{|\beta_{2,HDF}|}, \tag{4.22}$$

The operator B is realized using a dispersion-shifted HNLF [95]. The HNLF introduces a nonlinear phase shift, which is the same as that of a corresponding transmission fiber of length Δz, if the nonlinearity of the HDF is absent. For example, if $\Delta z = L_a$, the first HNLF provides the same nonlinear phase shift as that accumulated over the last span of the fiber-optic link. The transmission in HNLF is described by

$$u_{HN,out} = u_{HN,in} e^{i\gamma_{HN} L_{HN,eff} |u_{HN,in}|^2}, \tag{4.23}$$

$$L_{HN,eff} = \frac{1 - \exp(-\alpha_{HN} L_{HN})}{\alpha_{HN}}, \tag{4.24}$$

where α_{HN}, γ_{HN} and L_{HN} are the loss coefficient, nonlinear coefficient and length of the HNLF, respectively. From Eq. (4.23), the total phase shift introduced by HNLF is $\gamma_{HN} L_{HN,eff} |u_{HN,in}|^2$. If the launch power to the HNLF is increased, its length can

be reduced to have a fixed nonlinear phase shift. As a result, the insertion loss of HNLF can be reduced by decreasing its length. Therefore, an amplifier is introduced after the OPC (see Amp.1 in Fig. 4.1(b)). To offset the loss due to HDF and HNLF, a tiny amplifier is introduced after the HNLF (see Figs. 4.1(b) and 1(c)).

Since the HDF will also introduce nonlinear phase shift, now we will consider the HDF nonlinearity. Let us first consider the case of $\Delta z = L_a$ in the presence of the HDF nonlinearity. Let the nonlinear phase shifts of HDF$_j$, HNLF$_j$ and the transmission fiber, $N - j + 1$ be ϕ_{HDF}, ϕ_{HN} and ϕ_{TR}, respectively. The set of HDF$_j$ and HNLF$_j$, $j = 1, 2, \ldots, N$ compensates for the nonlinear phase shift of the corresponding transmission fiber, $N - j + 1$. Then, we have

$$\phi_{TR} = \phi_{HDF} + \phi_{HN}, \tag{4.25}$$

where

$$\phi_r = \gamma_r P_r L_{r,eff}, \tag{4.26}$$

and

$$L_{r,eff} = \frac{1 - \exp(-\alpha_r L_r)}{\alpha_r}. \tag{4.27}$$

r = HDF, HN, TR and P_r is the launch power to the fiber type r. Using Eq. (4.26) in Eq. (4.25), we find

$$L_{HN,eff} = \frac{\phi_{TR} - \phi_{HDF}}{\gamma_{HN} P_{HN}}. \tag{4.28}$$

If the dispersion of the HDF were to be zero, Eq. (4.28) holds true exactly. However, because of the large dispersion of the HDF, Eq. (4.28) is approximate and it should be used as a rough guide to optimize the HNLF length.

For the case of $\Delta z = L_a/2$, the first set of HDF and HNLF in Fig. 4.1(c) compensates for the nonlinear effects of the second half of the last span of the transmission fiber. Since the nonlinear phase shift due to the second half is quite small, we do not really need an amplifier following the OPC. So, the first amplifier is placed after the first set of the HDF and HNLF (see Fig. 4.1(c)). The analytical length of HDFs and HNLFs can be calculated as before. Also, the lengths of HDFs which are calculated analytically can be used directly and the lengths of HNLFs need to be optimized numerically.

It is desirable that the HDF and HNLF have high dispersion and high nonlinearity, respectively and they are of the shorter lengths so that their insertion losses are minimum. If the SSMF is used as the transmission fiber, the dispersion of the HDF should be anomalous. However, a HDF with anomalous dispersion is not commercially available. Instead, in this subsection, we have used the negative dispersion fiber (NDF) [96] as the transmission fiber so that the conventional DCF with high normal dispersion can be used as the HDF.

In this thesis, we neglect the higher-order dispersion while introducing OBP, since it can be compensated in digital domain.

4.2.2 Simulation results and discussions

We simulated a single-channel fiber-optic system with the following parameters: symbol rate = 25 Gsymbols/s, modulation=32 QAM, transmission fiber dispersion $\beta_2 =$ 5ps^2 /km, transmission fiber loss = 0.2 dB/ km, nonlinear coefficient $\gamma = 2.2\text{W}^{-1}$ km^{-1}, amplifier spacing L_a =80 km, spontaneous emission noise factor $n_{sp} = 1.5$. The parameters of the OBP module at the receiver side are: dispersion of the HDF

= 140 ps^2 /km, loss of the HDF = 0.4 dB/ km, nonlinear coefficient of the HDF = 4.4 W^{-1} km^{-1}, loss of the HNLF = 0.3 dB/m, and the nonlinear coefficient of the HNLF = 2000 W^{-1} km^{-1}. To simulate pulse propagating in fibers, standard SSFS is used with a nonlinear phase per step of 0.0005 rad.

We employ two OBP step size realizations to compensate for the fiber impairment in the transmission link. One is that the step size equals to the amplifier spacing L_a; the other is that the step size equals to half the amplifier spacing. In the case of $\Delta z = L_a$, we numerically optimized the gain of the first amplifier to obtain the best performance. The optimum gain is found to be 4.8 dB. Then, we optimized the HNLF length numerically to obtain the minimum BER. We found the optimum HNLF length as 3.1 m at the transmission fiber launch power of 1 dBm. The analytical length found using Eq. (4.28) is 3.2 m in good agreement with numerics. Total loss due to HDF and HNLF is 2.07 dB, which is compensated by the in-line amplifiers in OBP. The amplifiers in OBP have a n_{sp} of 1.5.

In the case of $\Delta z = L_a/2$, the gain of the first amplifier and lengths of HNLFs are numerically optimized. The first amplifier compensates for the loss of the first set of HDF and HNLF, and it gives an excess gain. The optimum excess gain is 3 dB. At 1 dBm transmission fiber launch power, the numerically optimized lengths of HNLF_1, HNLF_2, HNLF_3 are 0.28 m, 10.6 m, and 2.4 m, respectively. The corresponding analytical lengths are 0.28 m, 11.9 m and 1.5 m, respectively.

Fig. 4.2 shows the BER as a function of the launch power in different system configurations when the transmission distance is 800 km. The dashed line and the solid line represent the BER of the OBP with step size equaling to L_a and $L_a/2$, respectively. In order to compare the OBP with the other schemes, we calculated the

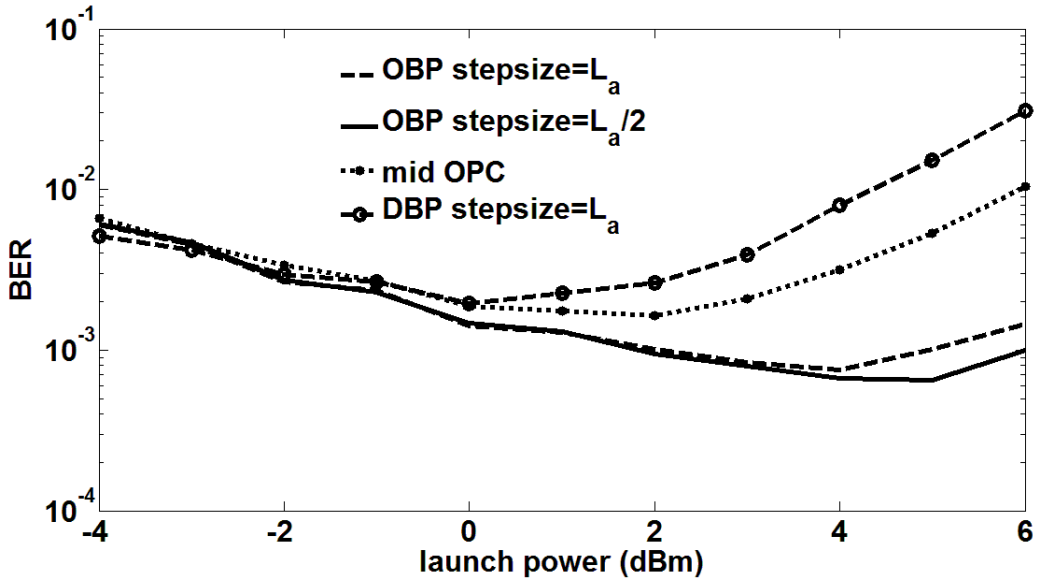

Figure 4.2: BER Vs launch power. Transmission distance = 800 km.

BER of the DBP with $\Delta z = L_a$ and the midpoint OPC. The scheme of midpoint OPC is shown in Fig. 4.3. In the single-channel simulation of the system based on

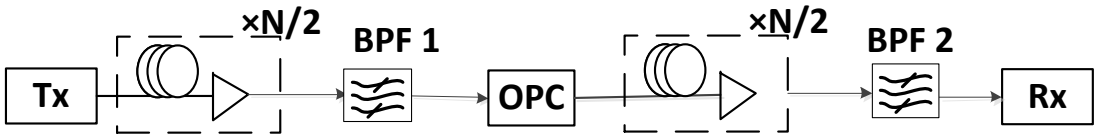

Figure 4.3: Schematic of midpoint OPC.

DBP, eight samples per symbol are used in the transmission link and after the analog to digital converter (ADC), two samples per symbol are used. As shown in Fig. 4.2, the four schemes have almost the same performance if the launch power is less than 0 dBm when the nonlinear effects are small. Beyond 0 dBm launch power, OBP with $\Delta z = L_a/2$ has the best tolerance to nonlinearity. When the step size equals L_a, the minimum BER for OBP is 8×10^{-4}, while the minimum BER for DBP is about

2×10^{-3}. The relatively poor performance of the DBP as compared to the OBP is mainly attributed to the fact that the nonlinear HDF in OBP provides distributed nonlinearity compensation and partly due to the lower number of samples per symbol of DBP [57]. Midpoint OPC does not perform well enough due to the unsymmetrical power profile with respect to the location of the OPC.

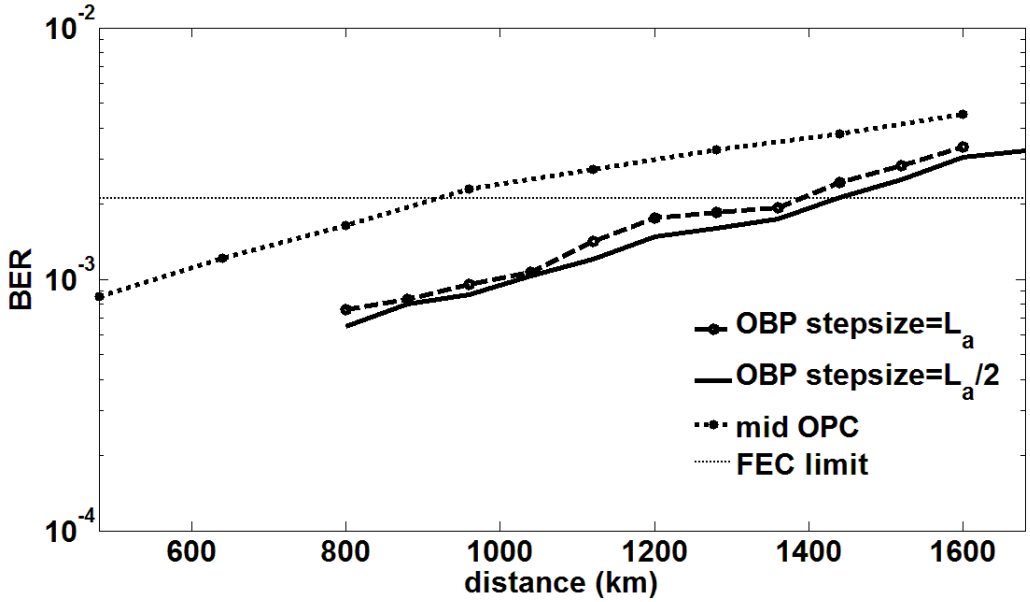

Figure 4.4: BER Vs transmission distance.

For different distances, a minimum BER (see Fig. 4.2) can be obtained for each scheme by optimizing the launch power. Fig. 4.4 shows the dependence of the minimum BER on the transmission distance. Using the midpoint OPC, the maximum reach is about 880 km, which can be increased to 1360 km with OBP, $\Delta z = L_a$ and to 1440 km with OBP, $\Delta z = L_a/2$.

4.3 OBP with optimal step size for fiber optic transmission systems using OPC, FBGs and HNLFs

4.3.1 System setup

In this subsection, we developed another OBP scheme using FBGs and HNLFs. Since the dispersion coefficient of FBGs can be negative, standard single mode fibers are used as transmission fibers. From Eqs. (4.12) and (4.13), if the effective nonlinear coefficient, $\gamma'(z)$ of the OBP fiber increases exponentially with distance (or equivalently, optical power increases exponentially with distance), the output of the OBP fiber would be the conjugate of the transmitter output in the absence of noise. But it is hard to design a fiber with such a property. Instead, we divide the OBP fiber into M sections of length l_j, $j = 1, 2, \ldots, M$. If the sections are sufficiently small, the propagation in each of the sections is approximated by a single symmetrical SSFS, i.e.,

$$u_b(t, z_{j-1} + l_j) \cong e^{iD(t)l_j/2} e^{i\int_{z_{j-1}}^{z_{j-1}+l_j} \gamma'(z)|u_b(t,z)|^2 dz} e^{iD(t)l_j/2} u_b(t, z_{j-1}), \tag{4.29}$$

$z_j = \sum_{k=1}^{j} l_k$, $z_0 = 0$ and $z_M = L_a$. We use symmetrical SSFS in this subsection since it can obtain higher accuracy. The dispersion operator is realized by the FBG with $\gamma = 0$ and the nonlinear operator is realized by the dispersion-shifted HNLF with $\beta_2 = 0$. We consider two cases.

Case (i) Uniform spacing: The OBP fiber has M equal sections of lengths $l_j = L_a/M$, $j = 1, 2, \ldots, M$. Each section of the OBP fiber is realized by a combination of FBGs and HNLF. The accumulated dispersion, ξ_j and nonlinear phase shift, ϕ_j of

the jth section provided by FBGs and HNLF, respectively, are

$$\xi_j = \beta_2 l_j, \tag{4.30}$$

$$\phi_j = \gamma L_{eff,j}|q_{b,j}|^2 = \gamma_{HN} L_{HN,eff,j}|q_{b,j}^2|. \tag{4.31}$$

where

$$L_{eff,j} = \frac{e^{\alpha l_j} - 1}{\alpha}, \tag{4.32}$$

$$L_{HN,eff,j} = \frac{1 - e^{-\alpha_{HN} L_{HN,j}}}{\alpha_{HN}}, \tag{4.33}$$

$q_{b,j}$ is the input field of the jth section, γ_{HN}, α_{HN} and $L_{HN,j}$ are nonlinear coefficient, loss coefficient and length of the jth HNLF, respectively.

Case (ii) Minimum area mismatch (MAM): As shown in Fig. 4.5(b), exponentially increasing effective nonlinear coefficient, $\gamma'(z)$ (solid line) can be approximated by a stepwise increasing function (dashed line) using MAM method (see Chapter 3). In Fig. 4.5(b), we see that the area mismatch, Δ_1, for the first section is $a_1 + a_2$ where

$$a_1 = \gamma_1 x_0 - \gamma \left(\frac{e^{\alpha x_0} - 1}{\alpha} \right), \tag{4.34}$$

$$x_0 = \frac{1}{\alpha} \mathrm{In} \left(\frac{\gamma_1}{\gamma} \right), \tag{4.35}$$

$$a_2 = -\gamma_1 (l_1 - x_0) + \frac{\gamma e^{\alpha l_1} - \gamma_1}{\alpha}. \tag{4.36}$$

Total area mismatch of both the sections is $\Delta_1 + \Delta_2 = \sum_{j=1}^{4} a_j$. The section length l_j and effective nonlinear coefficients γ_1 and γ_2 are so chosen that $\Delta_1 + \Delta_2$ is minimum under the constraint that the total area under the exponential curve is same as that

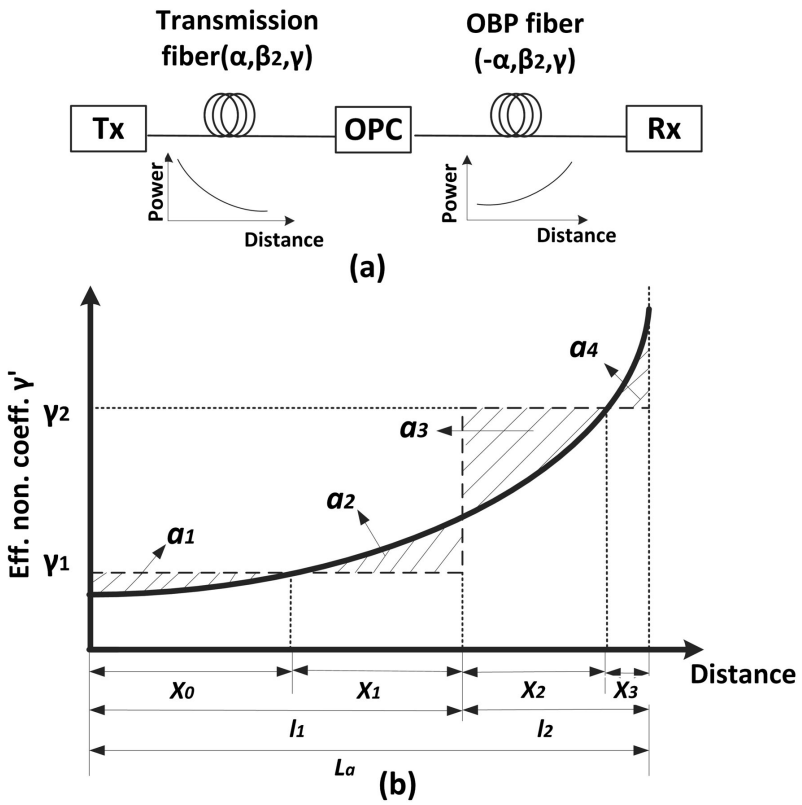

Figure 4.5: (a) Block diagram of a fiber-optic link with OBP; (b) Effective nonlinear coefficient and its stepwise approximation for the number of steps per span $M = 2$.

under the stepwise curve. The detailed optimization method can be found in Chapter 3 using the Lagrange multiplier. The results are that, for 2 steps per span case, when $\gamma = 1.1$ W^{-1}km^{-1}, $L_a = 80$ km, loss $= 0.2$ dB/km, $l_1 = 55.8$ km, $\gamma_1 = 4.81$ W^{-1}km^{-1}, $\gamma_2 = 27.3$ W^{-1}km^{-1} and $\lambda = -0.149$.

The propagation in each OBP fiber section is approximated by the SSFS. The nonlinear coefficient of the jth HNLF need not be γ_j, but the nonlinear phase shift imparted by the jth HNLF should be

$$\int_{z_{j-1}}^{z_{j-1}+l_j} \gamma'(z)|u_b(t,z)|^2 dz \cong \gamma_j l_j |u_b(t, z_{j-1})|^2, \tag{4.37}$$

$$\gamma_j l_j = \gamma_{HN} L_{HN,eff,j}, \quad j = 1, 2, \ldots, M. \tag{4.38}$$

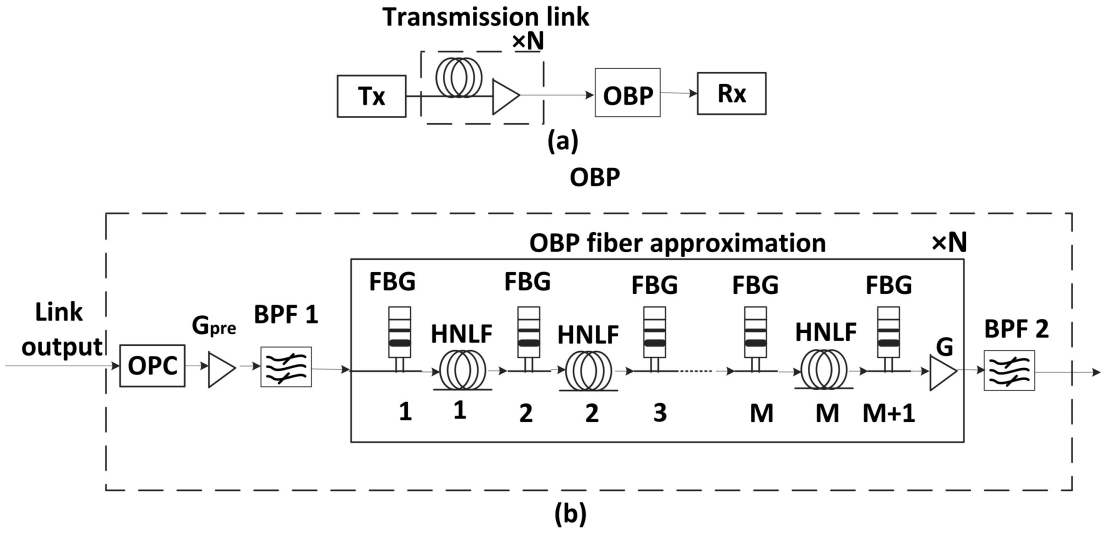

Figure 4.6: (a) Schematic of a fiber-optic link with OBP; (b) block diagram of the OBP. Tx, transmitter; Rx, receiver; BPF, bandpass filter.

So far we considered the compensation of dispersion and nonlinearity of a single-span fiber-optic link. Now we consider the compensation of a transmission system

consisting of multiple spans. Fig. 4.6(a) shows a schematic of a fiber-optic link consisting of N spans of transmission fiber and the OBP module. The OBP is applied after the whole transmission link. The schematic of the OBP module is shown in Fig. 4.6(b). The output of the OPC passes through a pre-amplifier of gain G_{pre} so that lengths of HNLFs can be reduced. As a result, the insertion loss of HNLFs can be reduced. A band pass filter BPF1 is introduced after the pre-amplifier to remove the out of band ASE noise. The OBP fiber shown in Fig. 4.5(a) is approximated by M sections consisting of FBGs and HNLFs. To compensate for the losses of FBGs and HNLFs, an amplifier of gain G is used. Since there are N spans in the transmission system, cascaded OBPs with each OBP consisting of M sections are required. A band pass filter BPF2 is introduced after the cascaded OBPs to maximize the signal-to-noise ratio (SNR).

4.3.2 Simulation results

We simulate a single-channel and single-polarization fiber-optic system with OBP at the receiver with 25 Gsym/s symbol rate and 32 QAM. SSMF is used as the transmission fiber, with the following parameters, $\beta_2 = -21$ ps^2/km, $\gamma = 1.1$ W^{-1}km^{-1}, and $\alpha = 0.046$ km^{-1}. The amplifier spacing L_a is 80 km and the gain of the amplifier is 16 dB. The spontaneous emission noise factor n_{sp} is 1.5 for all the amplifiers (in-line amplifiers as well as OBP amplifiers). Noise loading is done on the per amplifier basis. The parameters for OBP are as follows: loss of FBG = 1.8 dB [97], nonlinear coefficient of FBG = 0 W^{-1}km^{-1}, loss of the HNLF = 0.3 dB/m, dispersion coefficient of the HNLF = 0 ps^2/km and the nonlinear coefficient of the HNLF = 2000 W^{-1}km^{-1} [95]. The gain of the pre-amplifier G_{pre} is 14 dB. Gain of the amplifiers

in the cascaded OBP, G, is 5.7 dB when $M = 2$, which exactly compensates for the losses due to FBGs and HNLFs. In the case of $M = 2$, lengths of HNLFs are $L_{HN,1}$= 0.2036 (0.0963) m, $L_{HN,2}$ = 0.7876 (0.9534) m for MAM (uniform spacing). 8 and 2 samples per symbol are used for optical propagation (both forward and backward) and for digital processing, respectively. A coherent receiver is used with the local oscillator laser linewidth (=Transmitter laser linewidth)=22 kHz. A feedforward carrier recovery algorithm is used for phase estimation [98]. Digital filters are not used for dispersion compensation as the OBP compensates for dispersion. Second order Gaussian filters with bandwidths 80 GHz and 50 GHz are used prior to the OBP (BPF1 in Fig. 4.6(b)) and after the OBP (BPF2), respectively. Gain of the pre-amplifier and filter bandwidths are optimized to obtain the minimal BER. The gain of the pre-amplifier is so chosen that the power launched to the first FBG is 14 dB higher than the power launched to the transmission fiber. It is possible to choose a lower gain of the pre-amplifier and in that case, lengths of HNLFs become longer and because of the losses in HNLFs, there would be slight performance degradation.

Figure 4.7 shows the BER as a function of the SSMF launch power at 800 km. For a 10 span system and $M = 2$, 30 FBGs and 20 HNLFs are required for OBP to compensate for dispersion and nonlinearity of the whole transmission link. As can be seen, for the given M, the OBP system with sections designed using the MAM (Case 2) outperforms that designed using the uniformly spaced sections (Case 1). For $M = 2$ case, the minimum BER for MAM is 1×10^{-3}, while the minimum BER for uniform spacing scheme is 2×10^{-3}. For the case of $M = 3$, the minimum BER for MAM is 7×10^{-4}, and the minimum BER for uniform spacing scheme is about 1×10^{-3}. Also, from Fig. 4.7 we can see that the MAM scheme has a better nonlinear

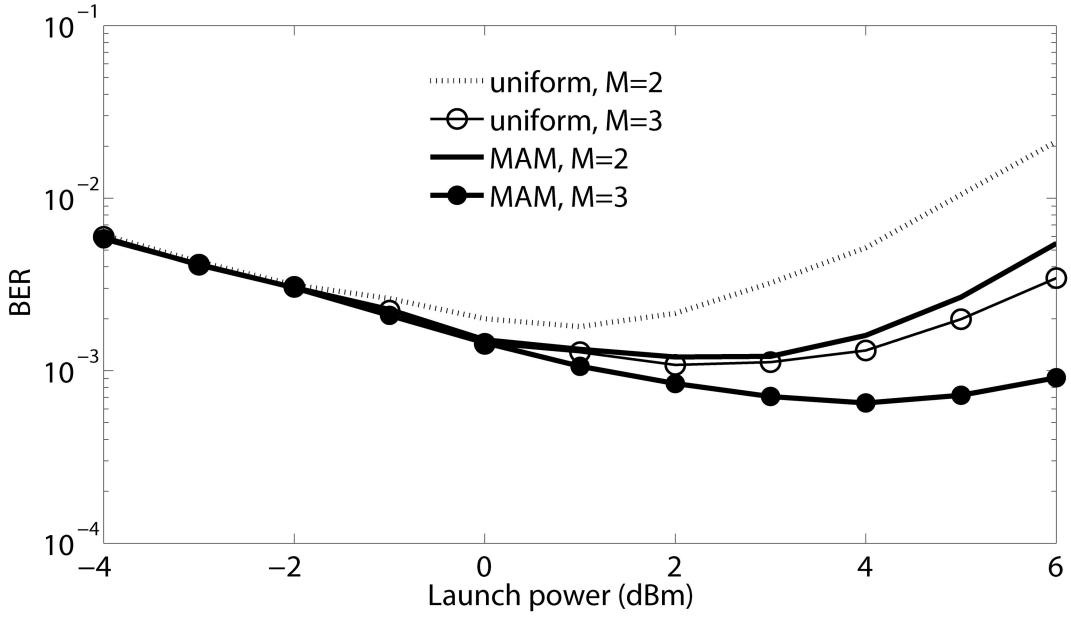

Figure 4.7: BER versus launch power for various OBP schemes. Transmission distance = 800 km.

tolerance.

The minimum BER (such as the minimum point in Fig. 4.7) is plotted as a function of the transmission reach in Fig. 4.8. At the FEC limit of 2.1×10^{-3}, the transmission reach is limited to 560 km for $M = 1$, which can be increased to 1200 km and 1680 km for $M = 3$ with uniform spacing and $M = 3$ with MAM, respectively. Thus, we see that the MAM technique leads to significant reach enhancement as compared to uniform spacing for the given M. If nearly ideal OBP is employed with lossless FBGs and HNLFs and a very small step size of 1 km, transmission reach can be increased to 2960 km. With MAM, $M = 8$, the maximum reach is 2880 km, which is 97% of the reach obtained using the nearly ideal OBP. For the case of nearly ideal OBP, the optimal signal launch power corresponding to the 2960 km transmission link is 6 dBm. If the system were to be linear, there should be no

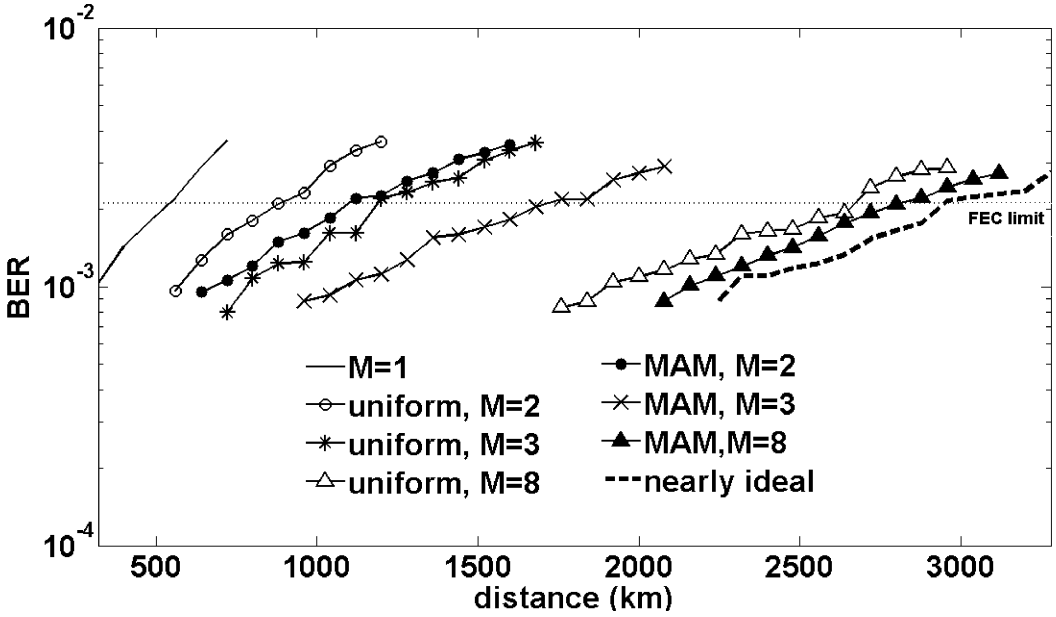

Figure 4.8: BER versus transmission distance for various OBP schemes.

limit on the achievable reach assuming that the launch power to the transmission fiber can be increased arbitrarily. The maximum reach of 2960 km for the nearly ideal case is due to signal-ASE nonlinear interaction. Although receiver-based ideal OBP can compensate for the deterministic (bit-pattern dependent) nonlinear effects exactly, signal-ASE nonlinear interaction cannot be compensated for by the receiver-based ideal OBP. In addition, the interaction of PMD and nonlinearity could lead to performance degradations which cannot be recovered by the ideal OBP. However, this effect is not considered in our simulation. All the fibers or optical devices in this chapter are assumed to be ideal. However, in real implementation, there may be fluctuation of the length of HDF and HNLF; the optical phase conjugator may introduce signal distortion; there will be group delay ripple for FBGs, and etc. All these may degrade the system performance, but we can use DSP to compensate for the distortions.

4.4 Conclusions

In conclusion, we have investigated an optical back propagation scheme to compensate for fiber dispersion and nonlinearity. The optical transmission system consists of transmission fibers, an OPC, and an OBP module. The OPC is used to obtain the conjugated signal of the fiber output, which makes compensation of fiber distortions by OBP realizable. The OBP module is a concatenation of HDFs and HNLFs, and it is similar to solving the NLSE in optical domain. When the step size equals to the span length, the OBP scheme outperforms that of the DBP with the same step size. The OBP performance can be further improved by using a smaller step size without bringing extra computational cost.

Also, we have developed another optical back propagation scheme to compensate the dispersion and nonlinearity of the transmission fibers in real time. The scheme consists of an optical phase conjugator, fiber Bragg gratings and highly nonlinear fibers. Each span of the transmission fiber can be divided into M sections and, the dispersion and nonlinearity of the each section are compensated for by fiber Bragg gratings and a highly nonlinear fiber, respectively. We have developed a technique to find the optimal step size (lengths of each section) using the minimum area mismatch constraint and the method of Lagrange multipliers. The results indicate that for the given M, the OBP system with sections designed using the proposed MAM technique outperforms that designed using the uniformly spaced sections. This implies that for the given transmission performance, the number of optical components can be reduced using MAM as compared to uniform spacing. The MAM technique also leads to significant reach enhancement as compared to uniform spacing for the given step size.

Chapter 5

Ideal optical back propagation using dispersion-decreasing fiber

5.1 Introduction

The maximum reach of a long haul fiber optic system with advanced modulation formats is mainly limited by fiber nonlinear impairments. The back propagation techniques can be used to compensate for dispersion and nonlinear effects of the transmission fiber (TF). The compensation schemes can be divided into three types: digital [56–58, 60, 61, 79, 80, 87–89, 99], optical [74, 81, 93, 100–104], and the combination of both [72]. The OBP has many advantages/disadvantages over DBP. (i) A very large bandwidth ($\sim$ 4 THz) is available for OBP while the bandwidth of the DBP is limited by the bandwidth of the coherent receiver. (ii) DBP requires significant computational resources, especially for WDM systems and hence it is currently limited to off-line signal processing. In contrast, OBP provides compensation in real

time and it can compensate for nonlinear impairments in WDM systems. (iii) Number of samples per symbol available for DBP is limited by the sampling rate of the ADC. Although it is possible to do upsampling on the digital signal processor, it leads to additional computational complexity. However, for OBP, the signal processing is done on the analog optical waveform. (iv) OBP requires a real fiber which has loss. So, amplifiers are needed to compensate for fiber loss in the OBP section which increases the noise in the system.

In [81, 93], an OBP scheme consisting of OPC, DCF/FBG, and highly nonlinear fiber (HNLF) is investigated. DCF/FBG is used to compensate for dispersion, and HNLF is used to compensate for nonlinearity. The dispersion and nonlinear effects are compensated in a split-step fashion analogous to SSFS used to solve the NLSE. Although this technique is quite effective for a single channel, for a WDM system, small step size is required and hence the insertion losses due to DCF/FBG and HNLF increase which limit the transmission performance. In this chapter, we investigate the possibility of introducing a single optical device which can exactly compensate for dispersion and nonlinearity. A dispersion-decreasing fiber (DDF) with a specific dispersion profile is found to meet our requirements [105].

In the proposed scheme, an OPC is placed at the end of the transmission link which is followed by N spans of DDFs where N is the number of TF spans. The DDFs introduce a small amount of losses which are compensated by amplifiers placed in the OBP section. Numerical simulation results show that the OBP with DDF outperforms DBP and midpoint-OPC schemes. The transmission reach of a WDM system can be significantly enhanced using the proposed scheme as compared to linear compensation in the receiver or DBP.

Existing digital compensation schemes including DBP and perturbation-based techniques compensate for fiber nonlinear effects based on the information of signal propagation path and link parameters such as dispersion profiles and nonlinear coefficient. Such compensation schemes can be implemented in a point-to-point link. However, in the case of fiber optic networks, the digital equalizer at node j has no access to the channels that are dropped at node $j-1$ and hence, it is impossible to fully compensate for inter-channel nonlinear impairments in digital domain. In contrast, if the OBP module is placed at every amplifier site or at every node, it compensates for both intra- and inter- channel nonlinear impairments and the system becomes nearly linear (except for nonlinear phase noise and nonlinear PMD), as shown in Fig. 5.1(b).

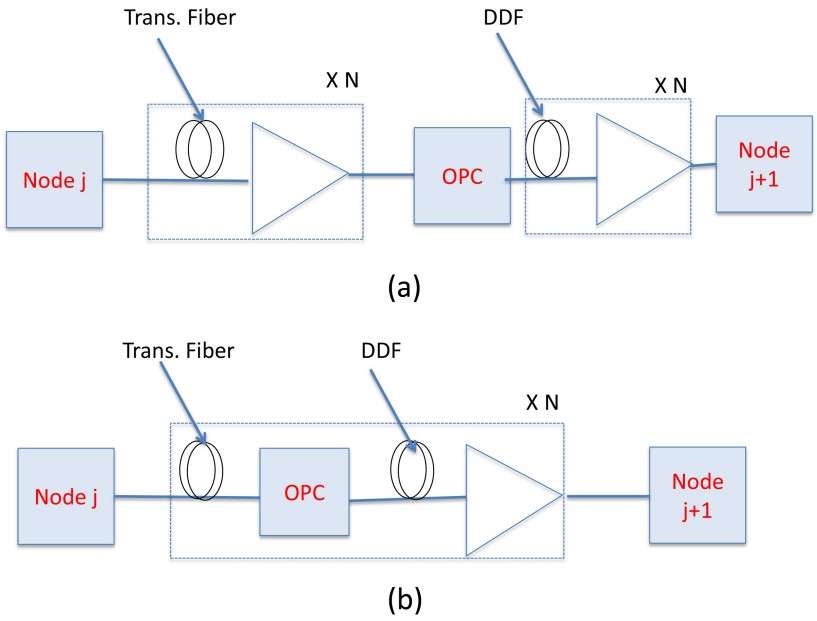

Figure 5.1: Schematic of fiber optic system using DDF. (a) DDFs are placed at the end of the transmission link. (b) DDFs are placed at every node.

5.2 Optical back propagation theory

The evolution of the optical field envelope in a fiber optic link is described by the NLSE,

$$\frac{\partial q}{\partial z} = i[D(t) + N(t,z)]q(t,z), \tag{5.1}$$

where D and N operator are given in Eqs. (4.2) and (4.3). The output signal field of the fiber pass through an OPC, as shown in Fig. 5.2(a), and then the output of OPC propagate through an ideal optical backpropagation fiber (OBPF) that is identical to the TF except that the sign of the loss coefficient of OBPF is inverted. The output of the OBPF is the conjugated signal of the input. Thus, the input field envelope can be

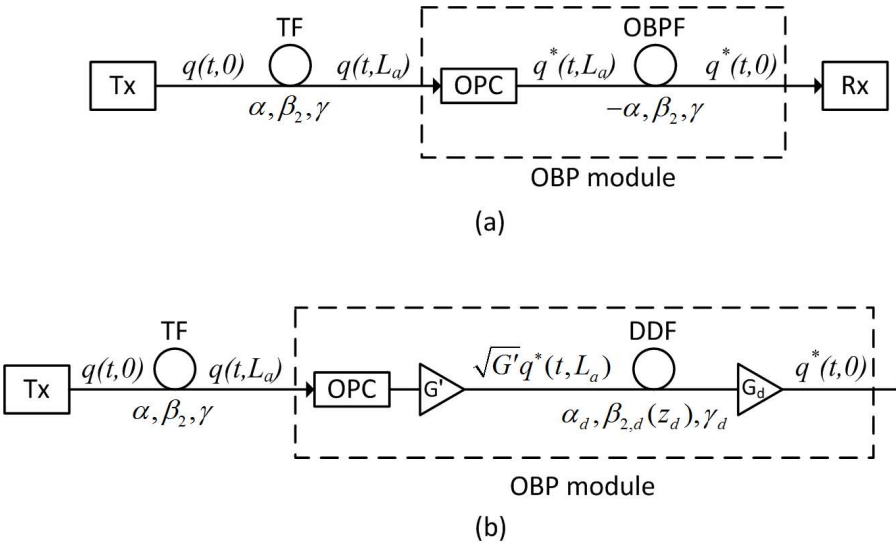

Figure 5.2: A single-span fiber optic system with (a) OBP using an ideal optical back propagation fiber with negative loss coefficient, (b) OBP using a DDF and amplifiers. Tx: transmitter, TF: transmission fiber, OPC: optical phase conjugator, OBPF: optical back propagation fiber, DDF: dispersion-decreasing fiber, Rx: receiver.

recovered by performing a phase conjugation in the electrical domain at the receiver,

(see Chapter 4 for mathematical derivation). The governing equation for OBP is

$$\frac{\partial q_b}{\partial z_b} = i[D(t) + N^*(t, z_b)]q_b(t, z_b), \tag{5.2}$$

with $q_b(t, 0) = q^*(t, L_a)$, and z_b is the distance in OBPF. Using

$$q_b = \sqrt{P_{in}} e^{-\alpha(L_a - z_b)/2} u_b, \tag{5.3}$$

and

$$dz'_b = \beta_2 dz_b, \tag{5.4}$$

Eq. (5.2) can be rewritten as

$$i\frac{\partial u_b}{\partial z'_b} - \frac{1}{2}\frac{\partial^2 u_b}{\partial t^2} + \frac{\gamma P_{in}}{\beta_2} e^{-\alpha(L_a - z_b)} |u_b|^2 u_b = 0, \tag{5.5}$$

where P_{in} is the power launched to the TF. Eq. (5.5) describes the field propagation in an ideal fiber with a constant β_2 and a negative loss coefficient (or equivalently the power increasing with distance) that exactly compensates for dispersion and nonlinearity of the TF. However, it is hard to realize such a fiber in practice. For an ideal OBP, we like to have a short length of a fiber (so that its insertion loss is small) which provides the same response as that of the ideal OBPF given by Eq. (5.5). Here, we derive an equivalent way of realizing Eq. (5.5) by using amplifiers and a DDF with positive loss coefficient α_d and a dispersion profile $\beta_{2,d}(z_d)$ [see Fig. 5.2(b)]. The optical field envelope in the DDF is described by

$$i\frac{\partial q_b}{\partial z_d} - \frac{\beta_{2,d}(z_d)}{2}\frac{\partial^2 q_b}{\partial t^2} + \gamma_d |q_b|^2 q_b + i\frac{\alpha_d}{2} q_d = 0, \tag{5.6}$$

where α_d and γ_d are the loss and nonlinear coefficients of DDF, respectively, z_d is the distance in the DDF, $q_b(t,0) = \sqrt{G'}q^*(t,L_a)$, and G' is the gain of the amplifier preceding DDF. Using transformations

$$q_d = \sqrt{P_d}e^{-\alpha_d z_d/2}u_b, \tag{5.7}$$

and

$$dz'_d = \beta_{2,d}(z_d)dz_d, \tag{5.8}$$

Eq. (5.6) can be rewritten as

$$i\frac{\partial u_b}{\partial z'_b} - \frac{1}{2}\frac{\partial^2 u_b}{\partial t^2} + \frac{\gamma_d P_d e^{-\alpha_d z_d}}{\beta_{2,d}(z_d)}|u_b|^2 u_b = 0, \tag{5.9}$$

where $P_d = GP_{in} = G'e^{-\alpha L_a}P_{in}$ is the input power of the DDF. Eqs. (5.5) and (5.9) are identical only if

$$dz'_b = dz'_d, \tag{5.10}$$

and

$$\frac{\gamma P_{in}}{\beta_2}e^{-\alpha(L_a - z_b)} = \frac{\gamma_d P_d e^{-\alpha_d z_d}}{\beta_{2,d}(z_d)}. \tag{5.11}$$

Substituting Eqs. (5.4) and (5.8) in Eq. (5.10), we find

$$\beta_2\frac{dz_b}{dz_d} = \beta_{2,d}(z_d), \tag{5.12}$$

$$w \equiv \beta_2 z_b = \int_0^{z_d}\beta_{2,d}(z_d)dz_d, \tag{5.13}$$

$$\frac{dw}{dz_d} = \beta_{2,d}(z_d), \tag{5.14}$$

Substituting Eqs. (5.13) and (5.14) in Eq. (5.11), we obtain

$$\frac{dw}{dz_d}e^{\alpha w/\beta_2} = \left(\frac{\gamma_d P_d \beta_2}{\gamma P_{in}}\right) e^{\alpha L_a} e^{-\alpha_d z_d}. \tag{5.15}$$

Integrating Eq. (5.15), we find

$$\frac{1}{\alpha}\left(e^{\frac{\alpha}{\beta_2}w(z_d)} - 1\right) = \left(\frac{\gamma_d P_d}{\gamma P_{in}}\right) e^{\alpha L_a} \frac{1 - e^{-\alpha_d z_d}}{\alpha_d}. \tag{5.16}$$

Simplifying Eq. (5.16), we obtain

$$w(z_d) = \frac{\beta_2}{\alpha}\ln\left(1 + \frac{\gamma_d G\alpha}{\gamma e^{-\alpha L_a}}\frac{1 - e^{-\alpha_d z_d}}{\alpha_d}\right), \tag{5.17}$$

$$\beta_{2,d} = \frac{e^{-\alpha_d z_d}}{\frac{\gamma e^{-\alpha L_a}}{\gamma_d G} + \alpha\left(\frac{1-e^{-\alpha_d z_d}}{\alpha_d}\right)}\beta_2. \tag{5.18}$$

The length of DDF L_d is found as follows. Total accumulated dispersion of the ideal OBPF [Fig. 5.2(a)] should be the same as that of the DDF, i.e.,

$$\beta_2 L_a = w(L_d) = \int_0^{L_d} \beta_{2,d}(z_d)dz_d, \tag{5.19}$$

or

$$L_d = -\frac{1}{\alpha_d}\ln\left[1 - \frac{\alpha_d \gamma e^{-\alpha L_a}}{\gamma_d G\alpha}\left(e^{\alpha L_a} - 1\right)\right]. \tag{5.20}$$

If the dispersion profile of the DDF is tailored to satisfy Eq. (5.18), the combination of the amplifiers and DDF provides the ideal response described by Eq. (5.5), and hence, signal-signal nonlinear interactions can be exactly compensated. The amplifier with gain $G_d = e^{\alpha_d L_d}$ is introduced after the DDF [see Fig. 5.2(b)] to compensate for

the loss of DDF. Fig. 5.3 shows the dispersion profiles of DDF that satisfy Eq. (5.18). As can be seen, relatively shorter length of DDF can compensate for the dispersion and nonlinear effects of the TF.

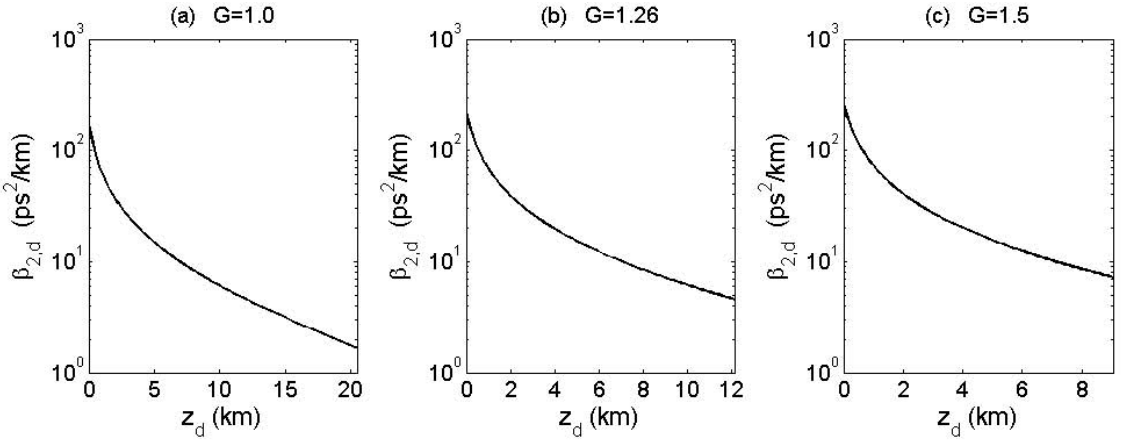

Figure 5.3: Dispersion profiles of DDF. TF parameters: α=0.2 dB/km, β_2=5 ps^2/km, γ=2.2 W^{-1}km^{-1}, L_a=60 km. DDF parameters: α_d=0.4 dB/km, γ_d=4.86 W^{-1}km^{-1}. (a) G=1.0: $\beta_{2,d}(0)$=175.1 ps^2/km, L_d=20.5 km, (b) G=1.26: $\beta_{2,d}(0)$=220.6 ps^2/km, L_d=12.1 km, (c) G=1.5: $\beta_{2,d}(0)$=262.6 ps^2/km, L_d=9.0 km.

So far we considered the compensation of dispersion and nonlinearity of a single-span fiber optic link. For a multiple-span transmission system, Fig. 5.4 shows the schematic of a WDM fiber optic transmission system consisting of M transmitters, N spans of TFs, the OBP module, and M coherent receivers. The OBP is applied at the end of the transmission link. A pre-amplifier with gain G is introduced so that the required dispersion profile and length of the DDF can be adjusted according to Eqs. (5.18) and (5.20), respectively. A BPF is introduced to remove the out of band ASE noise. During back propagation, amplifiers with gain G_d are used to fully compensate for the loss of each span of DDF.

In DBP, the compensation of fiber dispersion and nonlinearity is implemented in a step-wise manner and the performance is usually limited by the step size which has

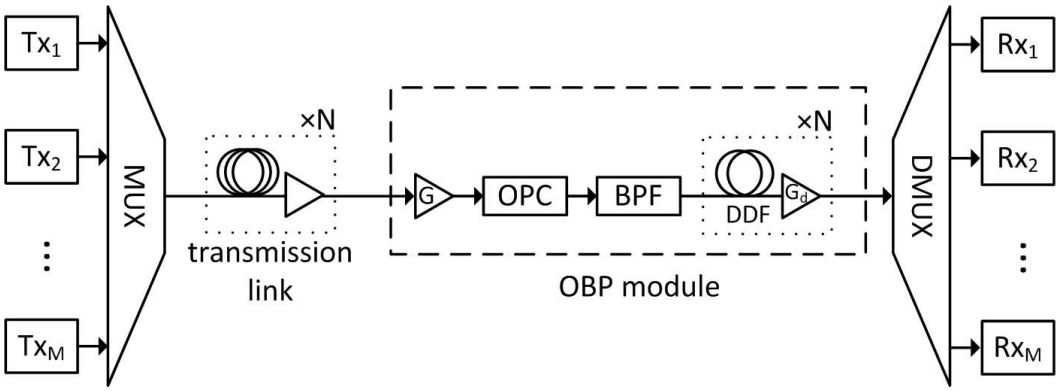

Figure 5.4: Schematic diagram of a WDM fiber optic transmission system with OBP. MUX: multiplexer, BPF: band pass filter, DMUX: demultiplexer.

to be traded off against computational cost or system complexity. In WDM systems, the required computational load may prevent DBP from real time implementation. In the OBP with DDF, the compensation of dispersion and nonlinearity is realized by a gradually decreasing dispersion profile, which inherently has a very small step size. The DDF with exponentially dispersion decreasing fibers have been fabricated before [106, 107]. The step size of the order of a few meters in DDF can be realized and hence, nearly ideal OBP can be realized using DDF. The DDF can be fabricated by tapering the fiber during drawing process which alters the waveguide contribution to the dispersion [106]. The maximum dispersion required for OBP fiber is of the same order as the commercially available dispersion compensation fiber and of the same sign.

5.3 Simulation results and discussions

We simulate a WDM fiber optic transmission system with OBP at the receiver with the following parameters: number of WDM channels = 5, channel spacing = 100

GHz, symbol rate per channel = 25 Gsymbols/s, modulation = 32 QAM, number of symbols simulated = 32768 per channel. The linewidths of the transmitter and local oscillator lasers are 100 kHz each. The dispersion, loss, and nonlinear coefficients of the TF are $\beta_2 = 5$ ps^2/km, $\alpha = 0.2$ dB/km, and $\gamma = 2.2$ W^{-1}km^{-1}, respectively. This type of fiber has been fabricated before and it is known as negative dispersion fiber (NDF) [96, 108]. The amplifier spacing is 60 km, and the spontaneous emission noise factor is $n_{sp} = 1.5$. The BPF shown in Fig. 5.4 is a second order Gaussian filter with full bandwidth of 450 GHz. For the DDF, $\alpha_d = 0.4$ dB/km, $\gamma_d = 4.86$ W^{-1}km^{-1}, and $L_d = 12.1$ km [see Fig. 5.3(b)]. The corresponding amplifier gain for compensating the DDF loss is 4.84 dB. Standard SSFS is used to simulate forward signal propagating in fibers with a nonlinear phase per step of 0.0005. In all the simulations, 32 samples per symbol are used in the transmission link so as to obtain a frequency window covering all the WDM channels. In DBP simulations, 2 samples per symbol are used after the ADC unless otherwise specified, while in OBP simulations, back propagation is in the optical domain and 32 samples per symbol are used. Using the method of [58], the coupled NLSE is used to compensate for the inter-channel nonlinear impairments ignoring FWM. However, the OBP scheme compensates for both XPM and FWM simultaneously. The central channel is demultiplexed using a second order Gaussian filter with full bandwidth of 50 GHz. In the coherent receiver, for OBP, two samples per symbol are used after the ADC and phase noise compensation is done using the approach of Ref. [98]. A LPF of bandwidth 25 GHz is used prior to phase noise compensation. For the DBP scheme, coupled NLSE is solved in digital domain prior to phase noise compensation. The optical and electrical filter bandwidths are optimized in both OBP and DBP schemes.

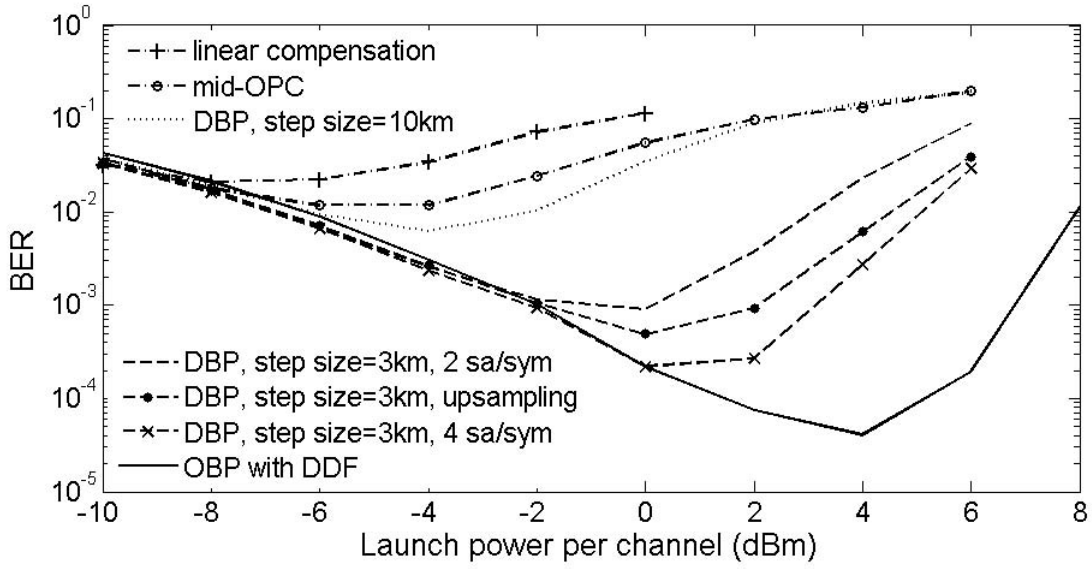

Figure 5.5: BER versus launch power per WDM channel. BER are calculated based on the central channel. (Number of WDM channels = 5, transmission distance = 1200 km.)

Fig. 5.5 shows the BER as a function of the launch power per WDM channel when the transmission distance is 1200 km. The solid curve represents the BER of OBP using DDFs, and the dashed and dotted curves represent the BER of DBP with 3 km and 10 km step sizes, respectively. The DBP step size of the simulated WDM system is limited by the walk-off length [58], which is 3.2 km. We found that there is no obvious performance improvement when a step size smaller than 3 km is chosen for DBP, consistent with the results of Ref. [58]. Also, Fig. 5.5 shows the simulation results of DBP with 4 samples/symbol ADC sampling rate and DBP with DSP upsampling [56] from 2 to 4 samples/symbol. The DBP performance can be improved by increasing ADC sampling rate or DSP upsampling, at the cost of increased system complexity and computational cost. The OBP outperforms DBP (2 samples/symbol, step size = 3 km) by 2.0 dB in Q-factor. The relatively poor

performance of DBP as compared to OBP is mainly due to the down sampling penalty and the lack of FWM compensation. The performance of midpoint OPC is worse than DBP, because the power profile is unsymmetrical with respect to the location of OPC. The performance of OBP is worse than that of DBP (with step size = 3 km) when the launch power is less than -2 dBm which is due to the optical signal to noise ratio (OSNR) penalty resulting from OBP amplifiers. The OSNR penalty due to OBP amplifiers is found to be 0.56 dB. From Fig. 5.5, it can also be seen that the DBP with a step size of 10 km performs worse than the DBP with a step size of 3 km even at lower launch powers (-10 dBm to -6 dBm) due to residual nonlinearity. The curve with "+" shows the case where no OBP (or DBP) is applied and fiber dispersion and laser phase noise are compensated in the receiver. As can be seen, the performance of this system is much worse than the system with DBP or OBP.

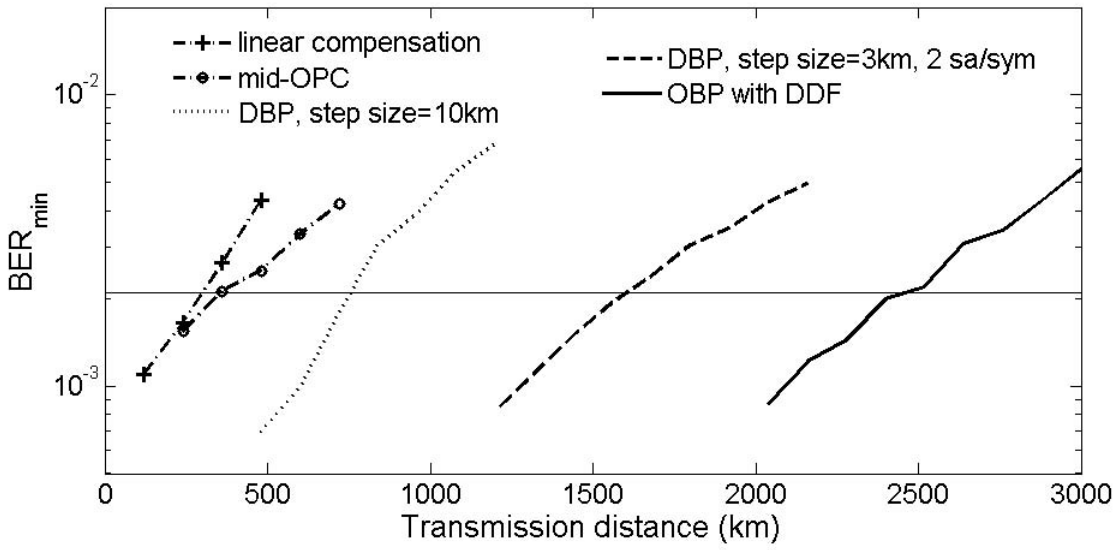

Figure 5.6: BER_{min} versus transmission distance. OSNR is 30.5 dB at the output of the fiber-optic link when launch power per channel is 0 dBm.

Fig. 5.6 shows the minimum BER as a function of transmission distance. The

BER_{min} is obtained by optimizing the launch power for each distance. At the BER of 2.1×10^{-3}, the transmission reaches of linear compensation only and midpoint OPC are 300 km and 360 km, respectively. For DBP with a 10 km step size and 2 samples/symbol sampling rate, the reach is 760 km, which can be increased to 1600 km by using a 3 km step size at the cost of more than tripling the computational effort. The transmission reach of OBP with DDF is 2460 km. Although the OBP fully compensates for signal-signal nonlinear interactions, it neither compensates for signal-ASE nonlinear interactions [27, 28, 32] nor mitigates nonlinear PMD [109], which are the limiting factors to enhance the reach in systems based on OBP. Instead of placing the OBP module at the receiver, it can be placed at each of the amplifier location. In such a scheme, signal-ASE nonlinear interactions can be compensated and better performance is expected.

The research work presented in this chapter is collaborative and my main contribution includes mathematical derivation of the dispersion profiles of DDF, and validation of the scheme to introduce DDF to fully compensate for deterministic fiber impairments. My contribution also includes a part of the modeling and simulation in Section 5.3.

5.4 Conclusions

We have investigated the performance of an OBP scheme consisting of an OPC and N spans of DDFs followed by amplifiers to compensate for dispersion and nonlinear effects of an N-span fiber optic WDM system. We have identified the conditions under which the nonlinear effects (both intra- and inter-channel nonlinearities) can be fully compensated and obtained an analytical expression for the novel dispersion

profile of the DDF which provides the exact compensation of intra- and inter-channel signal-signal nonlinear impairments. The performance of the proposed OBP scheme is compared with DBP and midpoint OPC and simulation results show that the transmission reach can be significantly enhanced using the OBP with DDF. In addition, OBP can be implemented in real time for WDM systems. The OBP scheme with DDF is also potential for applications in fiber optic network by placing the OBP module at the end of each span or at each node, since the compensation of a certain signal channel becomes independent of its propagation path and independent of the added/dropped channels within the propagation path.

Chapter 6

Impulse response of nonlinear Schrödinger equation and its implications for pre-dispersed fiber-optic communication systems

6.1 Introduction

The propagation dynamics of the pulse in a cubically nonlinear dispersive medium such as an optical fiber is described by the nonlinear Schrödinger equation (NLSE) [110, 111]. Optical soliton is a normal mode of the nonlinear system described by the NLSE, which can be integrated by means of inverse scattering transform (IST) [112, 113]. Zakharov and Shabat [111] solved the NLSE using IST and obtained soliton and breather solutions. The breathers or higher order solitons undergo periodic

compression and expansion with a soliton period. Impulse response approach to nonlinear dispersive propagation in fiber has been studied in the past [114, 115]. In Ref. [114] , the impulse response approach of linear system is extended to nonlinear system using a self-consistent time-transformation. In Ref. [115], an impulse response approach is used to calculate the multiplicative correction due to the interplay between chromatic dispersion and Kerr nonlinearity. In this chapter, we obtain an exact solution of the NLSE for an impulse input [116]. However, we found that there is a singularity in the phase. To remove this singularity, we introduced pre-dispersion which can be added either in electrical domain at the transmitter or in optical domain prior to transmission. The exact solution in this case has a phase factor which is described by the exponential integral. Next, we investigated the nonlinear interaction among pulses in a fiber due to periodically placed impulses at the input and analyzed the conditions under which they propagate over long distances without exchanging energy among them [116].

When a cluster of CW beams of different frequencies propagate in optical fiber, they exchange energy through the process known as four wave mixing (FWM). Eventually the amplitudes of CW beams reach an equilibrium in which there is no exchange of energy among them and they take secant-hyperbolic shape corresponding to soliton spectrum. There exists an alternate explanation in time domain. The dual of classical FWM is time-domain FWM or IFWM [24, 33–35] and the dual of CW signal is a Dirac delta function in time domain (CW signal is an impulse function in frequency domain). When a cluster of closely spaced impulses propagate in fiber, they exchange energy through IFWM. However, if the weights of the impulses have

secent-hyperbolic shapes, they do not exchange energy and propagate stably as solitons over long distances. In order to have soliton propagation, the impulses have to be infinitesimally closer. In this chapter, we have investigated if it is possible to propagate a large number of periodically placed impulses over large distances without exchanging energy among them. We found that if the impulse weights at the input have a secant-hyperbolic shape and a proper chirp factor, they propagate without change in shape over long distances just like the soliton of NLSE [116]. The amplitude of the soliton solution depends on system parameters such as pre-accumulated dispersion, separation between the impulses and the dispersion of the transmission fiber. When the impulses are infinitesimally closer, this solution becomes the classical soliton of the continuous NLSE. We have derived a discrete NLSE which describes the evolution of the discrete Fourier transform of the product of the impulse weights and a chirp factor. We note that the discrete NLSE can be easily obtained by discretizing the continuous NLSE. In such a discrete NLSE, the dispersion term would be directly proportional to fiber dispersion coefficient. However, in the discrete NLSE derived here, the effective dispersion term is inversely proportional to the square of the accumulated dispersion and the effective nonlinear term is inversely proportional to the absolute accumulated dispersion. It is not yet known if the discrete NLSE derived here can be integrated by IST. However, we have numerically found that the discrete NLSE admits higher order soliton solutions which undergo periodic compression and expansion with a certain period, similar to its continuous analogue.

In the context of discrete NLSE, if the effective dispersion length is much longer than the effective nonlinear length, the equation becomes significantly simplified. In this case, intra-channel cross-phase modulation (IXPM) and IFWM [12, 24, 33–35]

vanish in the transformed system. We have obtained nonlinear eigenmodes which form the natural basis for description of signal propagation and signal and noise nonlinear interaction in highly pre-dispersed fiber-optic systems. The work presented in this chapter may appear unrelated to the rest of the thesis. However, the pre-dispersion significantly simplifies the propagation equations, which would make the analysis easier and could potentially lead to simpler nonlinearity compensation schemes.

6.2 Impulse response

If we make a transformation that $A = u\exp(-\alpha z/2)$ in Eq. (2.1), the evolution of optical field envelope is described by lossless NLSE,

$$i\frac{\partial u}{\partial z} - \frac{\beta_2}{2}\frac{\partial^2 u}{\partial t^2} + \gamma_0 e^{-\alpha z}|u|^2 u = 0, \tag{6.1}$$

where α, β_2, and γ_0 are the loss, dispersion and nonlinear coefficients, respectively. In a linear fiber ($\gamma_0 = 0$), when an impluse is launched,

$$u(t,0) = A\delta(t), \tag{6.2}$$

the optical field in the fiber is

$$u(t,z) = \frac{A}{\sqrt{-i2\pi\beta_2 z}} e^{-i\frac{t^2}{2\beta_2 z}}. \tag{6.3}$$

In the presence of nonlinearity, we look for a solution of Eq. (6.1) in the form,

$$u(t,z) = \frac{A}{\sqrt{-i2\pi\beta_2 z}} e^{-i\frac{t^2}{2\beta_2 z}+iv(z)}, \tag{6.4}$$

Substituting Eq. (6.4) in Eq. (6.1), we obtain

$$\frac{A}{\sqrt{-i2\pi\beta_2 z}}\left[-\frac{i}{2z}-\frac{t^2}{2\beta_2 z^2}-\frac{dv(z)}{dz}+\frac{\beta_2}{2}\left(\frac{i}{\beta_2 z}+\frac{t^2}{\beta_2^2 z^2}\right)+\gamma_0 e^{-\alpha z}\frac{|A|^2}{2\pi|\beta_2|z}\right]=0. \tag{6.5}$$

Simplifying Eq. (6.5), we obtain

$$v(z)=\frac{\gamma_0|A|^2}{2\pi|\beta_2|}\int_0^z\frac{e^{-\alpha x}}{x}dx. \tag{6.6}$$

The integrand of Eq. (6.6) has a singularity, which should be expected due to the impulse input. The singularity can be avoided by using pre-dispersion. Suppose

$$\beta_2(z)=\begin{cases}\beta_{2-}, & \text{for } z<0\\ \beta_{2+}, & \text{for } z>0\end{cases} \tag{6.7}$$

$$\gamma=\begin{cases}0, & \text{for } z<0\\ \gamma_0, & \text{for } z>0.\end{cases} \tag{6.8}$$

Let $s_0=\int_{-L}^{0}\beta_{2-}(z)dz$ be the pre-accumulated dispersion. The pre-dispersion can be realized using a high dispersion fiber prior to transmission fiber or a digital dispersion filter in the DSP unit of the optical transmitter [12, 92]. Now for $z>0$, Eqs. (6.4) and (6.6) are modified as

$$u(t,z)=\frac{A}{\sqrt{-i2\pi s(z)}}e^{-i\frac{t^2}{2s(z)}+i\gamma_0\frac{|A|^2}{2\pi}\theta(z)}, \tag{6.9}$$

$$\theta(z)=\int_0^z\frac{e^{-\alpha x}}{s(x)}dx, \tag{6.10}$$

$$s(z) = s_0 + \beta_{2+} z. \tag{6.11}$$

$\theta(z)$ in Eq. (6.9) does not diverge only if $s_0 + \beta_{2+} z$ does not cross 0 for any z. In this chapter, we assume that pre-accumulated dispersion s_0 has the same sign as β_{2+} so that $s(z)$ does not cross 0. Under this condition, Eq. (6.10) can be written in a closed form as [117]

$$\theta(z) = e^{\alpha s_0/\beta_{2+}} \left[\mathrm{Ei}\left(\frac{-\alpha s(z)}{\beta_{2+}}\right) - \mathrm{Ei}\left(\frac{-\alpha s_0}{\beta_{2+}}\right)\right], \tag{6.12}$$

where $\mathrm{Ei}(x)$ is the exponential integral.

$$\mathrm{Ei}(x) = -\int_{-x}^{\infty} \frac{e^{-t}}{t} dt. \tag{6.13}$$

Equation (6.9) is an exact solution of the NLSE when the input (at $z = -L$) is a single impulse. Suppose the input consists of a train of impluses,

$$u_{in}(t) = \sum_{n=-N/2}^{N/2-1} A_n \delta(t - nT), \tag{6.14}$$

where N is the number of impulses, which is assumed to be large. The optical field in the transmission fiber for this input may be written as

$$u(t,z) = \sum_{n=-N/2}^{N/2-1} \frac{A_n(z) e^{-i(t-nT)^2/2s(z)}}{\sqrt{-i2\pi s(z)}}, \quad \text{for } z \geq 0. \tag{6.15}$$

In the absence of nonlinear interaction with the neighboring pulses, we have

$$A_n(z) = A_n(0) e^{i\gamma_0 |A_n(0)|^2 \theta(z)/2\pi}. \tag{6.16}$$

Equation (6.16) includes the effect of SPM only. However, due to IXPM and IFWM, [24, 33–35] the pulses undergo amplitude/phase shifts. Substituting Eq. (6.15) in Eq. (6.1), we find

$$i\sum_n \frac{dA_n}{dz} e^{-i\frac{(t-nT)^2}{2s(z)}} + \frac{\gamma_0 e^{-\alpha z}}{2\pi|s(z)|}\sum_k\sum_l\sum_m A_k A_l A_m^* F_{klm} = 0, \tag{6.17}$$

where $F_{klm} = e^{-i\left[(t-kT)^2+(t-lT)^2-(t-mT)^2\right]/2s(z)}$. Multiplying Eq. (6.17) by $e^{i(t-jT)^2/2s(z)}$ and integrating from $-t$ to t with $t\to\infty$, we find

$$i\sum_n \frac{dA_n}{dz}\delta_{jn} + \frac{\gamma_0 e^{-\alpha z}}{2\pi|s(z)|}\sum_k\sum_l\sum_m A_k A_l A_m^* Y_{klm,j} = 0, \tag{6.18}$$

where δ_{jn} is a Kronecker delta function and

$$\begin{aligned} Y_{klm,j} &= \lim_{t\to\infty}\frac{1}{2t}\int_{-t}^{t} F_{klm} e^{i(\tau-jT)^2/2s(z)} d\tau \\ &= \lim_{t\to\infty}\frac{1}{2t} e^{-i(k^2+l^2-m^2-j^2)T^2/2s(z)}\int_{-t}^{t} e^{i(k+l-m-j)\tau T/s(z)} d\tau. \end{aligned} \tag{6.19}$$

$Y_{klm,j}$ will be non-zero only if $m = k+l-j$. In this case,

$$Y_{klj} \equiv Y_{klm,j} = e^{-i\left[k^2+l^2-(k+l-j)^2-j^2\right]T^2/2s(z)}. \tag{6.20}$$

So, now Eq. (6.18) becomes

$$i\frac{dA_j}{dz} + \frac{\gamma_0 e^{-\alpha z}}{2\pi|s(z)|}\sum_k\sum_l A_k(z) A_l(z) A_{k+l-j}^* Y_{klj} = 0. \tag{6.21}$$

In the absence of nonlinear effects ($\gamma_0 = 0$), from Eq. (6.21) we find

$$\frac{dA_j}{dz} = 0, \tag{6.22}$$

which indicates that there is no interaction among pulses in a linear medium. Let

$$U_k(z) = e^{-ik^2T^2/2s(z)}, \tag{6.23}$$

where k is an integer. Equation (6.20) may be written as

$$Y_{klj} = U_k U_l U^*_{k+l-j} e^{ij^2T^2/2s(z)}. \tag{6.24}$$

Let

$$B_k(z) = A_k(z)U_k(z). \tag{6.25}$$

Using Eqs. (6.23)-(6.25) in Eq. (6.21), we find

$$i\frac{dB_j}{dz} + \frac{j^2T^2\beta_{2+}}{2s^2(z)}B_j + \frac{\gamma_0 e^{-\alpha z}}{2\pi|s(z)|}\sum_k\sum_l B_k B_l B^*_{k+l-j} = 0. \tag{6.26}$$

The second term is similar to dispersion in NLSE. If we take the Fourier transform of Eq. (6.1), the second term would be $\beta_2\omega^2\widetilde{u}(\omega,z)/2$, where $\widetilde{u}(\omega,z) = \mathcal{F}\{u(t,z)\}$, $\mathcal{F}$ denotes the Fourier transformation. Therefore, in Eq. (6.26), $\beta_{2+}/s^2(z)$ may be interpreted as the effective dispersion. However, unlike $u(t,z)$, $B_j(z)$ is a discrete variable and hence, we consider the discrete Fourier transform (DFT),

$$\mathrm{DFT}\{B_j; j \to m\} = \widetilde{B}_m = \sum_{j=-N/2}^{N/2-1} B_j e^{-i2\pi jm/N}. \tag{6.27}$$

Taking the discrete Fourier transform of Eq. (6.26) and noting that a convolution becomes product in spectral domain (and vice versa), we find

$$i\frac{d\widetilde{B}_m}{dz} - \frac{\beta_{2+}T^2}{2s^2(z)}\sum_{k=-N/2}^{N/2-1}\widetilde{B}_{m-k}\widetilde{x}_k + \frac{\gamma e^{-\alpha z}}{2\pi|s(z)|}|\widetilde{B}_m|^2\widetilde{B}_m = 0, \tag{6.28}$$

where

$$\widetilde{x}_k = \mathrm{DFT}\{j^2; j \to k\}. \tag{6.29}$$

Equation (6.28) may be interpreted as a discrete analogue of the NLSE. Since A_n may be interpreted as signal sample at nT, a discrete NLSE can be easily obtained for A_n [118, 119]. In such a discrete NLSE, the dispersion term would be directly proportional to fiber dispersion coefficient. However, in Eq. (6.28), the effective dispersion term is inversely proportional to the square of accumulated dispersion and the effective nonlinear term is inversely proportional to the absolute accumulated dispersion. The discrete NLSE in Eq. (6.28) does not describe A_n, instead it discribes the evolution of the DFT of B_n which is the product of A_n and U_n. In the absence of pre-dispersion ($s_0 = 0$), the effective dispersion term and the effective nonlinear term of Eq. (6.28) diverge at $z = 0$ and hence, pre-dispersion is essential for the solution of Eq. (6.28). In the terminology of Ref. [119], Eq. (6.28) is a discrete self-trapping (DST) equation of the form [120],

$$i\frac{d\widetilde{B}_m}{dz} + \epsilon\sum_k m_{jk}\widetilde{B}_k + \gamma|\widetilde{B}_m|^2\widetilde{B}_m = 0, \tag{6.30}$$

where $[m_{jk}]$ is a $f \times f$ coupling matrix. In Eq. (6.1), when $\alpha = 0$, dispersion and nonlinear coefficients are constants for $z > 0$ and hence, it admits soliton solutions.

However, in Eq. (6.28), the effective dispersion and nonlinear coefficients are varying with distance due to $s(z)$. If we choose the pre-dispersion such that $s_0 >> \beta_{2+} L_{tr}$ where L_{tr} is the length of the transmission fiber, we can approximate $s(z)$ as s_0. In this case with $\alpha = 0\ km^{-1}$, we look for a soliton solution of Eq. (6.28) in the form

$$\widetilde{B}_m(z) = \widetilde{B}_0 \text{sech}\left(\frac{m}{M}\right) e^{i\mu(z)}. \tag{6.31}$$

Equation (6.28) is numerically solved using the split-step Fourier method with the initial condition,

$$\widetilde{B}_m(0) = \widetilde{B}_0 \text{sech}\left(\frac{m}{M}\right). \tag{6.32}$$

Figure 6.1 shows the evolution of $|\widetilde{B}_m|^2$ in the transmission fiber. As can be seen, when $\widetilde{B}_0$ is less than a threshold $\widetilde{B}_{th}$, we see the broadening effect and when $\widetilde{B}_0 = \widetilde{B}_{th}$, the pulse shape is retained throughout. Figure 6.2 shows the evolution of $|B_n|^2$ obtained by taking the inverse discrete Fourier transform (IDFT) of $\widetilde{B}_m$. As can be seen, when $\widetilde{B}_0 < \widetilde{B}_{th}$ (Fig. 6.2a), the envelope of $|B_n|^2 (= |A_n|^2)$ becomes narrower which indicates that the pulses exchange energy among them resulting in the pulse at the center ($n = 0$) becoming stronger. When $\widetilde{B}_0 = \widetilde{B}_{th}$, pulses propagate long distances without exchanging energy among them.

Figure 6.3 shows the similar result by solving Eq. (6.1). The impulses of Eq. (6.14) are approximated by Gaussian pulses of short pulse widths,

$$A_n \delta(t - nT) \rightarrow \frac{A_n}{\sqrt{2\pi} T_0} e^{-\frac{(t-nT)^2}{2T_0^2}}, \tag{6.33}$$

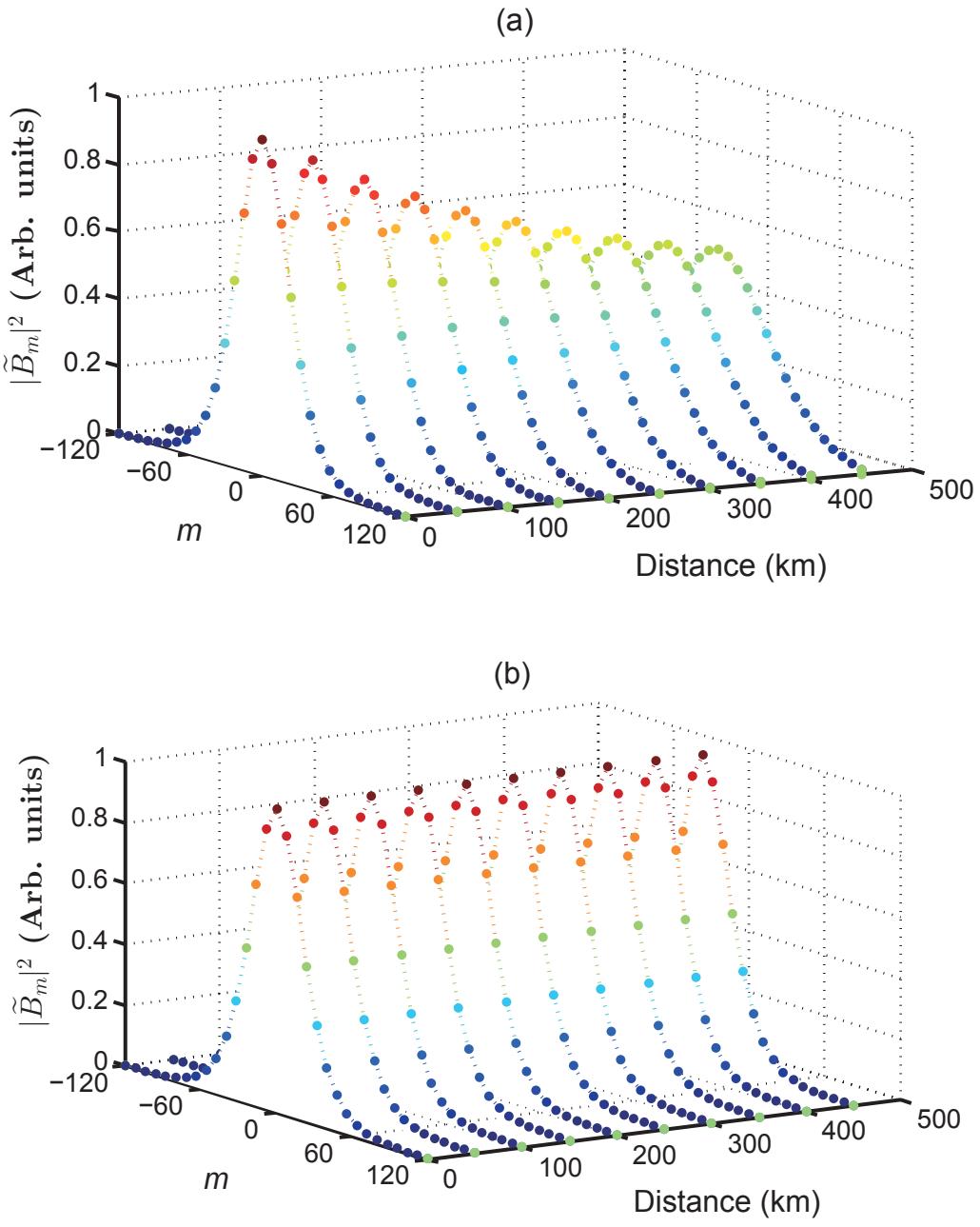

Figure 6.1: Evolution of $\widetilde{B}_m$ in the transmission fiber, (a) $\widetilde{B}_0 < \widetilde{B}_{th}$, $\widetilde{B}_0 = 10\ \sqrt{\text{mW}}\text{ps}$, (b) $\widetilde{B}_0 = \widetilde{B}_{th}$. $\widetilde{B}_{th} = 14.9\ \sqrt{\text{mW}}\text{ps}$, $M = 28$, $\alpha = 0\ \text{km}^{-1}$, $s_0 = -1.28 \times 10^4\ \text{ps}^2$, $\gamma_0 = 1.1\ \text{W}^{-1}\text{km}^{-1}$.

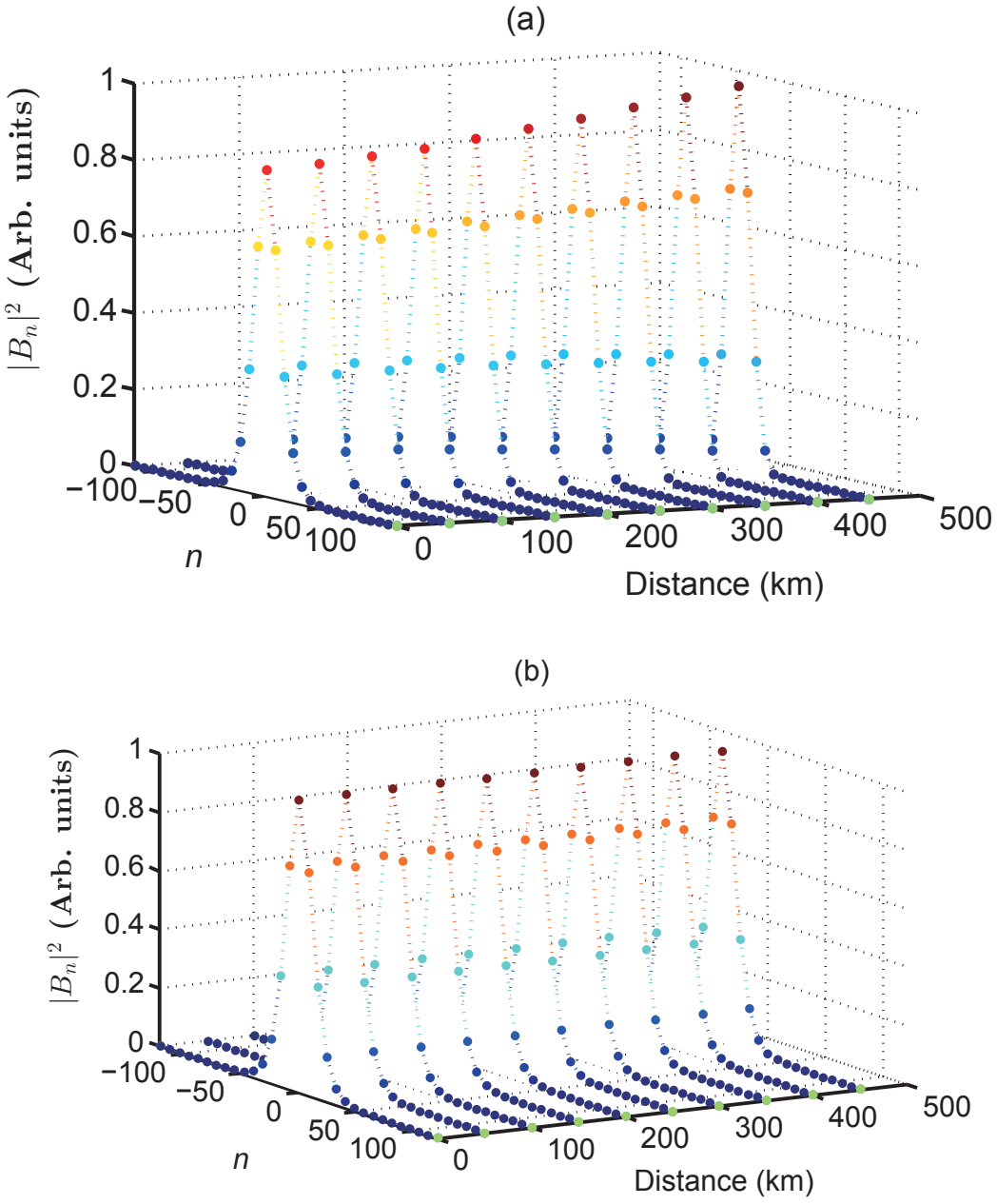

Figure 6.2: Evolution of B_m in the transmission fiber, (a) $\widetilde{B}_0 < \widetilde{B}_{th}$, (b) $\widetilde{B}_0 = \widetilde{B}_{th}$. The parameters are the same as in Fig. 6.1.

and Eq. (6.1) is solved with the following initial condition

$$u_{in}(t) = \sum_{n=-N/2}^{N/2-1} \frac{A_n(0) e^{-\frac{(t-nT)^2}{2T_0^2}}}{\sqrt{2\pi} T_0}, \tag{6.34}$$

where

$$A_n(0) = B_n(0) e^{i\frac{n^2 T^2}{2s_0}}, \tag{6.35}$$

$$B_n(0) = \text{IDFT}\left\{\widetilde{B}_m(0); m \to n\right\}, \tag{6.36}$$

and $\widetilde{B}_m(0)$ is given by Eq. (6.32). To obtain Fig. 6.3, the pre-accumulated dispersion is fully compensated at the receiver so that the pulse width of the Gaussian pulses at the output is the same as that at the input. As can be seen from Fig. 6.3, the envelope of Gaussian pulses propagate undistorted over the transmission fiber. If we had not properly chosen the input power, the nonlinear interaction among Gaussian pulses would broaden/compress the shape of the envelope. "×" in Fig. 6.3 show the power obtained by numerically solving Eq. (6.28) after converting $\widetilde{B}_m$ to A_n using Eqs. (6.23) and (6.25). The power required to form fundamental soliton is found to be

$$P_s = \frac{\beta_{2+} T^2}{4 s_0 \gamma_0 T_0^2}, \tag{6.37}$$

where T is the pulse separation and T_0 is the pulse width of the Gaussian pulses. Strictly speaking, the approximation of impulses by ultra-short Gaussian pulses is not really necessary. To test the validity of Eq. (6.28), in principle, Eq. (6.1) can be solved with the initial condition $u(t, 0)$ given by Eq. (6.15). However, the extraction of A_n from the transmission fiber output becomes hard.

As pointed in Ref. [119], DST is not typically integrable when $f > 2$. The

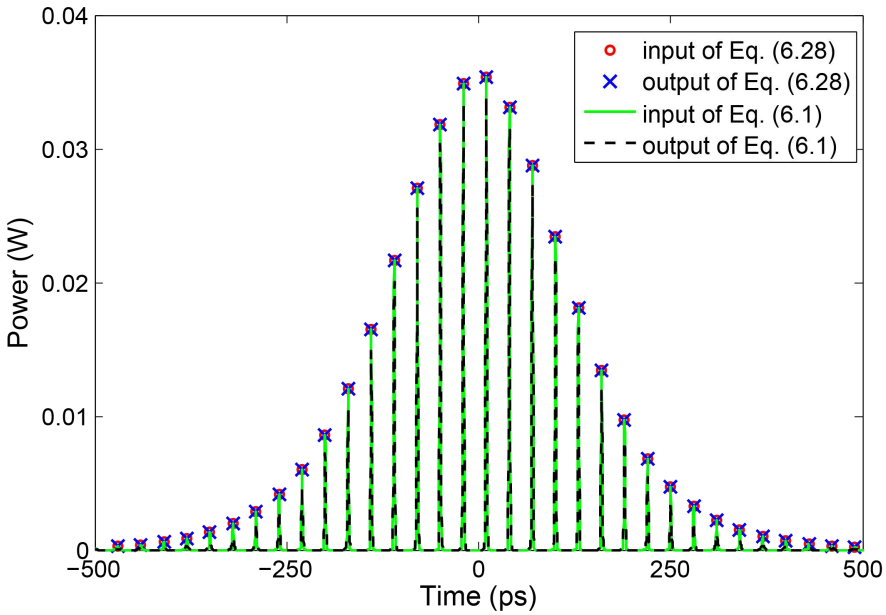

Figure 6.3: Comparison of discrete NLSE (Eq. (6.28)) and continuous NLSE (Eq. (6.1)). Peak power = 35.5 mw , $T = 10$ ps, $T_0 = 1$ ps, $s_0 = -1.28\times10^4$ ps^2, $\beta_{2+} = -20$ ps^2/km, $\gamma_0 = 1.1$ W^{-1}km^{-1}, transmission distance = 240 km.

integrability of Eq. (6.28) is not known yet, and to test if it admits high order soliton solutions, we solved Eq. (6.28) with the initial condition

$$\widetilde{B}_m(0) = 2\widetilde{B}_{th}\text{sech}\left(\frac{m}{M}\right). \tag{6.38}$$

Figure 6.4(a) shows the evolution of the second order soliton. As can be seen, it undergoes periodic compression just like its continuous analogue. The soliton period is found to be

$$z_0 = \frac{2s_0^2}{\pi M^2 T^2 |\beta_{2+}|}. \tag{6.39}$$

Figure 6.4(b) shows the evolution of $|B_n|^2$. When the envelope of $\widetilde{B}_m$ is compressed, the corresponding envelope of B_n is broadened and vice versa.

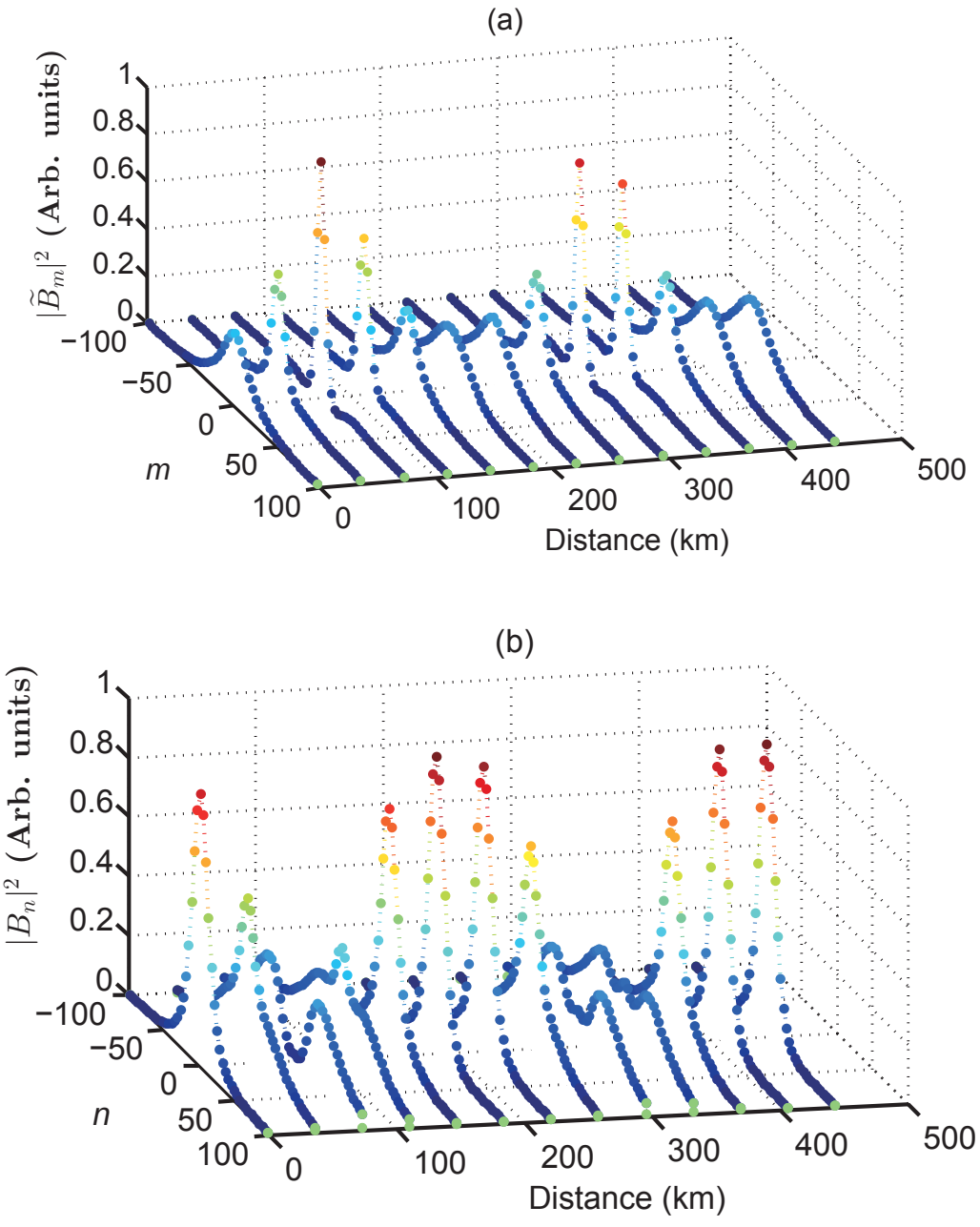

Figure 6.4: Evolution of second order soliton. $\widetilde{B}_0 = 29.8\sqrt{\text{mW}}\text{ps}$. The rest of the parameters are the same as in Fig. 6.1.

6.3 Nonlinear eigenmodes

When the effective dispersive effects are much weaker than the effective nonlinear effects in Eq. (6.28), i.e.,

$$\gamma P T_0^2/\pi >> \beta_{2+} T^2/|s(z)|, \tag{6.40}$$

where P is the peak power and T_0 is the half-width at $1/e$-intensity point of the Gaussian pulse that approximates the impulse, the second term in Eq. (6.28) can be ignored and we obtain

$$\frac{\partial \widetilde{B}_m}{\partial z} = i\frac{\gamma e^{-\alpha z}}{2\pi|s(z)|}|\widetilde{B}_m|^2 \widetilde{B}_m. \tag{6.41}$$

In Eq. (6.26), the last term is responsible for nonlinear interactions such as IXPM and IFWM among pulses. However, in Eq. (6.41), in the transformed system, these terms are absent and hence, the description of the nonlinear interactions becomes significantly simplified. Let

$$\widetilde{B}_m = Y_m e^{i\theta_m}. \tag{6.42}$$

Substituting Eq. (6.42) in Eq. (6.41), we find

$$Y_m = \text{const}, \tag{6.43}$$

$$\theta_m(z) = \theta_m(0) + \gamma|Y_m|^2 \int_0^z \frac{e^{-\alpha x}}{2\pi|s(x)|}dx. \tag{6.44}$$

The solution of Eq. (6.41) may be written as

$$\widetilde{B}_m(z) = \widetilde{B}_m(0)e^{\lambda_m z'}, \tag{6.45}$$

where

$$\lambda_m = i\gamma|\widetilde{B}_m|^2, \qquad z' = \frac{1}{2\pi}\int_0^z \frac{e^{-\alpha x}}{|s(x)|}dx. \tag{6.46}$$

When s_0 and β_{2+} have the same sign, z' can be written as

$$z' = \frac{e^{\alpha|s_0/\beta_{2+}|}}{2\pi}\left[\mathrm{Ei}\left(-\alpha\left|\frac{s(z)}{\beta_{2+}}\right|\right) - \mathrm{Ei}\left(-\alpha\left|\frac{s_0}{\beta_{2+}}\right|\right)\right]. \tag{6.47}$$

$\widetilde{B}_m$ may be interpreted as the nonlinear eigenmode of the fiber-optic system in the presence of pre-dispersion with the eigenvalue λ_m. These eigenmodes form a natural basis for the description of signal propagation, and signal and noise nonlinear interaction in highly pre-dispersed fiber-optic transmission systems. We note that using a different approach with stationary phase approximation, it has been shown that propagation equations can be considerably simplified in the presence of high pre-dispersion [55]. We found a few similarities and differences between Ref. [121] and our work. In this chapter, we introduce a transformation $B_k(z) = A_k(z)\exp\left(-ik^2T^2/2s(z)\right)$ in time domain, whereas in Ref. [121], the transformation $\hat{u}(z,\omega) \sim \hat{U}(z,\omega)\exp(-iC\omega^2/2)$ is used in frequency domain. In Ref. [121], when the system has a small value of path-average dispersion, the average dynamic of the pulse transmission is characterized only by the nonlinear phase shift. In contrast, from Eq. (6.28), it follows that when the system has a very large pre-accumulated dispersion, the pulse transmission is characterized only by the nonlinear phase shift given by Eq. (6.45). Even when the condition given by Eq. (6.40) is not met, i.e. when the pre-accumulated dispersion is moderate, the nonlinear eigenmode could serve as the unperturbed solution and a first order perturbation theory could be developed for the discrete NLSE of Eq. (6.28). An interesting fact is that the square of the accumulated dispersion appears in the

denominator of the second term in Eq. (6.28). This means that the effect of the second term becomes smaller for the fiber spans closer to receiver in a long haul system. Typically, in quasilinear fiber optic systems, dispersion length is much shorter than the nonlinear length. Hence linear solution (including dispersive effects) is treated as the unperturbed solution and first order correction due to nonlinear effects are calculated [35]. However, the computational complexity of the first order calculations scales as M^2 per sample where M is the number of neighbors with which the nonlinear interaction is significant and as a result, the digital compensation of fiber nonlinearities using first order perturbation theory is time-consuming [65, 122]. In contrast, if the nonlinear eigenmodes are treated as the unperturbed solution with the second term of Eq. (6.28) being treated as perturbation, the computational complexity is expected to be much smaller.

The research work presented in this chapter is collaborative and my contribution is derive the exact solution of NLSE for impulse input in the presence of pre-dispersion mathematically, as well as model and simulate the system numerically. Also, I find the power required to form the fundamental solition and the solition period.

6.4 Conclusions

In conclusion, we have derived an exact solution of NLSE for an impulse input in the presence of pre-dispersion. The exact solution has a phase factor that is described by the exponential integral. Next, we considered the nonlinear interaction among pulses in a fiber due to periodically placed impulses at the input. We found that these pulses will propagate stably over long distances if the complex weights of impulses at the input has a secant-hyperbolic envelope and a proper chirp factor. We have derived the

discrete version of the NLSE under the condition that the input of an optical fiber is a periodic train of impluses. When the accumulated pre-dispersion is large, the discrete NLSE admits soliton and breather solutions similar to its continuous analogue. In the discrete NLSE derived here, the effective dispersion term is inversely proportional to the square of the accumulated dispersion and the effect nonlinear term is inversely proportional to absolute of accumulated dispersion. The derived discrete NLSE has a solution only if the pre-accumulated dispersion is non-zero. In the context of discrete NLSE, if the effective dispersion length is much longer than the effective nonlinear length, we have obtained the nonlinear eigenmodes of the highly pre-dispersed fiber-optic system which could be useful for the description of signal propagation, and signal and noise interaction.

Chapter 7

Conclusions and future work

7.1 Conclusions

This thesis focuses on various schemes of split-step Fourier method to solve the nonlinear Schrödinger equation (NLSE), which is used to model optical pulses propagating in fibers. In addition, dispersive and nonlinear impairments in fiber-optic communication systems are discussed, and compensation techniques to mitigate them using DSP or optical devices are developed.

In Chapter 2, efficient schemes to solve the NLSE are discussed [84]. The fiber loss operator can be combined with dispersion or nonlinearity operators, and it is found that the schemes when loss is with nonlinearity outperform those when loss is with dispersion. The schemes with varying step size are more efficient than those with uniform step size, when the global error is large. In this thesis, it is proposed to use mimimum area mismatch (MAM) in which the step size distribution is optimized by minimizing the area mismatch of the power profile between the ideal curve and its stepwise approximation. The optimization problem is solved by the steepest descent

algorithm. Local error method is a scheme, in which the next step size is determined and adjusted by the local error of the current step. In this thesis, it is proposed to combine the MAM and local error method. The combined scheme is found to have higher computational efficiency than the other schemes studied in this thesis. For QPSK systems, when the global error is 10^{-8}, the number of FFTs needed for the conventional scheme (loss with dispersion and uniform step size) is 5.8 times that of the combined scheme. When the global error is 10^{-6}, the number of FFTs needed for the conventional scheme is 3.7 times that of the combined scheme.

Chapter 3 deals with a DBP scheme using optimal step size distribution to compensate for fiber distortions in a polarization division multiplexed fiber-optic communication system [83]. The optimization of the step sizes is obtained by minimizing the area mismatch between the exponential profile of the effective nonlinear coefficient or power profile and its stepwise approximation. Under the same computational complexity, DBP with optimal step sizes can obtain better performance. In simulations, vector NLSE and Manakov equations are used to model the forward propagation of the optical signals, and Manakov equations are used for backward propagation. In order to compensate for randomly changing birefringence when the vector NLSE is used for forward propagation, an adaptive LMS equalizer is utilized. Simulation results show that in both cases, DBP with optimal step size can significantly increase the system reach as compared to the uniform spacing scheme at the same computational load.

In Chapter 4, compensation of fiber dispersion and nonlinearity are realized by OBP, which is similar to DBP scheme except that the OBP module consists of optical devices [93]. Since fibers with negative Kerr nonlinear coefficient are not available, the

conjugation of the transmission signals are needed before OBP. Therefore, an optical phase conjugator is employed before OBP, and the conjugated signals then passes to the OBP module, which consists of high-dispersion fibers (HDFs) and highly nonlinear fibers (HNLFs). HDFs are mainly used to compensate for fiber dispersion, and HNLFs are used to compensate for fiber nonlinearity. It is shown in simulation that the OBP scheme outperforms the schemes using midpoint OPC and DBP with the same step size. Another OBP scheme with OPC is investigated, in which the OBP module consists of fiber Bragg gratings (FBGs) and HNLFs [81]. Dispersion and nonlinearity are compensated using FBGs and HNLFs, respectively, and several sections of FBGs and HNLFs are concatenated in a way similar to the split-step Fourier method, which is used to solve the NLSE. By minimizing the area mismatch between the ideal exponential curve of the effective nonlinear coefficient and its stepwise approximation, the accumulated dispersion and nonlinear phase shift are optimized. We simulated a single channel fiber-optic communication systems based on this OBP scheme, and the simulation results show that the optimized OBP scheme has a better performance than that use uniform spaced sections. Also, the benefit brought out by OBP is that it can be implemented in real time systems. However, DBP can only be limited to off-line signal processing recently.

In Chapter 5, an ideal optical back propagation (OBP) scheme to compensate for impairment of the transmission fibers is investigated [105]. The transmission link consists of N spans, and the output of the transmission fiber goes through an optical phase conjugator, N spans of dispersion-decreasing fibers (DDFs) and amplifiers. To compensate for the dispersive and nonlinear effects of the transmission fibers exactly, the nonlinear coefficient of the back propagation fiber needs to increase exponentially

with distance or equivalently the power in the back propagation fiber should increase exponentially if the nonlinear coefficient is constant. It is found that DDFs combined with amplifiers can be used to compensate for nonlinear effects exactly. The dispersion profile of the DDF is derived analytically. Numerical simulations of WDM fiber-optic systems show that the proposed OBP scheme can enhance the system reach significantly as compared to DBP. Although OBP may introduce insertion loss, it has many advantages: It has a very large bandwith, while DBP is limited by the bandwidth of the coherent receiver. OBP can be implemented in real time for WDM system, while DBP is limited to off-line signal processing due to its requirement of significant computational resources. In addition, OBP is potential for optical network, if the OBP module is placed at every span or at each node, but DBP can only be implemented at the transmitter or the receiver side.

In Chapter 6, an exact solution of NLSE is derived for impulse input in the presence of pre-dispersion [116]. The phase factor of the exact solution is obtained in a closed form using the exponential integral. The nonlinear interaction among discrete pulses train launched at the input is investigated, and the condition under which the envelope of these pulses keep unchanged is examined. It is found that if the complex weights of the impulses at the input have a secant-hyperbolic envelope and a proper chirp factor, they will propagate over long distances without exchanging energy. A discrete version of NLSE is derived to describe their propagation in fibers. The derived equation is a form of discrete self-trapping (DST) equation. In the context of discrete NLSE, if the effective dispersion length is much longer than the effective nonlinear length, the nonlinear eigenmodes of the highly pre-dispersed fiber-optic system is obtained, which may be useful for the description of signal propagation, and signal

and noise interaction.

7.2 Future work

This thesis provides various schemes to solve the NLSE using SSFS, which are used to model the optical pulse propagating in fibers. More accurate and efficient schemes to simulate forward propagation need to be investigated in the future work. In order to validate the theoretical derivation and simulation results, experiments need to be carried out. Through experiments, the performance of DBP and OBP schemes can be measured and the feasibility can be validated.

These days, DBP can only be implemented in off-line signal processing for WDM systems because of the enormous computational cost. The main computational complexity comes from the large number of steps and the FFT operations in each step. Improving the compensation accuracy and reducing the computational complexity of DBP is an important topic. Since perturbation theory can be used to solve NLSE analytically or semi-analytically, DBP based on SSFS combined with perturbation theory, which introduces perturbation theory in each step of DBP, may lead to a better DBP scheme.

Compared with DBP, OBP compensates for fiber distortions in real time using fibers and optical devices. Another interesting topic is to develop integrated optic devices to realize OBP. In Chaper 4, fiber Bragg gratings and highly nonlinear fibers are concatenated in a way similar to SSFS, and it may be possible to develop a single integrated optic device with alternating sections of Bragg gratings and highly nonlinear waveguides or multiple sections of the gratings written on the highly nonlinear waveguide. For the latter case, optimum section lengths calculated in Chapter 4 are

still applicable, but the split-step approximation is not required as dispersion and nonlinearity act simultaneously and hence, the performance would be better than that shown in Chapter 4 for a given number of steps. Silicon has a very large Kerr nonlinear coefficient and a small length of silicon waveguide can compensate for the nonlinear phase-shift occurring over kilometers of optical fiber. Also, a dispersive waveguide can be used to fulfill the dispersion operation. Hence, it may be possible to develop an OBP module on silicon chip. Also, if a single integrated optic device is developed to realize the function of DDF in Chapter 5, the design of fiber optic communication systems will become much more simplified and efficient.

Appendix A

Derivation of the leading error per step using SSFS

The derivation of the error per step for scheme I and II is as follows. The Baker-Hausdorff formular for two noncommuting operators $\hat{a}$ and $\hat{b}$ is [22]

$$\exp(\hat{a})\exp(\hat{b}) = \exp\left(\hat{a}+\hat{b}+\frac{1}{2}[\hat{a},\hat{b}]+\frac{1}{12}\left[\hat{a}-\hat{b},[\hat{a},\hat{b}]\right]+\ldots\right), \tag{A.1}$$

where $[\hat{a},\hat{b}] = \hat{a}\hat{b}-\hat{b}\hat{a}$. By using the Baker-Hausdorff formular twice, we obtain

$$\begin{aligned}\exp\left(\frac{\hat{a}}{2}\right)\exp(\hat{b})\exp\left(\frac{\hat{a}}{2}\right) = \exp\Bigg(\hat{a}+\hat{b}+\frac{1}{12}\hat{b}\hat{b}\hat{a}-\frac{1}{6}\hat{b}\hat{a}\hat{b}+\frac{1}{12}\hat{a}\hat{b}\hat{a}-\frac{1}{24}\hat{a}\hat{a}\hat{b}\\ -\frac{1}{24}\hat{b}\hat{a}\hat{a}+\frac{1}{12}\hat{a}\hat{b}\hat{b}\Bigg).\end{aligned} \tag{A.2}$$

Let us set the right hand side of Eq. (A.2) equal to $\exp(H+E)$, where

$$H = \hat{a}+\hat{b}, \tag{A.3}$$

$$E = \frac{1}{12}\hat{b}\hat{b}\hat{a} - \frac{1}{6}\hat{b}\hat{a}\hat{b} + \frac{1}{12}\hat{a}\hat{b}\hat{a} - \frac{1}{24}\hat{a}\hat{a}\hat{b} - \frac{1}{24}\hat{b}\hat{a}\hat{a} + \frac{1}{12}\hat{a}\hat{b}\hat{b}. \tag{A.4}$$

In the symmetric SSFS, let

$$\hat{a} = h\hat{D}, \quad \hat{b} = h\hat{N}. \tag{A.5}$$

From Eq. (A.4), we find that $E \propto h^3$. Using Taylor expansion, we find

$$\begin{aligned}
\exp(H+E) &= 1 + (H+E) + \frac{(H+E)^2}{2!} + \frac{(H+E)^3}{3!} + \dots \\
&= \left(1 + H + \frac{H^2}{2!} + \frac{H^3}{3!}\right) + \Big[E + \frac{1}{2}\left(E^2 + HE + EH\right) \\
&\quad + \frac{1}{6}\left(E^3 + HE^2 + H^2E + EH^2 + E^2H + HEH + EHE\right)\Big] + \dots \\
&\approx \exp(H) + E + O(h^4).
\end{aligned} \tag{A.6}$$

In Eq. (A.6), E is $O\left(h^3\right)$ and the higher order terms such as E^2 and HE are $O\left(h^6\right)$ and $O\left(h^4\right)$, respectively. So the leading error term for symmetric SSFS is E. When loss is with dispersion (scheme I),

$$\hat{a}_1 = \hat{D}_1 h = \left(-\frac{i}{2}\beta_2\frac{\partial^2}{\partial T^2} - \frac{\alpha}{2}\right)h, \tag{A.7}$$

$$\hat{b}_1 = \hat{N}_1 h = i\gamma|A_{l1}|^2 h, \tag{A.8}$$

and the leading error is

$$\begin{aligned} E_I &= \left(\frac{1}{12}\hat{b}_1\hat{b}_1\hat{a}_1 - \frac{1}{6}\hat{b}_1\hat{a}_1\hat{b}_1 + \frac{1}{12}\hat{a}_1\hat{b}_1\hat{a}_1 - \frac{1}{24}\hat{a}_1\hat{a}_1\hat{b}_1 - \frac{1}{24}\hat{b}_1\hat{a}_1\hat{a}_1 + \frac{1}{12}\hat{a}_1\hat{b}_1\hat{b}_1\right) A(0,T) \\ &= \left(\frac{i}{24}\beta_2\gamma^2|A_{l1}|^4\frac{\partial^2}{\partial T^2} - \frac{i}{12}\beta_2\gamma^2|A_{l1}|^2\frac{\partial^2}{\partial T^2}|A_{l1}|^2 - \frac{i}{48}\beta_2^2\gamma\frac{\partial^2}{\partial T^2}|A_{l1}|^2\frac{\partial^2}{\partial T^2}\right. \\ &\quad \left. + \frac{i}{96}\beta_2^2\gamma\frac{\partial^4}{\partial T^4}|A_{l1}|^2 + \frac{i}{96}\beta_2^2\gamma|A_{l1}|^2\frac{\partial^4}{\partial T^4} + \frac{i}{24}\beta_2\gamma^2\frac{\partial^2}{\partial T^2}|A_{l1}|^4\right) h^3 A(0,T). \end{aligned} \tag{A.9}$$

When loss is with nonlinearity (scheme II), let

$$\hat{a}_2 = \hat{D}_2 h = -\frac{i}{2}h\beta_2\frac{\partial^2}{\partial T^2}, \tag{A.10}$$

$$\hat{b}_2 = -\frac{\alpha}{2}h + i\gamma h_{eff}|A_{l2}|^2, \tag{A.11}$$

and the leading error now is

$$\begin{aligned} E_I &= \left(\frac{1}{12}\hat{b}_2\hat{b}_2\hat{a}_2 - \frac{1}{6}\hat{b}_2\hat{a}_2\hat{b}_2 + \frac{1}{12}\hat{a}_2\hat{b}_2\hat{a}_2 - \frac{1}{24}\hat{a}_2\hat{a}_2\hat{b}_2 - \frac{1}{24}\hat{b}_2\hat{a}_2\hat{a}_2 + \frac{1}{12}\hat{a}_2\hat{b}_2\hat{b}_2\right) A(0,T) \\ &= \left(\frac{i}{24}h_{eff}\beta_2\gamma^2|A_{l2}|^4\frac{\partial^2}{\partial T^2} - \frac{i}{12}h_{heff}\beta_2\gamma^2|A_{l2}|^2\frac{\partial^2}{\partial T^2}|A_{l2}|^2 - \frac{i}{48}h\beta_2^2\gamma\frac{\partial^2}{\partial T^2}|A_{l2}|^2\frac{\partial^2}{\partial T^2}\right. \\ &\quad \left. + \frac{i}{96}h\beta_2^2\gamma\frac{\partial^4}{\partial T^4}|A_{l2}|^2 + \frac{i}{96}h\beta_2^2\gamma|A_{l2}|^2\frac{\partial^4}{\partial T^4} + \frac{i}{24}h_{eff}\beta_2\gamma^2\frac{\partial^2}{\partial T^2}|A_{l2}|^4\right) hh_{eff}A(0,T). \end{aligned} \tag{A.12}$$

Bibliography

[1] T. H. Maiman, "Stimulated optical radiation in ruby," *Nature*, vol. 187, pp. 493–494, 1960.

[2] K. Kao and G. A. Hockham, "Dielectric-fibre surface waveguides for optical frequencies," in *Proceedings of the Institution of Electrical Engineers*, vol. 113, no. 7. IET, 1966, pp. 1151–1158.

[3] F. Kapron, D. B. Keck, and R. D. Maurer, "Radiation losses in glass optical waveguides," *Applied Physics Letters*, vol. 17, no. 10, pp. 423–425, 1970.

[4] I. Hayashi, M. Panish, P. Foy, and S. Sumski, "Junction lasers which operate continuously at room temperature," *Applied Physics Letters*, vol. 17, no. 3, pp. 109–111, 1970.

[5] G. P. Agrawal, *Lightwave technology: telecommunication systems*. John Wiley & Sons, 2005.

[6] R. J. Sanferrare, "Terrestrial lightwave systems," *AT&T technical journal*, vol. 66, no. 1, pp. 95–107, 1987.

[7] D. Gloge, A. Albanese, C. Burrus, E. Chinnock, J. Copeland, A. Dentai, T. Lee, T. Li, and K. Ogawa, "High-speed digital lightwave communication using leds

and pin photodiodes at 1.3 μm," *Bell System Technical Journal*, vol. 59, no. 8, pp. 1365–1382, 1980.

[8] J. Yamada, S. Machida, and T. Kimura, "2 gbit/s optical transmission experiments at 1.3 â¿ m with 44 km single-mode fibre," *Electronics Letters*, vol. 17, no. 13, pp. 479–480, 1981.

[9] T. Miya, Y. Terunuma, T. Hosaka, and T. Miyashita, "Ultimate low-loss single-mode fibre at 1.55 μm," *Electronics Letters*, vol. 15, no. 4, pp. 106–108, 1979.

[10] L. Cohen, C. Lin, and W. French, "Tailoring zero chromatic dispersion into the 1.5? 1.6? m low-loss spectral region of single-mode fibres," *Electronics Letters*, vol. 12, no. 15, pp. 334–335, 1979.

[11] N. S. Bergano and H. Kidorf, "Global undersea cable networks," *Optics Photonics News*, vol. 12, no. 3, pp. 32–35, 2001.

[12] S. Kumar and M. J. Deen, *Fiber Optic Communications: Fundamentals and Applications*. Wiley, 2014.

[13] M. Born and E. Wolf, *Principles of optics: electromagnetic theory of propagation, interference and diffraction of light*. Cambridge university press, 1999.

[14] G. P. Agrawal, *Fiber-Optic Communication Systems*. John Wiley & Sons, 1997.

[15] C. D. Poole and J. Nagel, "Polarization effects in lightwave systems," *Optical Fiber Telecommunications IIIA*, pp. 114–161, 1997.

[16] F. Bruyere, "Impact of first-and second-order pmd in optical digital transmission systems," *Optical Fiber Technology*, vol. 2, no. 3, pp. 269–280, 1996.

[17] P. Wai and C. Menyak, "Polarization mode dispersion, decorrelation, and diffusion in optical fibers with randomly varying birefringence," *Lightwave Technology, Journal of*, vol. 14, no. 2, pp. 148–157, 1996.

[18] M. Karlsson, "Polarization mode dispersion induced pulse broadening in optical fibers," *Optics letters*, vol. 23, no. 9, pp. 688–690, 1998.

[19] G. J. Foschini, R. Jopson, L. E. Nelson, and H. Kogelnik, "The statistics of pmd-induced chromatic fiber dispersion," *Journal of lightwave technology*, vol. 17, no. 9, p. 1560, 1999.

[20] M. Karlsson, J. Brentel, and P. A. Andrekson, "Long-term measurement of pmd and polarization drift in installed fibers," *Journal of Lightwave Technology*, vol. 18, no. 7, p. 941, 2000.

[21] J. Fini and H. Haus, "Accumulation of polarization-mode dispersion in cascades of compensated optical fibers," *Photonics Technology Letters, IEEE*, vol. 13, no. 2, pp. 124–126, 2001.

[22] G. P. Agrawal, *Nonlinear Fiber Optics*. Academic Press, 2007.

[23] R. W. Boyd, *Nonlinear optics*. Academic press, 2003.

[24] R.-J. Essiambre, B. Mikkelsen, and G. Raybon, "Intra-channel cross-phase modulation and four-wave mixing in high-speed tdm systems," *Electron. Lett.*, vol. 35, no. 18, pp. 1576–1578, 1999.

[25] K. Inoue, K. Nakanishi, K. Oda, and H. Toba, "Crosstalk and power penalty due to fiber four-wave mixing in multichannel transmissions," *Lightwave Technology, Journal of*, vol. 12, no. 8, pp. 1423–1439, 1994.

[26] K. Inoue, "Influence of fiber four-wave mixing in multichannel return-to-zero (rz) signal transmissions," *Photonics Technology Letters, IEEE*, vol. 8, no. 2, pp. 293–295, 1996.

[27] J. P. Gordon and L. F. Mollenauer, "Phase noise in photonic communications systems using linear amplifiers," *Opt. Lett.*, vol. 15, no. 23, pp. 1351–1353, 1990.

[28] S. Kumar, "Effect of dispersion on nonlinear phase noise in optical transmission systems," *Opt. Lett.*, vol. 30, no. 24, pp. 3278–3280, 2005.

[29] A. Mecozzi, "Limits to long-haul coherent transmission set by the kerr nonlinearity and noise of the in-line amplifiers," *Journal of lightwave technology*, vol. 12, no. 11, pp. 1993–2000, 1994.

[30] S. Kumar, "Analysis of nonlinear phase noise in coherent fiber-optic systems based on phase shift keying," *J. Lightwave Technol.*, vol. 27, no. 21, pp. 4722–4733, 2009.

[31] K.-P. Ho and H.-C. Wang, "Effect of dispersion on nonlinear phase noise," *Optics letters*, vol. 31, no. 14, pp. 2109–2111, 2006.

[32] D. Yang and S. Kumar, "Intra-channel four-wave mixing impairments in dispersion-managed coherent fiber-optic systems based on binary phase-shift keying," *J. Lightwave Technol.*, vol. 27, no. 14, pp. 2916–2923, 2009.

[33] P. Mamyshev and N. Mamysheva, "Pulse-overlapped dispersion-managed data transmission and intrachannel four-wave mixing," *Opt. Lett.*, vol. 24, no. 21, pp. 1454–1456, 1999.

[34] S. Kumar, J. C. Mauro, S. Raghavan, and D. Q. Chowdhury, "Intrachannel nonlinear penalties in dispersion-managed transmission systems," *J. Select. Topics Quantum Electron.*, vol. 8, no. 3, pp. 626–631, 2002.

[35] A. Mecozzi, C. B. Clausen, and M. Shtaif, "Analysis of intrachannel nonlinear effects in highly dispersed optical pulse transmission," *Photon. Technol. Lett.*, vol. 12, no. 4, pp. 392–394, 2000.

[36] A. Mecozzi and et al., "System impact of intra-channel nonlinear effects in highly dispersed optical pulse transmission," *Photonics Technology Letters, IEEE*, vol. 12, no. 12, pp. 1633–1635, 2000.

[37] A. V. Cartaxo, "Cross-phase modulation in intensity modulation-direct detection WDM systems with multiple optical amplifiers and dispersion compensators," *J. Lightwave Technol.*, vol. 17, no. 2, pp. 178–190, 1999.

[38] Z. Jiang and C. Fan, "A comprehensive study on XPM-and SRS-induced noise in cascaded IM-DD optical fiber transmission systems," *J. Lightwave Technol.*, vol. 21, no. 4, pp. 953–960, 2003.

[39] T.-K. Chiang, N. Kagi, M. Marhic, and L. G. Kazovsky, "Cross-phase modulation in fiber links with multiple optical amplifiers and dispersion compensators," *J. Lightwave Technol.*, vol. 14, no. 3, pp. 249–260, 1996.

[40] R. Hui, K. Demarest, and C. T. Allen, "Cross-phase modulation in multispan WDM optical fiber systems," *J. Lightwave Technol.*, vol. 17, no. 6, pp. 1018–1026, 1999.

[41] D. Marcuse, A. Chraplyvy, and R. Tkach, "Dependence of cross-phase modulation on channel number in fiber WDM systems," *J. Lightwave Technol.*, vol. 12, no. 5, pp. 885–890, 1994.

[42] R. Hui, Y. Wang, K. Demarest, and C. Allen, "Frequency response of cross-phase modulation in multispan WDM optical fiber systems," *Photon. Technol. Lett.*, vol. 10, no. 9, pp. 1271–1273, 1998.

[43] M. Shtaif and M. Eiselt, "Analysis of intensity interference caused by cross-phase modulation in dispersive optical fibers," *Photon. Technol. Lett.*, vol. 10, no. 7, pp. 979–981, 1998.

[44] S. Kumar and D. Yang, "Second-order theory for self-phase modulation and cross-phase modulation in optical fibers," *J. Lightwave Technol.*, vol. 23, no. 6, pp. 2073–2080, 2005.

[45] P. Johannisson and M. Karlsson, "Perturbation analysis of nonlinear propagation in a strongly dispersive optical communication system," *J. Lightwave Technol.*, vol. 31, no. 8, pp. 1273–1282, 2013.

[46] S. N. Shahi, S. Kumar, and X. Liang, "Analytical modeling of cross-phase modulation in coherent fiber-optic system," *Opt. Express*, vol. 22, no. 2, pp. 1426–1439, 2014.

[47] R. Dar, M. Feder, A. Mecozzi, and M. Shtaif, "Properties of nonlinear noise in long, dispersion-uncompensated fiber links," *Opt. Express*, vol. 21, no. 22, pp. 25 685–25 699, 2013.

[48] R. Dar and et al, "Time varying isi model for nonlinear interference noise," in *Optical Fiber Communication Conference*. Optical Society of America, 2014, p. W2A.62.

[49] A. Mecozzi and R.-J. Essiambre, "Nonlinear shannon limit in pseudolinear coherent systems," *J. Lightwave Technol.*, vol. 30, no. 12, pp. 2011–2024, 2012.

[50] R. Dar, M. Shtaif, and M. Feder, "New bounds on the capacity of the nonlinear fiber-optic channel," *Opt. Lett.*, vol. 39, no. 2, pp. 398–401, 2014.

[51] P. Poggiolini, A. Carena, V. Curri, G. Bosco, and F. Forghieri, "Analytical modeling of nonlinear propagation in uncompensated optical transmission links," *Photon. Technol. Lett.*, vol. 23, no. 11, pp. 742–744, 2011.

[52] A. Carena, V. Curri, G. Bosco, P. Poggiolini, and F. Forghieri, "Modeling of the impact of nonlinear propagation effects in uncompensated optical coherent transmission links," *J. Lightwave Technol.*, vol. 30, no. 10, pp. 1524–1539, 2012.

[53] P. Poggiolini, "The GN model of non-linear propagation in uncompensated coherent optical systems," *J. Lightwave Technol.*, vol. 30, no. 24, pp. 3857–3879, 2012.

[54] G. Bosco, R. Cigliutti, A. Nespola, A. Carena, V. Curri, F. Forghieri, Y. Yamamoto, T. Sasaki, Y. Jiang, and P. Poggiolini, "Experimental investigation of

nonlinear interference accumulation in uncompensated links," *Photon. Technol. Lett.*, vol. 24, no. 13, p. 1230, 2012.

[55] S. Turitsyn, M. Sorokina, and S. Derevyanko, "Dispersion-dominated nonlinear fiber-optic channel," *Opt. Lett.*, vol. 37, no. 14, pp. 2931–2933, 2012.

[56] X. Li, X. Chen, G. Goldfarb, E. Mateo, I. Kim, F. Yaman, and G. Li, "Electronic post-compensation of WDM transmission impairments using coherent detection and digital signal processing," *Opt. Express*, vol. 16, no. 2, pp. 880–888, 2008.

[57] E. Ip and J. M. Kahn, "Compensation of dispersion and nonlinear impairments using digital backpropagation," *J. Lightwave Technol.*, vol. 26, no. 20, pp. 3416–3425, 2008.

[58] E. Mateo, L. Zhu, and G. Li, "Impact of XPM and FWM on the digital implementation of impairment compensation for WDM transmission using backward propagation," *Opt. Express*, vol. 16, no. 20, pp. 16 124–16 137, 2008.

[59] E. F. Mateo and G. Li, "Compensation of interchannel nonlinearities using enhanced coupled equations for digital backward propagation," *Appl. Opt.*, vol. 48, no. 25, pp. F6–F10, 2009.

[60] E. F. Mateo, F. Yaman, and G. Li, "Efficient compensation of inter-channel nonlinear effects via digital backward propagation in WDM optical transmission," *Opt. Express*, vol. 18, no. 14, pp. 15 144–15 154, 2010.

[61] L. B. Du and A. J. Lowery, "Improved single channel backpropagation for intra-channel fiber nonlinearity compensation in long-haul optical communication systems," *Opt. Express*, vol. 18, no. 16, pp. 17 075–17 088, 2010.

[62] L. Zhu and G. Li, "Folded digital backward propagation for dispersion-managed fiber-optic transmission," *Opt. Express*, vol. 19, no. 7, pp. 5953–5959, 2011.

[63] L. Zhu and G. LI, "Nonlinearity compensation using dispersion-folded digital backward propagation," *Opt. Express*, vol. 20, no. 13, pp. 14 362–14 370, 2012.

[64] E. F. Mateo, X. Zhou, and G. Li, "Improved digital backward propagation for the compensation of inter-channel nonlinear effects in polarization-multiplexed WDM systems," *Opt. Express*, vol. 19, no. 2, pp. 570–583, 2011.

[65] Z. Tao, L. Dou, W. Yan, L. Li, T. Hoshida, and J. C. Rasmussen, "Multiplier-free intrachannel nonlinearity compensating algorithm operating at symbol rate," *J. Lightwave Technol.*, vol. 29, no. 17, pp. 2570–2576, 2011.

[66] Y. Gao, J. C. Cartledge, A. S. Karar, S. S.-H. Yam, M. OSullivan, C. Laperle, A. Borowiec, and K. Roberts, "Reducing the complexity of perturbation based nonlinearity pre-compensation using symmetric edc and pulse shaping," *Opt. Express*, vol. 22, no. 2, pp. 1209–1219, 2014.

[67] Y. Gao, A. S. Karar, J. C. Cartledge, S. S.-H. Yam, C. Sullivan, Maurice Oand Laperle, A. Borowiec, and K. Roberts, "Joint pre-compensation and selective post-compensation for fiber nonlinearities," *Photon. Technol. Lett.*, vol. 26, no. 17, pp. 1746–1749, 2014.

[68] A. J. Antos and D. K. Smith, "Design and characterization of dispersion compensating fiber based on the LP_{01} mode," *J. Lightwave Technol.*, vol. 12, no. 10, pp. 1739–1745, 1994.

[69] K. Hill, K. Takiguchi, F. Bilodeau, B. Malo, T. Kitagawa, S. Thériault, D. Johnson, and J. Albert, "Chirped in-fiber bragg gratings for compensation of optical-fiber dispersion," *Opt. Lett.*, vol. 19, no. 17, pp. 1314–1316, 1994.

[70] D. M. Pepper and A. Yariv, "Compensation for phase distortions in nonlinear media by phase conjugation," *Opt. Lett.*, vol. 5, no. 2, pp. 59–60, 1980.

[71] R. A. Fisher, B. Suydam, and D. Yevick, "Optical phase conjugation for time-domain undoing of dispersive self-phase-modulation effects," *Opt. Lett.*, vol. 8, no. 12, pp. 611–613, 1983.

[72] D. Rafique and A. D. Ellis, "Nonlinearity compensation via spectral inversion and digital back-propagation: A practical approach," in *Optical Fiber Communication Conference*. Optical Society of America, 2012, p. OM3A.1.

[73] C. Paré, N. Doran, A. Villeneuve, and P.-A. Bélanger, "Compensating for dispersion and the nonlinear kerr effect without phase conjugation," *Optics letters*, vol. 21, no. 7, pp. 459–461, 1996.

[74] S. Kumar and D. Yang, "Optical backpropagation for fiber-optic communications using highly nonlinear fibers," *Opt. Lett.*, vol. 36, no. 7, pp. 1038–1040, 2011.

[75] R. Hardin and F. Tappert, "Applications of the split-step fourier method to the numerical solution of nonlinear and variable coefficient wave equations," *Siam Rev*, vol. 15, no. 2, p. 423, 1973.

[76] G. Bosco, A. Carena, V. Curri, R. Gaudino, P. Poggiolini, and S. Benedetto, "Suppression of spurious tones induced by the split-step method in fiber systems

simulation," *IEEE Photonics Technology Letters*, vol. 12, no. 5, pp. 489–491, 2000.

[77] O. V. Sinkin, R. Holzlöhner, J. Zweck, and C. R. Menyuk, "Optimization of the split-step fourier method in modeling optical-fiber communications systems," *Journal of lightwave technology*, vol. 21, no. 1, pp. 61–68, 2003.

[78] F. Yaman and G. Li, "Nonlinear impairment compensation for polarization-division multiplexed WDM transmission using digital backward propagation," *Photonics J.*, vol. 2, no. 5, pp. 816–832, 2010.

[79] E. Ip, "Nonlinear compensation using backpropagation for polarization-multiplexed transmission," *J. Lightwave Technol.*, vol. 28, no. 6, pp. 939–951, 2010.

[80] R. Asif, C.-Y. Lin, M. Holtmannspoetter, and B. Schmauss, "Optimized digital backward propagation for phase modulated signals in mixed-optical fiber transmission link," *Opt. Express*, vol. 18, no. 22, pp. 22 796–22 807, 2010.

[81] S. Kumar and J. Shao, "Optical back propagation with optimal step size for fiber optic transmission systems," *Photon. Technol. Lett.*, vol. 25, pp. 523–526, 2013.

[82] W. Forysiak, F. Knox, and N. Doran, "Average soliton propagation in periodically amplified systems with stepwise dispersion-profiled fiber," *Opt. Lett.*, vol. 19, no. 3, pp. 174–176, 1994.

[83] J. Shao, S. Kumar, and X. Liang, "Digital back propagation with optimal step

size for polarization multiplexed transmission," *Photon. Technol. Lett.*, vol. 25, no. 23, pp. 2327–2330, 2013.

[84] J. Shao, X. Liang, and S. Kumar, "Comparison of split-step fourier schemes for simulating fiber optic communication systems," *IEEE Photonics J.*, vol. 6, no. 4, p. 7200515, 2014.

[85] G. H. Weiss and A. A. Maradudin, "The baker-hausdorff formula and a problem in crystal physics," *Journal of Mathematical Physics*, vol. 3, no. 4, pp. 771–777, 1962.

[86] H. Simon, "Adaptive filter theory 4th ed," *Prentice Hall*, 2002.

[87] D. S. Millar, S. Makovejs, C. Behrens, S. Hellerbrand, R. I. Killey, P. Bayvel, and S. J. Savory, "Mitigation of fiber nonlinearity using a digital coherent receiver," *J. Select. Topics Quantum Electron.*, vol. 16, no. 5, pp. 1217–1226, 2010.

[88] D. Rafique and A. D. Ellis, "Impact of signal-ASE four-wave mixing on the effectiveness of digital back-propagation in 112 Gb/s PM-QPSK systems," *Opt. Express*, vol. 19, no. 4, pp. 3449–3454, 2011.

[89] G. Gao, X. Chen, and W. Shieh, "Influence of PMD on fiber nonlinearity compensation using digital back propagation," *Opt. Express*, vol. 20, no. 13, pp. 14 406–14 418, 2012.

[90] M. Matsumoto, Y. Akagi, and A. Hasegawa, "Propagation of solitons in fibers with randomly varying birefringence: Effects of soliton transmission control," *J. Lightwave Technol.*, vol. 15, no. 4, pp. 584–589, 1997.

[91] Z. Chen and S. Kumar, "A fiber-optic transmission system based on differential polarization-shift keying," *Opt. Commun.*, vol. 284, no. 16, pp. 4064–4069, 2011.

[92] S. J. Savory, "Digital filters for coherent optical receivers," *Opt. Express*, vol. 16, no. 2, pp. 804–817, 2008.

[93] J. Shao and S. Kumar, "Optical backpropagation for fiber-optic communications using optical phase conjugation at the receiver," *Opt. Lett.*, vol. 37, no. 15, pp. 3012–3014, 2012.

[94] M. Lax, J. Batteh, and G. Agrawal, "Channeling of intense electromagnetic beams," *Journal of Applied Physics*, vol. 52, no. 1, pp. 109–125, 1981.

[95] J. Y. Leong, P. Petropoulos, J. H. Price, H. Ebendorff-Heidepriem, S. Asimakis, R. C. Moore, K. E. Frampton, V. Finazzi, X. Feng, T. M. Monro *et al.*, "High-nonlinearity dispersion-shifted lead-silicate holey fibers for efficient 1-μm pumped supercontinuum generation," *Lightwave Technology, Journal of*, vol. 24, no. 1, pp. 183–190, 2006.

[96] I. Tomkos, D. Chowdhury, J. Conradi, D. Culverhouse, K. Ennser, C. Giroux, B. Hallock, T. Kennedy, A. Kruse, S. Kumar *et al.*, "Demonstration of negative dispersion fibers for DWDM metropolitan area networks," *J. Select. Topics Quantum Electron.*, vol. 7, no. 3, pp. 439–460, 2001.

[97] H. Fews, M. Stephens, A. Straw, W. Forysiak, B. Nayar, and L. Gleeson, "Experimental comparison of fibre and grating-based dispersion compensation schemes for 40 channel 10gb/s dwdm systems," 2006.

[98] T. Pfau, S. Hoffmann, and R. Noé, "Hardware-efficient coherent digital receiver concept with feedforward carrier recovery for m-QAM constellations," *J. Lightwave Technol.*, vol. 27, no. 8, pp. 989–999, 2009.

[99] Y. Gao, J. H. Ke, K. P. Zhong, J. C. Cartledge, and S. Yam, "Assessment of intrachannel nonlinear compensation for 112 Gb/s dual-polarization 16QAM systems," *J. Lightwave Technol.*, vol. 30, no. 24, pp. 3902–3910, 2012.

[100] M. D. Pelusi, "WDM signal all-optical precompensation of Kerr nonlinearity in dispersion-managed fibers," *Photon. Technol. Lett.*, vol. 25, no. 1, pp. 71–74, 2013.

[101] A. Yariv, D. Fekete, and D. M. Pepper, "Compensation for channel dispersion by nonlinear optical phase conjugation," *Opt. Lett.*, vol. 4, no. 2, pp. 52–54, 1979.

[102] S. Watanabe and M. Shirasaki, "Exact compensation for both chromatic dispersion and Kerr effect in a transmission fiber using optical phase conjugation," *J. Lightwave Technol.*, vol. 14, no. 3, pp. 243–248, 1996.

[103] P. Minzioni, I. Cristiani, V. Degiorgio, L. Marazzi, M. Martinelli, C. Langrock, and M. Fejer, "Experimental demonstration of nonlinearity and dispersion compensation in an embedded link by optical phase conjugation," *Photon. Technol. Lett.*, vol. 18, no. 9, pp. 995–997, 2006.

[104] M. Morshed, L. B. Du, B. Foo, M. D. Pelusi, and A. J. Lowery, "Optical phase

conjugation for nonlinearity compensation of 1.21-Tb/s pol-mux coherent optical OFDM," in *OptoElectronics and Communications Conference and Photonics in Switching*. Optical Society of America, 2013, p. PD3_4.

[105] X. Liang, S. Kumar, and J. Shao, "Ideal optical backpropagation of scalar NLSE using dispersion-decreasing fibers for WDM transmission," *Opt. Express*, vol. 21, no. 23, pp. 28 668–28 675, 2013.

[106] S. V. Chernikov, D. Richardson, D. Payne, and E. Dianov, "Soliton pulse compression in dispersion-decreasing fiber," *Opt. Lett.*, vol. 18, no. 7, pp. 476–478, 1993.

[107] A. J. Stentz, A. F. Evans, and R. W. Boyd, "Dramatically improved transmission of ultrashort solitons through 40 km of dispersion-decreasing fiber," *Opt. Lett.*, vol. 20, no. 17, pp. 1770–1772, 1995.

[108] J. Conradi, S. Kumar, and S. S. Rosenblum, "Negative dispersion single mode waveguide fiber," 2002, uS Patent 6,430,346.

[109] C. Xie, "Interchannel nonlinearities in coherent polarization-division-multiplexed quadrature-phase-shift-keying systems," *Photon. Technol. Lett.*, vol. 21, no. 5, pp. 274–276, 2009.

[110] A. Hasegawa and F. Tappert, "Transmission of stationary nonlinear optical pulses in dispersive dielectric fibers. I. Anomalous dispersion," *Appl. Phys. Lett.*, vol. 23, no. 3, pp. 142–144, 1973.

[111] V. E. Zakharov and A. B. Shabat, "Exact theory of two-dimensional self-focusing and one-dimensional self-modulation of waves in nonlinear media," *Sov. Phys. JETP.*, vol. 34, pp. 62–69, 1972.

[112] G. L. Lamb Jr, *Elements of Soliton Theory*. Wiley-Interscience, 1980.

[113] P. G. Drazin and R. S. Johnson, *Solitons: An Introduction*. Cambridge University Press, 1989, vol. 2.

[114] Y. Xiao, D. N. Maywar, and G. P. Agrawal, "New approach to pulse propagation in nonlinear dispersive optical media," *J. Opt. Soc. Am. B*, vol. 29, no. 10, pp. 2958–2963, 2012.

[115] E. Ciaramella and E. Forestieri, "Analytical approximation of nonlinear distortions," *Photon. Technol. Lett.*, vol. 17, no. 1, pp. 91–93, 2005.

[116] S. Kumar, J. Shao, and X. Liang, "Impulse response of nonlinear schrödinger equation and its implications for pre-dispersed fiber-optic communication systems," *Opt. Express*, vol. 22, no. 26, pp. 32 282–32 292, 2014.

[117] I. S. Gradshtejn and I. M. Ryzhik, *Table of Integrals, Series and Products*. Academic Press, 1965.

[118] M. Ablowitz and B. Prinari, "Nonlinear schrodinger systems: Continuous and discrete," *Scholarpedia*, vol. 3, no. 8, p. 5561, 2008.

[119] J. C. Eilbeck and M. Johansson, "The discrete nonlinear schrödinger equation-20 years on," in *Conference on Localization and Energy Transfer in Nonlinear Systems*, 2003, p. 44.

[120] J. C. Eilbeck, P. Lomdahl, and A. Scott, "The discrete self-trapping equation," *Physica D: Nonlinear Phenomena*, vol. 16, no. 3, pp. 318–338, 1985.

[121] M. J. Ablowitz and T. Hirooka, "Managing nonlinearity in strongly dispersion-managed optical pulse transmission," *J. Opt. Soc. Am. B*, vol. 19, no. 3, pp. 425–439, 2002.

[122] X. Liang and S. Kumar, "Multi-stage perturbation theory for compensating intra-channel nonlinear impairments in fiber-optic links," *Opt. Express*, vol. 22, no. 24, pp. 29 733–29 745, 2014.